The Pennsylvania State University

The Graduate School

THE STRUCTURE AND DYNAMICS OF THE NUCLEOSOME AT A SINGLE MOLECULE LEVEL

A Dissertation in

Chemistry

by

Mai T. Huynh

Submitted in Partial Fulfillment

of the Requirements

for the Degree of

Doctor of Philosophy

May 2023

The dissertation of Mai T. Huynh was reviewed and approved by the following:

Tae-Hee Lee
Professor of Chemistry
Dissertation Advisor
Chair of Committee

Lu Bai
Associate Professor of Biochemistry and Molecular Biology and of Physics

Mark Hedglin
Assistant Professor of Chemistry

Ruobo Zhou
Assistant Professor of Chemistry

Philip Bevilacqua
Distinguished Professor of Chemistry
Distinguished Professor of Biochemistry and Molecular Biology
Department Head, Chemistry

ABSTRACT

The basic unit of packaging for a eukaryotic genome is the nucleosome. The kinetics of numerous DNA-templated processes, including transcription elongation by RNA Polymerase II (Pol II), are controlled by dynamic interactions between DNA and histones in the nucleosome. The global and local stability of the nucleosome can be regulated by a number of elements, such as histone modifications and histone chaperones. By utilizing single-molecule FRET measurements with chemically modified histones, we investigated the effects of histone H2B ubiquitylations at K34 (H2BK34ub) and K120 (H2BK120ub) on the structure of the nucleosome and the interactions between two nucleosomes as well as the potential effects of histone H3 acetylation at K56 (H3K56ac), histone H2B ubiquitylations at K34 (H2BK34ub) and K120 (H2BK120ub) and H3K79 trimethylation ($H3K79me_3$) on the kinetics of transcription elongation by Pol II. We found that whereas H2BK120 ubiquitylation has no effect on the nucleosome structure or internucleosomal contacts, H2BK34 ubiquitylation expands the DNA gyre gap in the nucleosome and stabilizes long- and short-range interactions. We also observed that H3K56 acetylation and H2B ubiquitylation suppress pauses and decrease pause durations close to the nucleosome entry, while $H3K79me_3$ shortens pause durations and speeds up RNA elongation close to the nucleosome center. Additionally, we discovered that H2BK34ub promotes partial nucleosome rewrapping upon Pol II passage. All these results imply that H3K56ac and $H3K79me_3$ promote Pol II progression perhaps by disrupting the local nucleosome structure, while H2B ubiquitylations promote transcription elongation and aid in maintaining the chromatin structure by inducing and stabilizing nucleosome intermediates. Overall, our findings outline the processes by which these changes, when joined by a network of regulatory proteins, enable transcription in various nucleosome areas and assist in maintaining the structure of the chromatin during active transcription.

TABLE OF CONTENTS

LIST OF FIGURES

LIST OF TABLES

ACKNOWLEDGEMENTS

I would like to express my deepest appreciation to my primary mentor, Dr. Tae-Hee Lee for his guidance and patience during my Ph.D. study. His immense knowledge and continuous support through all stages of work have made this journey an inspirational experience for me.

In addition to my advisor, I would like to express my sincere gratitude to my committee members, Drs. Lu Bai, Mark Hedglin, and Xin Zhang, for their thoughtful criticisms and recommendations that have shaped my graduate studies. Additionally, I would also like to extend my thanks to Dr. Ruobo Zhou for his willingness to give time to serve as a member of my dissertation committee.

I would like to thank all of our collaborators who have contributed to my research initiatives throughout the years. I would like to acknowledge Dr. Joseph Reese for providing plasmids expressing yeast RNA Polymerase II, TFIIS, FACT, and Nhp6, Dr. Song Tan for plasmids expressing human histones, and Dr. Robert McGinty for ubiquitylated H2B histone proteins. I would like to also offer my thanks to the Genomics Core Facility (Huck) and Proteomics & Mass Spectrometry Core Facility (Huck), especially to Tatiana Laremore for her technical expertise.

For the work presented in this dissertation, I would like to thank all federal funding sources. All projects leading up to this dissertation were supported by NIH grants R01GM123164 and R01GM130793 to T.-H.L., R35GM136353 to J.C.R., R35GM133498 to R.K.M., and by IDB RAS government programs of basic research in 2022 No. 0088-2021-0007 to W.K. However, the findings and conclusions described in this dissertation do not necessarily reflect the view of the funding agencies.

My deepest gratitude to both my past and present lab members for their assistance at every stage of my research projects. They are Dr. Bhaswati Sengupta, Subhra Das, Dr. Satya Yadav, Dr. Shi Ho Kim, and Jia Gao, whom I always consider as not only colleagues but also as dear friends. I appreciate the times they have offered to examine my papers and presentations, provide me with helpful scientific advice, or just be a source of support and encouragement during tough times.

Finally, but the most importantly, I would like to thank all of family and friends back in my home country for their unending support despite our long distance. My parents, Tin Huynh and Thao Ho, deserve a special mention for their affection and unwavering belief in me throughout my entire life. A special thanks to Truc Huynh, my sister and my biggest supporter, for always being there for me and doing everything she could to get me through this challenging PhD journey.

Mai T. Huynh
The Pennsylvania State University
May 2023

Chapter 1

Introduction

1.1. Overview on chromatin

Around two meters of linear DNA are stored in each human cell as genetic material. DNA must be tightly packed into the chromosomal structure in order to fit it within the nucleus's constrained space. Heterochromatin, which is more compact and typically transcriptionally silent, and euchromatin, which is more accessible and transcriptionally active, are two physically and functionally distinct domains on the chromosome. Chromatins have a “beads on a string” structure (Kornberg 1974). The “beads” are nucleosomes whereas the string is the linker DNA (Fig. 1-1). The nucleosome, which repeats across the genome every 160 to 240 bp, is the essential component of chromatin and serves as the molecular basis of the dynamic gene regulatory mechanisms in chromatin. The nucleosome is made up of an octameric complex containing the core histone proteins, which is wrapped around by ~145 to ~147 bp of DNA (Luger et al. 1997a, Davey et al. 2002). Adjacent nucleosomes are joined together through linker DNA, which is frequently bound with linker histone (e.g, histone H1 or H5).

Chromatin dynamics regulates various eukaryotic DNA-templated biological processes, including the epigenetic regulation of gene expression, DNA replication, DNA recombination, gene transcription, and DNA damage repair. Epigenetic modifications have strong impacts on how genes are regulated. Examples of these modifications are DNA methylation, histone post-

translational modifications (PTMs), and histone variations, all of which have the ability to regulate nucleosome stability (Yankulov 2015, Berger 2007, Kouzarides 2007).

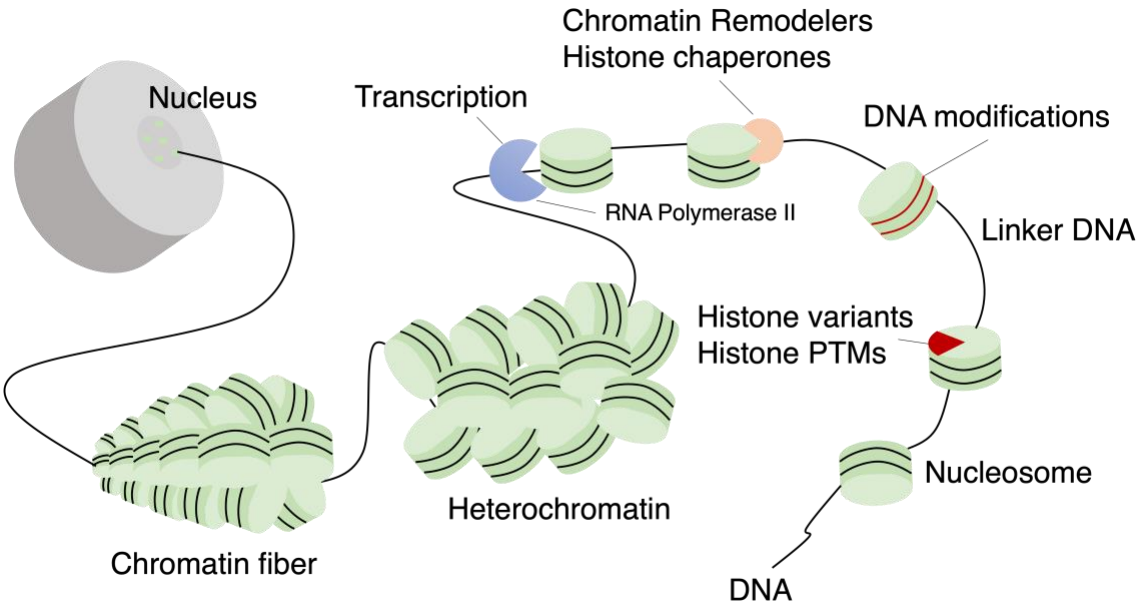

Figure **1-1**: A diagram depicting various aspects of chromatin regulation.

1.2. Nucleosome structure and dynamics

The nucleosome is composed of an octameric histone core containing two H2A-H2B histone dimers and one $(H3\text{-}H4)_2$ histone tetramer. The histone core is wrapped around 147 bp DNA (Luger et al. 1997a, Davey et al. 2002). Four histone heterodimers - two of each H2A/H2B and H3/H4-constitute the histone core (Fig. 1-2). Each of the four core histone proteins-H2A, H2B, H3 and H4-is present in two copies in the central histone octamer. DNA is periodically in contact with the histone octamer. The nucleosome dyad is located at the centered base pair on the

nucleosome. DNA contact sites are identified by superhelical locations (SHL), which indicate superhelical turns from the dyad (SHL 0) and range from SHL-7 to SHL 7 (Fig. 1-2). There is a primary periodicity of about 10 base pairs between two adjacent superhelical locations. The interactions between histones and DNA are maintained and modulated by a wide range of ionic interactions, nonpolar contacts, direct and water-mediated hydrogen bonds, and the alignment of helix dipoles with respect to phosphate backbone ions (Luger et al. 1997a, Davey et al. 2002).

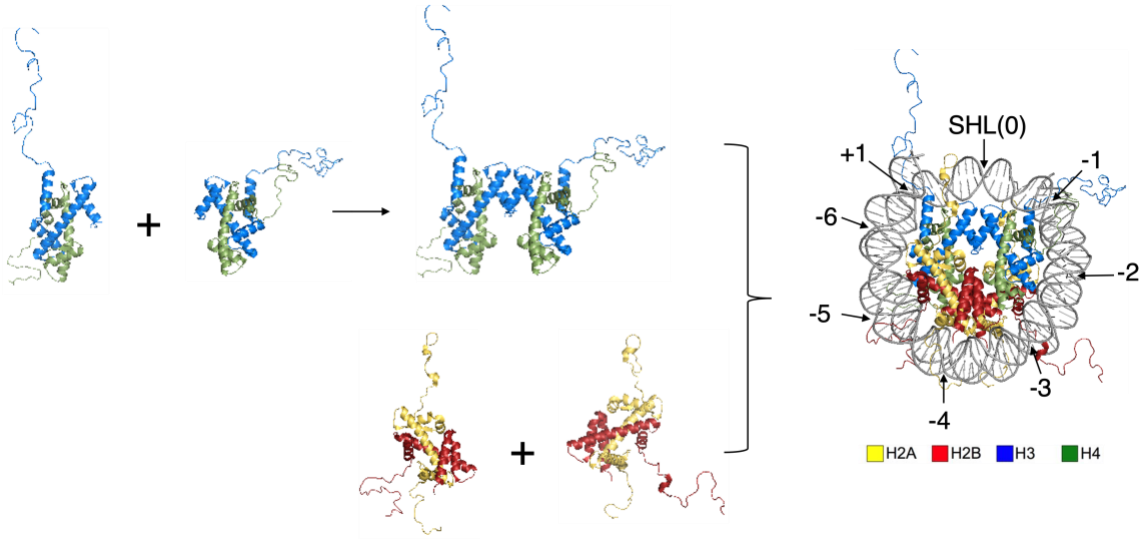

Figure **1-2**: Structure of the nucleosome core particle (PDB: 1kx5).

The nucleosome is composed of a short stretch of DNA wrapping around an octameric complex containing two copies of histone H2A-H2B and one copy of $(H3\text{-}H4)_2$ tetramer. DNA contacts with histone proteins via electrostatic interactions and these contact sites are identified as superhelical locations (in short, SHL). The dyad is designated as SHL(0). The range between the nucleosome entry site and the nucleosome exit site is from SHL(-7) to SHL(7) with 10 base pair periodicity.

Intact nucleosomes possess strong DNA-histone interactions, thus imposing physical barriers on enzymes translocating along nucleosomal DNA and limit DNA accessibility (Bednar

et al. 1999, Kireeva et al. 2005, Jin et al. 2010, Studitsky et al. 2016). These stable DNA-histone interactions regulate the efficiency of different genomic transactions, including chromatin remodeling and transcription by RNA Polymerase II (Pol II). However, despite possessing strong DNA-histone interactions, nucleosome structure can still be quite dynamic both in terms of composition and conformation. The nucleosome can undergo histone exchange to incorporate histone variants or histone post-translational modifications (PTMs), which can alter its structure and dynamics. DNA breathing, also known as fast DNA unwrapping and rewrapping, is a manifestation of the underlying structural dynamics that is present in the nucleosome.

In fact, DNA dynamics of the nucleosome has been a subject of multiple studies in conjunction of various types of histone PTMs (Bowman and Poirier 2015c). Past studies have shown that histone PTMs near the dyad influence the release of histone from DNA during disassembly but do not affect DNA unwrapping, whereas the nucleosomes with histone PTMs close to the DNA entry-exit site encourage spontaneous DNA unwrapping and the binding of regulatory components (Simon et al. 2011, Brehove et al. 2015). Hence, the primary role of the nucleosome is to act as a dynamic platform for several biological processes, not to restrict DNA accessibility.

1.3. Histone modifications and functions

The nucleosome can serve as a scaffold for chromatin enzyme binding, and it can experience various histone post-translational modifications (PTMs) (Yankulov 2015, Berger 2007, Kouzarides 2007). Those modifications can have either activating or repressive roles in transcription depending on their location (Zentner and Henikoff 2013, Xu, Zhang and Grunstein 2005, Black, Van Rechem and Whetstine 2012, Weake and Workman 2008). Histone PTMs can

exert their regulatory effects on gene expression by modulating the interactions among histone proteins, DNA, and various transcription factors (Cosgrove and Wolberger 2005, Cosgrove, Boeke and Wolberger 2004, Bannister and Kouzarides 2011). The effects of histone PTMs can be direct, such as altering DNA-histone and nucleosome-enzyme interactions, or indirect, such as recruiting more enzymes in cascading processes at the nucleosome and higher levels. The nucleosome is the basic building block of chromatin (Luger et al. 1997a, Davey et al. 2002). Therefore, changes at the nucleosome level provides the foundation to the understanding of chromatin dynamics and interactions with multiple enzymes and factors. Among all histone PTMs, histone acetylation, methylation and ubiquitylation are among the most common occurring PTMs in human cells and have been actively researched in the recent years (Zentner and Henikoff 2013, Xu et al. 2005, Black et al. 2012, Weake and Workman 2008).

1.3.1. Histone acetylation

Lysine acetylation at H3K56C is associated with active transcription (Xu et al. 2005). Past studies have proposed that it facilitates spontaneous DNA dynamics and is responsible for increased DNA accessibility. The number of acetylated H3K56C nucleosomes having DNA unwrapped at the entry position is reported as twice as the one recorded for non-acetylated nucleosomes (Neumann et al. 2009b). However, at the internal position near the dyad where the interactions between DNA and histones are the strongest, the fractions of the nucleosomes having unwrapped DNA for both cases are similar. Such phenomenon supports an increase in spontaneous histone-DNA interface opening only at the entry point of the DNA on the acetylated H3K56C nucleosome.

On the other hand, Kashlev and Bustamante *et al.* observed decreased pause densities and durations in the entry region (-115 to -35 bp) in acetylated nucleosomes when all lysine residues

get mutated to glutamine (Bintu et al. 2012). Yet, the values for both cases are similar in the region around the dyad (-35 to +5 bp) and the exit region (+5 to +85 bp). Notably, around 91% of non-acetylated nucleosomes show cooperative DNA unwrapping in the entry region while only 56% are noted for acetylated nucleosomes, thus implying that acetylation destabilizes the entry region of the nucleosomes.

Our previously published results also found that spontaneous DNA opening motion at the nucleosome termini decreases upon H3K56C acetylation (Lee and Lee 2019). The spontaneous DNA opening rate is 1.9-fold higher in acetylated H3K56C nucleosomes than in non-acetylated ones while maintaining the relatively constant closing rate at 50 mM NaCl. In the presence of histone chaperone Nap1, the DNA opening rate escalates to 5.9-fold difference between acetylated H3K56C and non-acetylated nucleosomes. Our rationale is that Nap1 binding requires a larger gap than averagely induced by spontaneous DNA opening. The rate at which DNA opens enough for Nap1 binding in acetylated H3K56C nucleosomes is approximately 5.9-fold greater than in non-acetylated ones (5.8 and 1.1 sec-1, respectively), assuming the same Nap1 binding success rate. This is reasonable considering H3K56C acetylation weakens histone-DNA interactions, thus increasing the likelihood of having a wider spontaneous histone-DNA gap. Hence, the effect of histone acetylation gets magnified upon Nap1 binding.

1.3.2. Histone ubiquitylations

Histone H2B ubiquitylation has been found at K34 and K120 (Weake and Workman 2008). These H2B ubiquitylations have been associated mostly with facilitated transcription (Wu et al. 2014, Tanny et al. 2007). The coding region of actively transcribed genes has been found to have histone H2B momentarily ubiquitinated and then deubiquitinated (Weake and Workman

2008). Mammalian heteromeric RNF20/40 complex catalyzes the majority of the H2B mono-ubiquitination , while various ubiquitin-specific proteases (USPs) catalyze its deubiquitylation.

A mutation that has the ubiquitin maker deleted has been shown to cause transcripts to accumulate more slowly and to lower levels. Hence, the ubiquitin marker may contribute to the facilitation of transcription (Fleming et al. 2008). Another research paper involving sedimentation velocity experiments revealed that the compaction of ubiquitinylated H2B-containing arrays was significantly reduced at 1 mM Mg^{2+}, suggesting that this histone PTM has the potential to disrupt higher-order chromatin structure folding and produces a more accessible fiber conformation (Fierz et al. 2011). More intriguingly, hub1-H2B, a protein that is comparable to ubiquitin in size and shape but has different surface residues, was not shown to have this impact, thus indicating that ubiquitinylated H2B does not rely solely on steric bulk effects (Fierz et al. 2011).

More recently, two separate biochemical and structural studies have found that H2BK34 ubiquitylation (H2BK34ub) weakens the interaction of the H2A-H2B dimer(s) with the nucleosome, enabling nucleosome opening and hexasome formation (Krajewski, Li and Dou 2018, Li et al. 2017, Ai et al. 2022). The ubiquitin moiety in H2BK34ub nucleosome resides between the two gyres of nucleosomal DNA, which results in the deformation of the two DNA chains. This may explain why H2BK34ub can accelerate transcription by promoting spontaneous DNA opening. However, there have not been any results published to confirm this proposal.

Another target for ubiquitylation at H2B is H2BK120. H2BK120 ubiquitylation (H2BK120ub) has much less of an impact on nucleosome stability than H2BK34 ubiquitylation (Krajewski et al. 2018). Chandrasekharan et al. demonstrated that the nucleosome stability is increased when the level of H2BK120ub increases, despite the fact that a mild nucleosome destabilizing effect of H2BK120ub was measured by in vitro Nap1-assited FRET-based assay from a different research group (Chandrasekharan et al. 2010, Fierz et al. 2012). More interestingly, optical tweezers experiments and thermal stability assays both support that

H2BK120ub stabilizes the proximal dimer and enhances the overall strength of the barrier for Pol II transcription through a nucleosome (Machida et al. 2016, Chen et al. 2019). Besides facilitating transcription, H2BK120ub has also been deemed necessary for the effective reassembly of the nucleosomes following Pol II-mediated transcription elongation (Fleming et al. 2008). Yet up to date, it is currently unclear how H2BK120ub influences nucleosome dynamics. In fact, because the epigenetic enzyme Dot1L recognizes H2BK120ub to methylate H3K79, H2BK120ub has primarily been studied in connection with H3K79 methylations (Worden et al. 2019, Spangler et al. 2022, Valencia-Sánchez et al. 2019).

1.3.3. Histone methylation

Histone H3K79 methylations have been linked to transcriptional activity (Schübeler et al. 2004, Wang et al. 2008, Yang et al. 2016). Although there has not been any research to demonstrate how H3K79 trimethylation (H3K79me$_3$) affects the nucleosome-mediated transcription, it is known to enhance transcription *in vitro* and to be related with highly active genes (Schübeler et al. 2004, Wang et al. 2008, Yang et al. 2016).

Genome-wide chromatin studies have shown that H3K79 methylation is enriched in areas that are actively engaged in transcription (Nguyen and Zhang 2011). A transcription assay using *in vitro* assembled chromatin templates and a highly purified Pol II transcription was designed to study the association of H3K79 methylation with transcription activation through p300-mediated histone acetylation (Yang et al. 2016). Transcription from H3K79-methylated chromatin was elevated, demonstrating a direct stimulatory effect of H3K79 methylation on chromatin transcription.

On the other hand, a structural study hinted on a possible role for H3K79me$_3$ (Lu et al. 2008). This histone PTM may induce a rearrangement of the histone surface although no change

was observed in the global structure of the nucleosome. H3K79 is located in the solvent-exposed C-terminal end of histone H3 where it can form a weak hydrogen bond with the main chain in the L2 loop of histone H4. The additional two methyl groups of H3K79me$_2$ cause the side chains to adopt different conformations that make them almost entirely solvent accessible. The molecular surface of the nucleosome as well as the local electrostatic potential are both affected by these two additional methyl groups. Specifically, a small hydrophobic pocket which is protected by the H4 residue Val70 and the H3 residue Leu82 gets exposed by H3K79me$_3$, thus modifying the local surface around the C-terminal end of H3 around SHL 2.5.

1.4. Transcription through the nucleosome

A series of studies have explored the structural dynamics and the function of the nucleosome at a molecular level as a general regulator of gene expression. It has been established that the nucleosomes impose physical barriers on enzymes translocating along nucleosomal DNA such as Pol II (Izban and Luse 1992, Bednar et al. 1999, Kireeva et al. 2005) . Previous studies have confirmed that the nucleosome can block Pol II progression during transcription elongation by imposing four different pauses on Pol II (Kujirai et al. 2018, Crickard et al. 2017). These stalled nucleosome positions correspond to certain pronounced DNA-histone interaction regions. Previously solved cryo-EM structures of Pol II-nucleosome complexes also confirm the two major pauses at the superhelical location -5 from the dyad or SHL(-5) and SHL(-1) (Kujirai et al. 2018) (Fig. 1-3). The structures also revealed weaker pauses at the SHL(-6) and SHL(-2) (Kujirai et al. 2018) (Fig. 1-3). Moreover, past research has found that Pol II can rarely overcome the barrier on its own and the assistance of certain nucleosome modifications or transcription factors is required (Hodges et al. 2009, Kulaeva et al. 2009). Instead, Pol II gets stalled or backtracked by

4-6 base pairs (Cheung and Cramer 2011, Lisica et al. 2016). TFIIS can relieve the Pol II backtracking by cleaving the RNA in front of the Pol II and align its active center to resume transcription elongation (Kettenberger, Armache and Cramer 2003, Kettenberger, Armache and Cramer 2004). Yet, in both cases, in order for Pol II to escape from the paused sites, Pol II needs to wait for spontaneous DNA fluctuations that eventually induce a large enough histone-DNA gap for Pol II to progress. In order to obtain a more open histone-DNA gap, the nucleosome can increase DNA accessibility in two major ways. One requires breaking the interactions between the nucleosome and DNA, thus resulting in the nucleosome in a more open state. The nucleosome can also recruit external proteins to the nucleosome core, thus inducing structural changes in the nucleosome which is favorable for transcription. All of these alterations typically involve the regulatory effects of histone post-translational modifications, histone variants, or nucleosome sliding or remodeling by histone chaperones or ATP-dependent remodeling complexes.

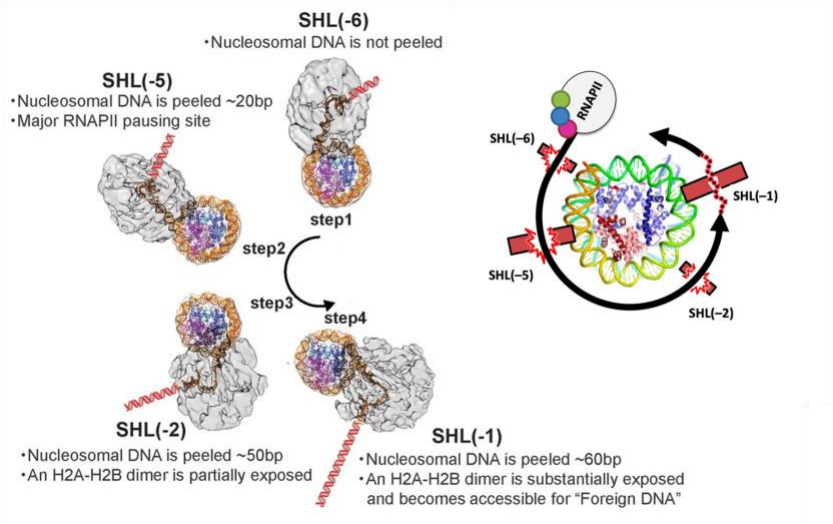

Figure **1-3**: An illustration of how Pol II transcribes through a nucleosome.

The nucleosomes impose four pauses on Pol II transcription based on solved cryo-EM structures: two major pauses on SHL(-5) and SHL(-1), and two minor pauses on SHL(-6) and SHL (-1). This figure is adapted from (Kujirai et al. 2018).

Another important aspect of transcription is how the nucleosome maintains its structure after Pol II progression. Prior research has suggested two main mechanisms for the recovery of the nucleosome structure (Kulaeva et al. 2009, Kulaeva and Studitsky 2010). The first one involves the exchange of the proximal H2A-H2B dimer on moderately transcribed genes. In this case, the interaction between DNA and the proximal histone dimer gets disrupted after Pol II passage along the nucleosomal DNA. Consequently, the proximal histone dimer may get evicted out of the nucleosome core, resulting in the formation of hexasome or unstable subnucleosome structure. The second scenario involves the displacement of the entire histone octamer during intense transcription. Past published reports proposed that the nucleosomes cannot self-assemble under physiological conditions spontaneously, thus requiring the assistance of transcription factors or binding proteins such as histone chaperones or chromatin remodelers.

Interestingly, a more recently published paper has shown that Pol II can help reassemble the nucleosome after transcription by promoting DNA rewrapping back around the histone core (Filipovski et al. 2022). They came up with a model that Pol II transcribes the nucleosome while both DNA regions ahead of Pol II and behind Pol II remain in contact with the nucleosome. Pol II encounters substantial barrier in the dyad region, and transcription of Pol II past the dyad can induce complete unwrapping of DNA downstream of Pol II. As a result, the nucleosome can transfer to the upstream DNA upon release of the downstream DNA from the octamer and the proximal and distal regions of the histone core swap. This phenomenon also complies with past publications which suggest that the nucleosome may not face any nucleosomal barrier past the dyad because at the stage, Pol II only transcribes the already unwrapped downstream DNA (Chen et al. 2019, Farnung et al. 2021).

Another study employing cryo-EM looked into how transcription elongation factors and histone chaperones affected Pol II ability to transcribe and reassemble nucleosomes (Ehara et al. 2022). They resolved several nucleosome intermediates during FACT-mediated transcription in

order to understand the mechanism via which FACT supports nucleosome reassembly. During transcription, the elongation complex can disassemble the nucleosome core as Pol II passes through the strong barrier at the nucleosomal dyad. With high affinity for histone proteins, FACT can then bind to histone proteins, and the resulting stabilized FACT-histone hexamer can move either upstream or downstream of DNA. Eventually, FACT can deposit the histone hexamer on the upstream DNA to form the hexasome and the remaining H2A-H2B dimer can be recruited to the hexasome to form the complete octasome.

1.5. Single-molecule FRET

The experimental method known as fluorescence resonance energy transfer (FRET) began to gain popularity around the turn of the century (Joo et al. 2008, Lerner et al. 2021). The theory behind FRET is that all molecules remain in their ground state, and they can get excited and move to higher electronic states when they come into contact with outside energy sources, like photons (Albrecht 2008). The fluorescence phenomenon originates from radiative energy released when a fluorescent molecule returns to its ground state. Different fluorescent molecules (often termed fluorophores) exhibit different fluorescence emission profiles determined by a particular wavelength and intensity. The emission profile of one fluorophore, which serves as the donor, must overlap with the absorption profile of the other, which serves as the acceptor, for FRET to occur between the two fluorophores (Fig. 1-4). The extent of this overlap is characterized by the overlap integral. Fluorescence resonance energy transfer is the non-radiative transmission of energy from an excited state fluorophore (referred as the donor) to a nearby second fluorophore (referred as the acceptor). When two fluorophores (the donor and the acceptor) are separated, no energy transfer occurs between the donor and the acceptor, thus

resulting in the absence of the acceptor emission (Fig. 1-4). When two fluorophores (the donor and the acceptor) are in close proximity and their transition dipoles are properly aligned, the two fluorophores can communicate through a dipole-dipole coupling mechanism to transfer energy (Fig. 1-4). Due to the efficient energy transfer between the donor and the acceptor, the intensity of the acceptor emission increases while the intensity of the donor emission decreases. The amount of energy transmitted per excited donor molecule is measured by the efficiency (E) of this transfer, which exhibits an inverse relationship with the sixth power of the distance (r) between the fluorophores (Albrecht 2008) (Fig. 1-4). The Förster distance, by definition, is the distance at which 50% of energy transfer (r_0) from the donor to the acceptor is observed (Albrecht 2008). Each donor-acceptor pair has a unique value for this parameter, known as r_0. A higher r_0 value allows for the monitoring of processes involving a greater change in distance. The energy transfer is only capable of occurring within a range of around 1 - 10 nanometers (100 angstroms) and is highly sensitive to the separation distance between fluorophores (Albrecht 2008). Because of its distance-dependent nature, FRET can be used to understand a variety of biophysical and biochemical phenomena, including protein folding, drug binding, DNA dynamics and nucleosome conformational changes . The relative changes between two moieties in a biomolecule can be monitored by utilizing a suitable donor-acceptor pair. Changes in the distance between two moieties in a biomolecule labeled with a FRET pair (one donor and one acceptor on each moiety) caused by intrinsic dynamics or conformational changes will result in the fluctuations in the FRET efficiency (E). These FRET efficiency fluctuations can be detected and used to estimate the distance change or rate of related conformational changes.

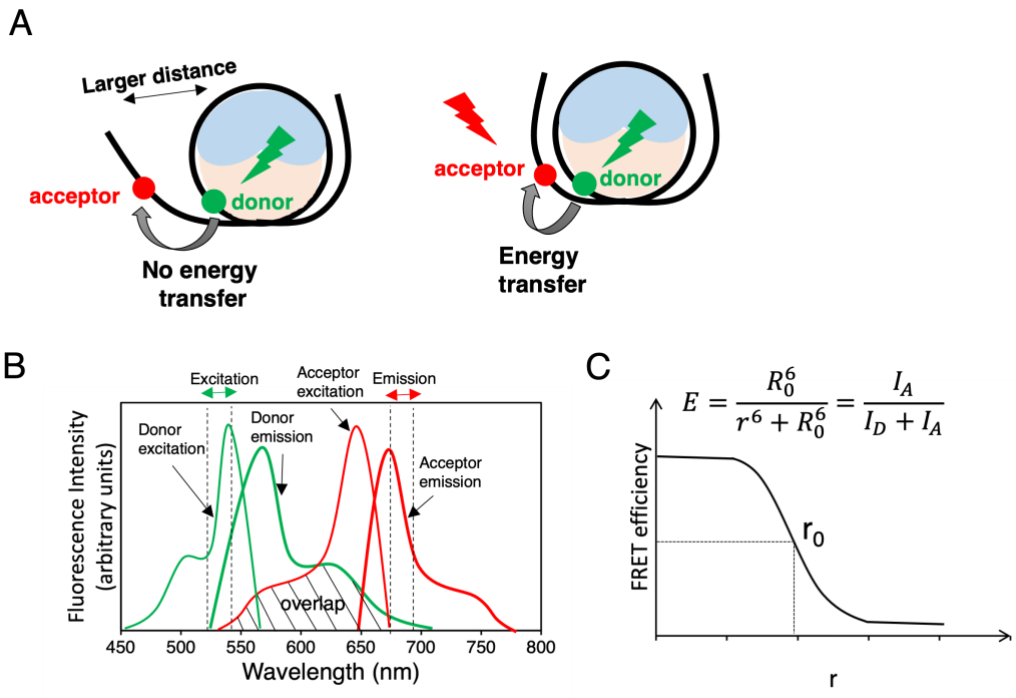

Figure **1-4**: Basic scheme illustrating the fundamentals of FRET.

(A) An example of a nucleosome with a labeled FRET pair on the DNA. The acceptor exhibits fluorescence signal as a result of energy transfer from the donor when both the donor and the acceptor are in close proximity. (B) FRET is generated by a spectral overlap between the emission spectrum of a donor dye (green line) and the absorption spectrum of an acceptor dye (red line). The spectral overlap is represented by shaded area. (C) FRET efficiency as a function of donor-acceptor distance. r_0 stands for the distance between a donor and an acceptor at which there is a 50% energy transfer.

1.6. Past literatures on single-molecule FRET studies of nucleosome structure and dynamics

Widom conducted the initial efforts to investigate the conformational variations of the nucleosomes using single-molecule fluorescence with fluorescence correlation spectroscopy (FCS) (Li et al. 2005). Shortly after, several studies using single-molecule FRET (smFRET) to examine nucleosome conformations and dynamics were published. M. Tomschik and his group

are among the first few groups that employed smFRET in their nucleosome research which eventually leads to their discovery that the nucleosomes adopt two distinct conformations: the closed conformation with tightly packaged DNA around the histone core and the open conformation with more loosened DNA around the histones (Tomschik et al. 2005, Tomschik, van Holde and Zlatanova 2009). After that, another two separate groups using a FRET pair on nucleosomal DNA successfully resolved three (sub)nucleosome populations: an intact nucleosome, a partially unwrapped nucleosome intermediate with slightly increased DNA accessibility, and another partially unwrapped intermediate with an even higher degree of DNA accessibility (Gansen et al. 2009, Ngo and Ha 2015). The spontaneous unwrapping of DNA tails, which might result in the removal of the H2A-H2B dimer, was noted as the rationale for the presence of these (sub)nucleosome populations. Moreover, Ngo et al. successfully detected that the nucleosomes slowly and spontaneously change their conformations over the course of several seconds, with varying degrees of unwrapping occurring at both DNA ends (Ngo and Ha 2015). In a separate work, Bohm et al. used a FRET pair with labeled DNA and either labeled histone $(H3\text{-}H4)_2$ tetramer or histone H2A-H2B dimer to examine how the nucleosomes spontaneously unfold (Böhm et al. 2011). According to this study, spontaneous DNA opening is required for the displacement of the histone H2A-H2B dimer, which confirmed earlier research on the (sub)nucleosome intermediates that partially unwrapped DNA may be induced by the loss of DNA-histone interactions. The nucleosomes are then proposed to go through a sequential disassembly and reassembly (Böhm et al. 2011). The H2A-H2B dimer dissociates before the $(H3\text{-}H4)_2$ tetramer does during the disassembly phase, and the order is reversed upon reassembly (Böhm et al. 2011).

smFRET has also been used to investigate the intrinsic features of nucleosome structure and dynamics under various environmental conditions. According to Gansen et al, the nucleosomes are destabilized at low nucleosome concentrations (around pM range) and high ionic

conditions (Gansen et al. 2009). By monitoring a FRET pair on nucleosomal DNA, they detected nucleosome fluctuations across varying monovalent salt concentrations with an increased population of partially unwrapped nucleosomes at higher salt concentrations (Gansen et al. 2009). The effects of high ionic conditions on nucleosome structure were further experimented in another paper by Ngo et al., where 50 mM to 1 M NaCl concentrations were used instead (Ngo and Ha 2015). They discovered that salt-induced nucleosome disassembly is reversible, thus proposing that histone H2A-H2B dimer(s) are still preserved in the nucleosome core (Ngo and Ha 2015). Lee et al. also employed three-color smFRET to study the histone eviction procedure with DNA labeled with a donor and an acceptor to form a first FRET pair for monitoring DNA motions, and the histone core tagged with a second acceptor to form a second FRET pair for tracking histone H2A-H2B dimer(s) location(s) in real-time. They found that the spontaneous unwrapping of the nucleosomal DNA mainly occurs prior to the displacement of H2A-H2B dimer without any histone chaperone (Lee and Lee 2017), thus confirming the nucleosome stability.

The implications of DNA modifications and histone PTMs (post-translational modifications) on nucleosome structure and dynamics have also been investigated using smFRET. For instance, a study examining the effects of DNA methylation on nucleosome dynamics was published by Lee et al. in 2015 (Lee et al. 2015). The authors utilized a three-color labeling scheme where DNA was labeled with a donor and an acceptor, and the histone core was labeled with a second acceptor to monitor both DNA and histone motions. They found that CpG methylation on DNA promotes DNA tightly rewrapping around the histone core, which results in stable tetrasome (DNA-$(H3\text{-}H4)_2$) formation while impairing the integration of the histone H2A-H2B dimer on the same CpG-methylated DNA [58]. The authors then proposed two potential mechanisms by which CpG methylation facilitates nucleosome assembly: either by a three step process where $(H3\text{-}H4)_2$ tetramer first deposits on the nucleosomal DNA, DNA then rewraps around the histone core, and lastly histone H2A-H2B dimer gets recruited to form a complete

nucleosome structure, or by the transfer of the complete histone octamer followed by DNA rewrapping (Lee et al. 2015).

Histone acetylation is an important histone PTM which has been known to be coupled with gene activation. The effects of histone acetylation on nucleosome dynamics were investigated by Neumann et al. in 2009 where the authors used a FRET pair on the DNA close to the nucleosome entry site to detect the structural alterations in the H3K56 acetylated nucleosomes (Neumann et al. 2009b). According to their findings, nucleosome breathing dynamics has increased seven-fold, which indicates that H3K56 acetylation enhances spontaneous DNA opening at DNA ends (Neumann et al. 2009b). This finding is consistent with the established role of H3K56 acetylation in enhancing gene expression. In another smFRET study on the functions of histone PTMs, H3K122 succinylation was selected due to its proposed ability to enhance transcription process and its prevalence in active genes. Shahidian et al. showed that H3K122 succinylated nucleosomes are considerably less stable than wild-type nucleosomes by monitoring a FRET pair on the nucleosomal DNA (Zorro Shahidian et al. 2021). They contrasted the acetylation and succinylation using both smFRET and biochemical experiments and concluded that nucleosome structure is indeed one of many variables that regulates transcription by destabilizing the intact nucleosome and making it more accessible to transcription factors (Zorro Shahidian et al. 2021).

In this subsection, I have covered a few studies that have been done using smFRET to directly study the structure and dynamics of the nucleosome that have been published to date. There are many more articles that have used smFRET to examine nucleosome alterations in association with other protein complexes including transcription factors (for example, FACT, Spt4/5, Rap1) (Crickard et al. 2017, Mivelaz et al. 2020, Safaric et al. 2022), chromatin remodelers (for example, Chd1, SWI/SNF, ISWI, INO80) (Blosser et al. 2009, Deindl et al. 2013, Sabantsev et al. 2019, Harada et al. 2016, Qiu et al. 2017, Gamarra et al. 2018, Zhou et al. 2018,

Johnson and Narlikar 2022), and epigenetic enzymes (for example, DOT1L) (Jang et al. 2019). All of these past studies have supported that smFRET is an effective tool for investigating the regulatory effects of various factors on the structure and dynamics of the nucleosome.

1.7. Scope of our research

The overall efficiency of transcription elongation depends on the DNA accessibility by the transcription machinery. As mentioned before, the nucleosome represents a barrier to Pol II and many transcription factors necessary for regulating gene expression (Bednar et al. 1999, Kireeva et al. 2005, Jin et al. 2010, Studitsky et al. 2016). Hence, the pause dynamics and its regulation have critical implications to the regulation of transcription elongation. The major factors controlling the regulation of the pause dynamics include histone tails, particular histone-DNA interactions, DNA sequence, and post-translational changes of histone proteins.

In my thesis, I focused on investigating the roles of various histone post-translational modifications (H3K56 acetylation, H2BK34 ubiquitylation, H2BK120 ubiquitylation, and H3K79 trimethylation) and histone chaperones (e.g., Nap1, FACT) on nucleosome stability and dynamics, especially in the process of transcription by Pol II. I utilized single-molecule FRET (smFRET) experiments with different labeling scheme combinations in order to gain more insights into changes in the nucleosome structure and dynamics brought about by these PTMs and histone chaperones.

Chapter 2

Nucleosome Dynamics during Transcription Elongation

This chapter is adapted with permission from (Huynh et al. 2020). Copyright 2020 American Chemical Society.

2.1. Abstract

The nucleosome is the basic packing unit of the eukaryotic genome. Dynamic interactions between DNA and histones in the nucleosome are the molecular basis of gene accessibility regulation that governs the kinetics of various DNA-templated processes such as transcription elongation by RNA Polymerase II (Pol II). Based on single-molecule FRET measurements with chemically modified histones, we investigated the nucleosome dynamics during transcription elongation and how it is affected by histone acetylation at H3 K56 and the histone chaperone Nap1, both of which can affect DNA-histone interactions. We observed that H3K56 acetylation dramatically shortens the pause duration of Pol II near the entry region of the nucleosome, while Nap1 induces no noticeable difference. We also found that the elongation rate of Pol II through the nucleosome is unaffected by the acetylation or Nap1. These results indicate that H3K56 acetylation facilitates Pol II translocation through the nucleosome by assisting paused Pol II to resume and that Nap1 does not affect Pol II progression. Following transcription, only a small fraction of nucleosomes remain intact, which is unaffected by H3K56 acetylation or Nap1. These results suggest that (i) spontaneous nucleosome opening enables Pol II progression, (ii) Pol

II mediates nucleosome reassembly very inefficiently, and (iii) Nap1 in the absence of other factors does not promote nucleosome disassembly or reassembly during transcription.

2.2. Introduction

The nucleosome is the most basic eukaryotic DNA packaging unit (Kornberg 1974, Kornberg 1977). A nucleosome core particle contains ~147 base pairs (bp) of DNA wrapped around a histone octamer core consisted of two H2A-H2B dimers and one $(H3\text{-}H4)_2$ tetramer (Luger et al. 1997a, Luger et al. 1997b, Davey et al. 2002). Many studies have explored the structural dynamics and the function of the nucleosome as a platform for gene regulation (Luger 2003, Akey and Luger 2003, Lorch, Maier-Davis and Kornberg 2006, Park and Luger 2006, De Koning et al. 2007, Park and Luger 2008). It has been established that nucleosomes impose physical barriers on enzymes translocating along nucleosomal DNA such as RNA Polymerase II (Pol II) (Morse 1989, Izban and Luse 1992, Chang and Luse 1997, Bednar et al. 1999, Kireeva et al. 2002, Kulaeva et al. 2009). Nucleosomes induce major pauses of Pol II at two regions – around the 15^{th} and the 45^{th} nucleotides from the nucleosome entry (Crickard et al. 2017, Kujirai et al. 2018). Recently published cryo-EM structures of Pol II-nucleosome complexes also confirm the two major pause locations (Kujirai et al. 2018). The pause around the 15^{th} nucleotide (nt) is at the super-helical location -5 from the dyad or SHL(-5) and the other at SHL(-1). The structures also revealed weaker pauses at SHL(-6) and SHL(-2). The pause dynamics of Pol II have critical implications in the kinetics of transcription elongation as the pause duration is the main determinant of the overall efficiency and rate of transcription elongation through the nucleosome (Hodges et al. 2009, Kwak and Lis 2013, Jonkers, Kwak and Lis 2014). Dynamic histone-DNA interactions are one of the major players in regulating the pause dynamics of Pol II.

The lysine residue K56 of histone H3 (H3K56) is at the entry and exit regions of the nucleosome and provides a positive charge for the histone core to interact with DNA (Ozdemir et al. 2005). Acetylation of this lysine residue facilitates spontaneous DNA dynamics that should increase DNA accessibility (Ozdemir et al. 2005, Neumann et al. 2009a, North et al. 2012, Kim, Lee and Lee 2015, Kim et al. 2016, Lee and Lee 2017, Bilokapic, Strauss and Halic 2018, Lee and Lee 2019). The number of nucleosomes with its DNA unwrapped at the entry region increases by two folds when acetylated at H3K56 (Kim et al. 2015). While this large extent of spontaneous DNA unwrapping has not been observed under other experimental conditions, data demonstrating transient unwrapping in the range of a few angstroms has been published based on single-molecule FRET and cryo-EM measurements (Kujirai et al. 2018, Bilokapic et al. 2018). However, this extent of unwrapping is not large enough to directly affect Pol II binding or progression. Decreased pause densities and durations in early regions of the nucleosome including the entry region were reported when all histone lysine residues were mutated to glutamine (Hodges et al. 2009, Bintu et al. 2012). However, the effect cannot be attributed solely to acetylation as glutamine mutation is limited in modeling acetylation (Allahverdi et al. 2010) and such extensive glutamine mutation may result in an altered nucleosome structure. Due to the lack of direct investigations based on a highly refined and pure experimental system, the consequences of H3K56 acetylation on the kinetics of Pol II progression through the nucleosome remain largely unknown.

We have reported that spontaneous DNA opening motion at the nucleosome termini is facilitated upon H3K56 acetylation while the overall structural integrity of the nucleosome is unaffected (Kim et al. 2015). The spontaneous DNA opening rate at 50 mM NaCl is 1.9-fold higher in H3K56 acetylated nucleosomes compared to non-acetylated ones while the closing rate is kept constant. This change results in a 1.5-fold longer dwell time in the open state upon acetylation (Kim et al. 2015), and can be interpreted as a 1.5-fold increase in the probability of

finding a nucleosome in an open state at any random moment. However, the rate of the histone chaperone Nap1 binding escalates by 5.9 folds (Lee and Lee 2019) that is far larger than 1.5 folds. The greater increase in the Nap1 binding rate is because H3K56 acetylation (H3K56ac) not only increases the opening rate, but also makes the average opening slightly larger and that Nap1 binding requires a much larger opening than the average opening. According to our rationale, the probability of DNA opening large enough for Nap1 binding dramatically increases upon H3K56 acetylation while that of opening by any distance becomes merely 1.5-fold higher. This principle can also be applied to other processes that require spontaneous DNA opening. For instance, a paused Pol II in the nucleosome would need opening of the histone-DNA interface to resume. A large effect of H3K56ac would be expected if a paused Pol II requires a large opening to resume, which it does.

Transcription factors and histone chaperones can also influence nucleosome dynamics by promoting or disrupting DNA-histone and histone-histone interactions (Akey and Luger 2003, Park and Luger 2006, Lorch et al. 2006, De Koning et al. 2007, Park and Luger 2008). The well-studied Nap1 belongs to a class of histone chaperones that can interact with positively charged histone proteins via its acidic patch, thus plays roles in histone transport, nucleosome assembly and disassembly (Ito et al. 1996, McQuibban, Commisso-Cappelli and Lewis 1998, Mosammaparast, Ewart and Pemberton 2002, McBryant et al. 2003, Park et al. 2005, Andrews et al. 2008, Andrews et al. 2010, Vlijm et al. 2012, Aguilar-Gurrieri et al. 2016). Nap1 facilitates the thermodynamic equilibrium of a DNA-histone mixture, mediating nucleosome assembly or eliminating DNA-histone interactions that do not lead to nucleosome formation (Andrews et al. 2008, Andrews et al. 2010). Despite its nanomolar affinity to histone H2A-H2B, Nap1 cannot bind H2A-H2B in canonical nucleosomes because its binding regions on the dimer are shielded by DNA (Andrews et al. 2010). Only when DNA-histone interaction is weakened, Nap1 can interact with histones in the nucleosome. As such, Nap1 can mediate both nucleosome assembly

and disassembly, although it remains unclear how on a molecular level Nap1 can mediate DNA-histone dynamics during transcription elongation by Pol II.

Here, we investigated the effects of H3K56ac and Nap1 on the dynamics of transcription elongation through the nucleosome. We employed single-molecule FRET experimental systems (Lee et al. 2019a) with chemically modified H3K56ac nucleosomes in order to monitor the nucleosome dynamics during transcription elongation by Pol II in real time in a time-resolved manner. Our results indicate that H3K56ac shortens the pause duration of Pol II at the nucleosome entry region by 4.0 folds and that H3K56ac has no effect on the next pause duration or elongation rates. Surprisingly, Nap1 has no effect on the Pol II progression kinetics. We did not observe any effect of H3K56ac or Nap1 on the already low efficiency of nucleosome reassembly upon Pol II passage. Our results strongly support that a large spontaneous opening of the nucleosome enables a paused Pol II to resume and that H3K56ac greatly facilitates this process. This effect would be very much pronounced on the overall rate of nucleosomal transcription as the pause durations are on the order a few to a few hundreds of seconds.

2.3. Materials and Methods

2.3.1. Nap1 and Nucleosome reconstitution

6xHis-Yeast nucleosome assembly protein 1 (Nap1) was expressed in *E. coli* and purified with Ni-NTA beads (Thermo Fisher Scientific, Waltham, MA) as reported in a previous publication (Tóth, Mazurkiewicz and Rippe 2005). Histone proteins were purchased from Histone Source at the Colorado State University. Histone H3 with K56 acetylation was prepared following published protocols (Li et al. 2011) (detailed protocol in Appendix A) and confirmed

by mass-spectrometric analysis (Fig. 2-1). The resulting histone H3 has a thioether linked sidechain of acetylated lysine at the residue C56, often denoted by $H3K_C56ac$. We will denote this acetylation by H3K56ac for simplicity.

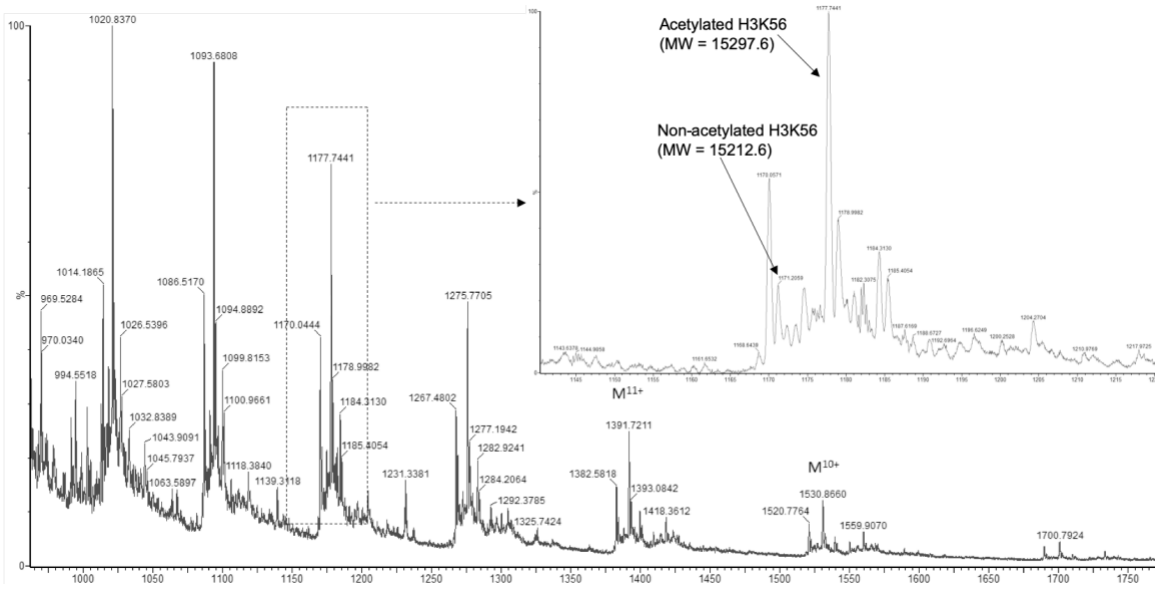

Figure **2-1**: Mass-spectrometric analysis of H3K56 acetylation.

Mass-spectrometric analysis confirms H3K56 acetylation (Mw = 15297.6, expected Mw = 15298). The areas under the peaks suggest that 90% of H3K56 were sucessfully acetylated although this is a rough estimation due to the complex fragmentation pattern.

Histone H2B T112C was unfolded and labeled with maleimide functionalized Cy5.5 in a labeling buffer containing 7M Guanidinium HCl and 20 mM Tris-HCl (pH 7.5). The resulting solution was incubated for 2 hours at room temperature and subsequently overnight at 4°C. Excess dye was removed with disposable PD-10 desalting columns (GE Healthcare). The labeling efficiency was 100% within the error of a UV-Vis spectroscopic measurement.

Five DNA fragments (see Table. 2-1 for sequences) were purchased from Integrated DNA Technologies (Coralville IA). The fragments were annealed and ligated to form the 601-DNA sequence (Lowary and Widom 1998). The EC-42 strands with a 13 nt extension to a G-less cassette were ligated to the nucleosome entry site. The amine functionalized C6 linkers coupled to the thymine nucleotides at the +34 and +112 positions from the entry site of the nucleosome, were labeled with NHS-ester functionalized Cy5 and Cy3, respectively.

Table **2-1**: Seven DNA fragments used to form the extended Widom 601 nucleosome positioning sequence in our measurements.

DNA fragment	Sequence (5' – 3')
F1	/5Phos/GCAG ATCGAGAATC CCGGTGCCGA GGCCGCTCAA
F2	/5Phos/ TTGG /iAmMC6T/CGTAGACAG CTCTAGCACC GCTTAAACGC ACGTACGCGC TGTCCCCCGC GTTTTAACCG CCAAGGGGAT TAC
F3	/5Phos/ TCC C/iAmMC6T/AGTCTCCA GGCACGTGTC AGATATATAC ATCCGAT
R1	ATCGGATGTA TATATCTGAC ACGTGCCTGG AGACTAGGGA GTAATCCCCT TGGCGGTTAA AACGCGGGG
R2	/5Phos/G ACAGCGCGTA CGTGCGTTTA AGCGGTGCTA GAGCTGTCTA CGACCAATTG AGCGGCCTCG GCACCGGGAT TCTCGAT
EC42 Template	/5Phos/CTGCGCCACCGCGGTCTAGAGGATCCCCGGGAGTGGAATGAGAAATGAGTGTGA AGATAGAGGAGAGATCAAAAAAATTA
EC42 Non-Template	CTCCTCTATCTTCACACTCATTTCTCATTCCACTCCCGGGGATCCTCTAGACCGCGGTGGC

Histone proteins were mixed in stoichiometric amounts and eluted through a gel filtration column to produce H2A-H2B dimers and $(H3\text{-}H4)_2$ tetramers separately (Luger, Rechsteiner and Richmond 1999a, Luger, Rechsteiner and Richmond 1999b). Nucleosomes were reconstituted by dialyzing a stoichiometric mixture of histones and DNA in a dialysis device (Slide-A-Lyzer MINI Dialysis Device, 7K MWCO, Thermo Fisher Scientific) against 1X TE (pH 8.0) buffer and decreasing salt concentrations of 850, 650, 500, 300, and 2.5 mM NaCl stepwise (Luger et al.

1999a, Luger et al. 1999b). The assembled transcription templates containing the nucleosome were confirmed by native PAGE (Fig. 2-2).

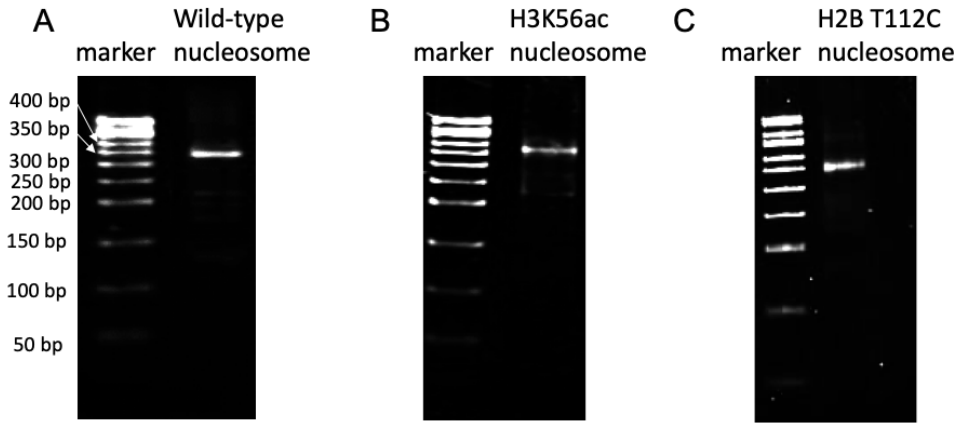

Figure **2-2**: Native PAGE analyses to confirm nucleosome reconsitution for wild-type nucleosome (A), H3K56ac nucleosome (B), and H2B T112C nucleosome (C).

2.3.2. Formation of transcription elongation complex

Transcription was performed in a buffer containing 60mM KCl, 1 mM $MnCl_2$, 50 mM K-HEPES (pH 7.8), 0.5mM DTT, and 10% glycerol. The transcription templates were added to 50 μL of transcription buffer to 10 nM along with 9.5 nM Pol II, 0.3mM UpG primer, 0.1 mg/mL BSA, and 2 units/μL RNasin RNase inhibitor to make a total volume of 91.5 μL. Pol II was prepared following published protocols (Crickard et al. 2017, Lee et al. 2019a). The mixture was incubated for 5 min at 30 °C, followed by the addition of ATP, CTP, and UTP to 1 mM to initiate transcription. The transcription elongation complexes were stopped and synchronyzed at a G-tract located at the 13^{th} nucleotide position into EC-42. The reaction mixture was diluted to 150 μL and incubated for 30 min at 30 °C.

2.3.3. Single-molecule FRET measurements

Microscope slides for Pol II immobilization and single-molecule FRET measurements were prepared as previously published (Lee et al. 2019a).

Microscope surface preparation

Microscope slides were purchased from G. Finkenbeiner Inc. (Waltham, MA). The slides were cleaned and coated with 1:5 biotin-PEG-silane and PEG-silane (Laysan Bio Inc., Arab AL). The sample channels were incubated with 0.1 mg/ml streptavidin, 0.1 mg/ml biotinylated protein A for 15 minutes each, and finally 300 nM 8WG16 ascites fluid antibody (Abnova, Taiwan) for 2 hours at room temperature, with each step followed by a washing step with a buffer containing 10 mM NaCl and 10 mM K-HEPES (pH 7.8). The transcription reaction mixture was injected into a channel and incubated for 5 min at room temperature. The imaging buffer (a complete set of NTP at 0.1 mM, 30 nM TFIIS, 0.4 unit/ml PCD, 4 mM PCA, and 1 mM Trolox in the transcription buffer) was used to wash unbound nucleosomes and resume transcription.

Nucleosome dynamics during transcription elongation by Pol II with and without Nap1

After adding the imaging buffer, Cy3 was excited with a 532 nm laser and fluorescence signals from both Cy3 and Cy5 were recorded with an electron multiplying CCD (EMCCD) camera. Recording started at around 100 sec after injecting the imaging buffer. Recording started at around 300 sec in the presence of Nap1. Nap1 (600 nM) was added to the imaging buffer. FRET data was collected for 30 min at a 250 ms time resolution. A total of 15 2-minute movies from different slide spots were recorded. The time window of measurements was limited to 30 minutes in order to avoid any spontaneous disassembly or decay of the nucleosomes. A total of 39 independent measurements were carried out on a total of 6 separate days.

Nucleosome states after transcription by Pol II

After adding the imaging buffer, 2 fluorescence images with 250 ms signal integration (= 2 x 250 ms) every 7.5 sec were taken with 532 nm excitation followed by 2 images taken with 635 nm excitation. In order to ensure full frame excitation during imaging, we used 750 ms excitation instead of 500 ms. This excitation and imaging scheme was employed to avoid premature photobleaching of Cy5.5 so that we can observe H2A-H2B-Cy5.5 displacement without complete dissociation from the elongation complex. Each movie was taken for 3 minutes during which Cy5.5 was excited for a total of 18 seconds. According to the typical photobleaching lifetime of Cy5.5 (42 sec) with 635 nm excitation under our conditions, the majority of Cy5.5 is not photobleached during imaging. Ten 3-minute movies from different slide spots were recorded and analyzed. A total of 38 independent measurements were carried out on a total of 6 separate days.

Single-molecule FRET data analysis

The time trajectories of fluorescence intensities from individual nucleosomes during transcription were collected and analyzed. The background intensities of fluorophores after photobleaching were used for background correction. Pause durations in each state and elongation times were estimated from the intensity trajectories of Cy3 and Cy5. Solely based on visual inspection, the durations of stable FRET states and the elongation times between two stable FRET states were measured. Histograms of the state durations and elongation times were generated and fit with a single exponential decay function. Pause durations and kinetic rate constants of transcription elongation were extracted from the fitting.

2.4. Results

2.4.1. A single-molecule FRET system reports nucleosome dynamics during transcription elongation by Pol II

We employed an *in vitro* transcription system based on single-molecule FRET (smFRET) to study the nucleosome dynamics during transcription elongation by Pol II as illustrated in figure 2-3 A. In the setup (Fig. 2-3 A), the nucleosomes are immobilized via Pol II and therefore always bound with Pol II during our observation. The changes in the fluorescence intensities of a FRET pair Cy3 and Cy5 enable us to quantify the extent of DNA unwrapping and potential rewrapping during the progression of Pol II through the nucleosome. In the absence of Pol II, the nucleosome does not show FRET dynamics within our observation time window of 30 min. We designed the FRET locations according to the published Pol II pause positions (Crickard et al. 2017, Kujirai et al. 2018) so that we can monitor the early dynamics of the nucleosome when Pol II translocases from the entry site through the region where a histone H2A-H2B dimer interacts strongly with DNA. Dynamic changes in the intensities of the FRET pair are evident (Fig. 2-3 C). The initial decrease in the FRET efficiency (~10 sec time point in Fig. 2-3 C) indicates that the DNA terminus is unwrapping. After initial DNA unwrapping, some Pol II stall, some proceed until the DNA is completely unwrapped, and some show signs of DNA rewrapping after polymerase passes. When Pol II stalls, the extent of DNA unwrapping also stalls, resulting in a stable FRET state whose lifetime is on the order of a few to few hundreds of seconds. Three stable FRET states were identified according to their FRET efficiencies – high-FRET (HF), mid-FRET (MF), and low-FRET (LF). The FRET efficiency distributions are shown in figure 2-3 D that verifies the three stable FRET states. A pause is a stochastic event with a low probability. As such, it is

rare to find a nucleosome that shows all three pauses. This is further exacerbated by pause durations longer than the photobleaching lifetimes of the fluorophores, making it impossible to tell whether a stable FRET event is due to a paused or an arrested state. Nevertheless, the pause locations overlap with experimentally-determined arrest points, and therefore, we can assign the three FRET states to the pause locations reported by a cryo-EM study (Kujirai et al. 2018). We assigned the HF state to the combination of pauses at SHL(-6) and (-5), MF to SHL(-2), and LF to SHL(-1). We assigned the highest FRET state (= HF state) to the paused state at SHL(-6) or (-5) as there is no change in the FRET distance between the intact nucleosome and the nucleosome with paused Pol II at SHL(-6) or at SHL(-5) (Fig. 2-4). The estimated FRET efficiency from the Cyro-EM structure of the SHL(-2) paused state (= 0.4) is in good agreement with the MF state FRET efficiency (= $0.37 \pm 0.00_2$). As the only remaining and major pause is at SHL(-1) and the estimated (<0.1, Fig. 2-4) and measured FRET efficiencies (= $0.07 \pm 0.00_2$) are in good agreement, we assigned the LF state to the SHL(-1) paused state. Previous biochemical studies also support these FRET assignments (Crickard et al. 2017, Kujirai et al. 2018).

A

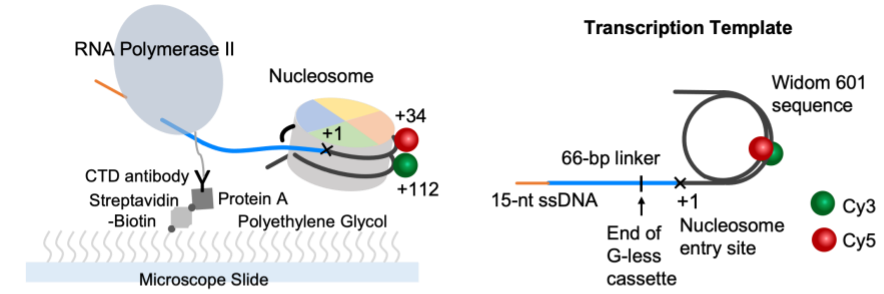

B

5'CTCCTCTATCTTCACACTCATTTCTCATTCCACTCCCGGGGATCCTCTAGACCGCGGTGGCGCAGATCGAGAATCC
CGGTGCCGAGGCCGCTCAATTGGT★CGTAGACAGCTCTAGCACCGCTTAAACGCACGTACGCGCTGTCCCCCGCGT
TTTAACCGCCAAGGGGATTACTCCCT★AGTCTCCA GGCACGTGTCAGATATATACATCCGAT 3'

3'ATTAAAAAAAACTAGAGAGGAGATAGAAGTGTGAGTAAAGAGTAAGGTGAGGGCCCCTAGGAGATCTGGCGCCACCG
CGTCTAGCTCTTAGGGCCACGGCTCCGGCGAGTTAACCAGCATCTGTCGAGATCGTGGCGAATTTGCGTGCATGCG
CGACAGGGGGCGCAAAATTGGCGGTTCCCCTAATGAGGGATCAGAGGTCCGTGCACAGTCTATATATGTAGGCTA 5'

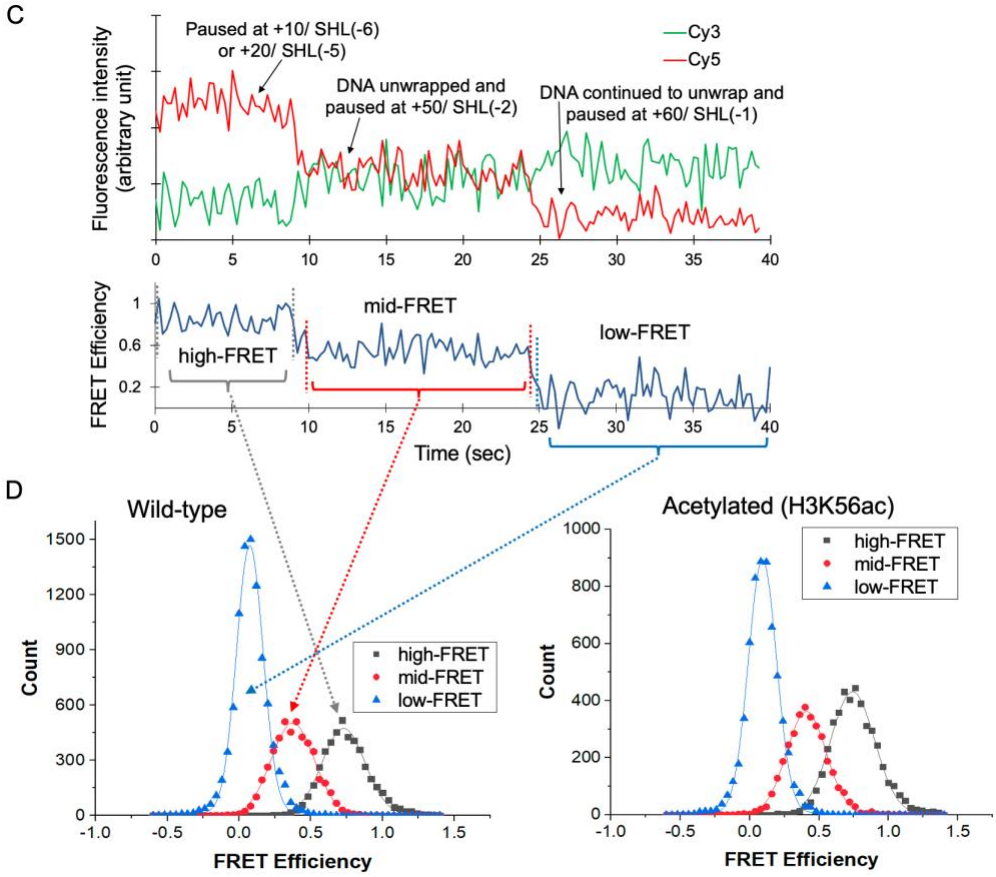

Figure **2-3**: A single-molecule FRET experimental system reports the dynamics of DNA unwrapping and rewrapping during transcription elongation by Pol II.

(A) Nucleosomes with a FRET pair were immobilized on a surface-passivated microscope slide via a series of conjugations shown, which is biotinylated poly(ethylene glycol) – streptavidin – biotinylated protein A – antibody of Pol II (C-terminal domain of the Rpb1 subunit) – Pol II/nucleosome (elongation complex). Since the nucleosomes are immobilized via Pol II, they are always bound with Pol II during our observation. Transcription-initated elongation complexes were formed by mixing Pol II, transcription template, ATP, CTP, and UTP. The complexes have Pol II stalled at the end of a G-less cassette. Nucleosomal DNA was labeled with a FRET pair, Cy3 and Cy5, at the +112th and +34th nucleotides from the entry site, respectively. Dynamic changes in the FRET pair intensities represent the DNA dynamics in the nucleosome. (B) DNA sequence of the transcription template including the Widom 601 sequence. The lower strand is the template strand. Each strand of the 601 sequence is linked to a 66-nucleotide DNA fragment (highlighted in blue) that contains a G-less cassette. The template strand had a 13-nucleotide extension to the 3' end (highlighted in orange). (C) Sample time trajectories of Cy3 and Cy5 fluorescence intensities and their FRET efficiency reveal mainly three stable FRET states, indicating three or more paused states of Pol II. The pause locations +10, +20, +50, and +60 are

counted from the nucleosome entry site (see panel A). The FRET time trajectories were manually cut into pieces such that each piece include only a single stable FRET state (see the vertical dotted lines in the FRET trajectory). These single FRET state events were grouped into three according to their FRET efficiency – high-, mid-, and low-FRET states. Each group was used to construct the corresponding FRET efficiency histogram shown in D. (D) Distributions of FRET efficiencies for the three states (HF, MF, and LF) from the wild-type and H3K56ac nucleosomes. Based on Gaussian fittings, HF ($0.73 \pm 0.00_2$), MF ($0.37 \pm 0.00_2$), LF ($0.07 \pm 0.00_2$) for wild-type nucleosomes, and HF ($0.74 \pm 0.00_3$), MF ($0.41 \pm 0.00_2$), LF ($0.09 \pm 0.00_2$) for H3K56ac nucleosomes were reported at 95% confidence interval. A subscript in the errors indicates that the number is not a significant figure.

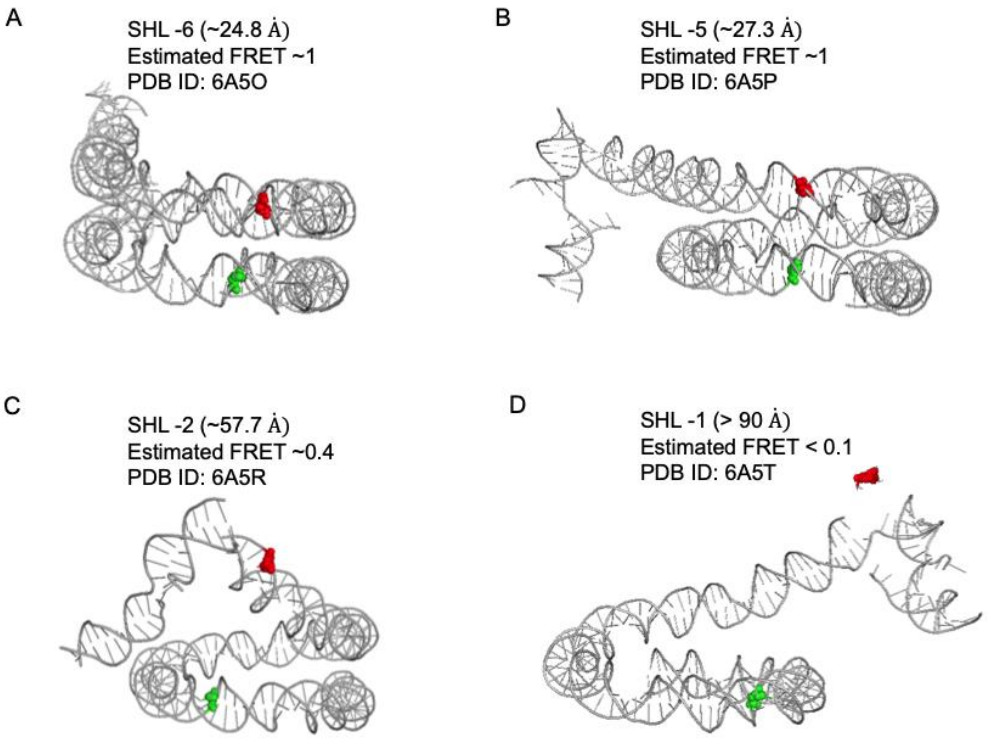

Figure **2-4**: FRET distance estimation from cryo-EM structures .

The distance between two fluorophores was estimated by measuring the distance between the two carbon atoms of the methyl groups attached to 5'C of Thymine bases at +34 and +112 locations. A value of 5.4 nm was used for the Forster radius of Cy3-Cy5 (Lee, Lee and Hohng 2010).

2.4.2. H3K56ac shortens the pause duration in the nucleosome entry region

We investigated whether H3K56 acetylation (H3K56ac) affects the pause dynamics in the nucleosome entry region (i.e. at SHL(-6) or (-5)) by examining the dwell time of the HF state with and without H3K56ac. The HF state dwell time distribution fits well to a single exponential decay function (Fig. 2-5). From the fitting results, we found that H3K56ac nucleosomes show a Pol II pause duration of 276 ± 37 sec that is a 4.0-fold decrease from the pause duration of 1104 ± 211 sec in the wild-type nucleosomes (Fig. 2-5 AB). One source of the fitting error in the acetylated case is the 10 % non-acetylated nucleosomes (Fig. 2-1). Regardless, the total error is much smaller than the difference induced by acetylation. These results, combined with our studies on the unwrapping of DNA from the end of H3K56ac nucleosomes, support our hypothesis that H3K56ac nucleosomes accelerate transcription through the entry by slightly increasing the average DNA opening size. This effect can result in a dramatic increase in the probability of rare openings (Lee and Lee 2019) that are large enough for Pol II passage, and subsequently, a significant increase in the success rate of escape attempts by Pol II. More detailed explanations about this mechanism are given in the discussion.

It is reasonable to postulate that H3K56ac would not affect the pause dynamics after Pol II passes through the entry region because H3K56 interacts with DNA only in the entry region. We analyzed the durations of the next pause at SHL(-2) which is represented by the MF state (Fig. 2-4). The total numbers of nucleosomes that we analyzed are 641 and 862 for the wild-type and H3K56ac nucleosomes, respectively. We selected nucleosomes showing all three FRET states (HF, MF, and LF states) starting from the HF state to evaluate the dwell time of the MF state. Some FRET trajectories start in the MF state because not all Pol II pauses in the HF state. We discarded the trajectories starting in the MF state because we could not pinpoint the onset of the MF state (46 % and 36 % of the total number of the nucleosomes monitored for wild-type and

acetylated nucleosomes). These nucleosomes represent likely the ones with no pauses in the entry region and filtering out these will not affect the analysis of pause dynamics. In many cases, the HF state skips the MF pause to go directly to the LF state, which we also excluded from the analysis (45% and 56% for wild-type and acetylated nucleosomes). Finally, we also discarded the data that showed arrested nucleosomes as they would remain in a stable FRET state until the fluorophores photobleached (5% and 2% for wild-type and acetylated nucleosomes). When we analyzed the data, no notable difference was found in the pause durations at SHL(-2) between the wild-type and H3K56ac nucleosomes (Fig. 2-5 CD). The pause durations in both cases are very short at around 5 sec, which is consistent with the weak swift pauses reported at SHL(-2) (Kujirai et al. 2018).

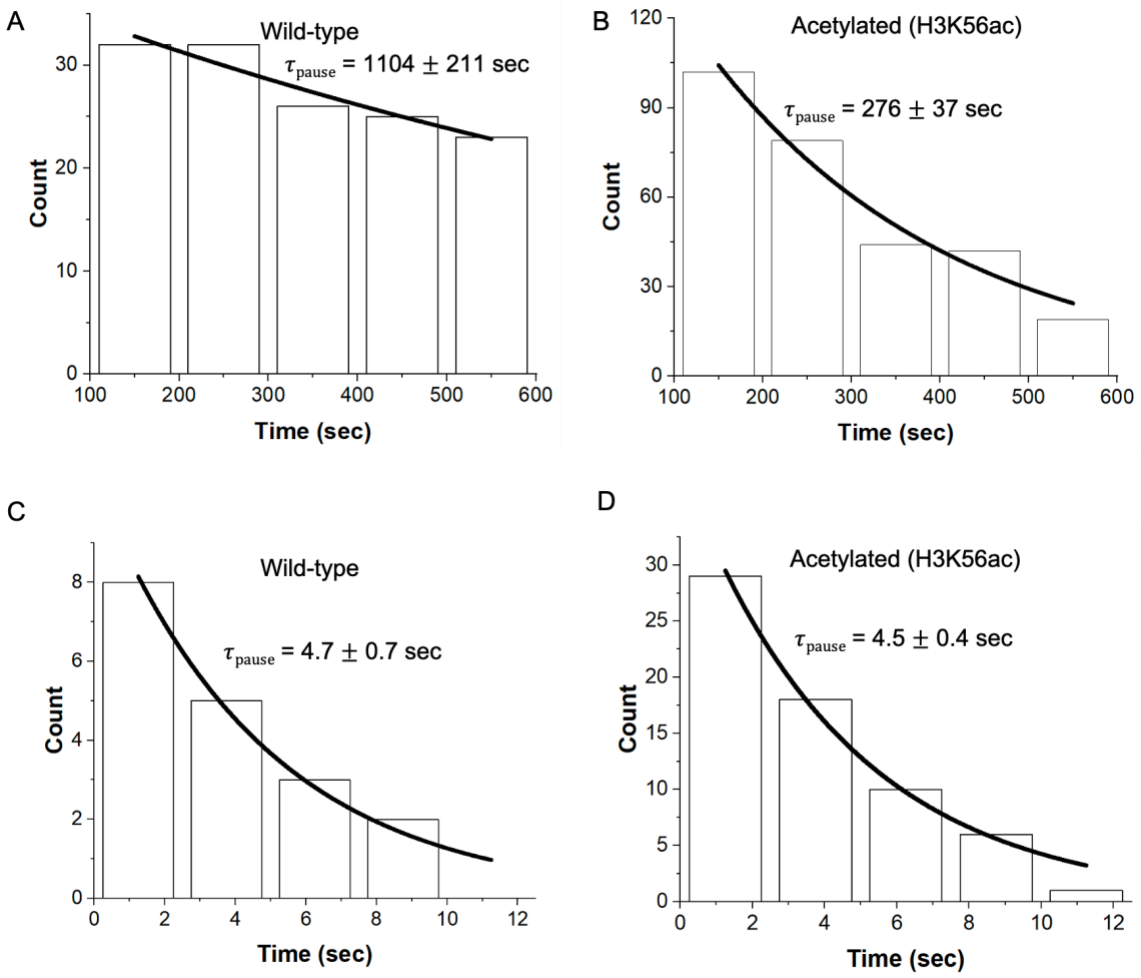

Figure **2-5**: Acetylation at H3K56 shortens Pol II pause duration only in the entry region.

Pause durations of Pol II in the nucleosome entry region for wild-type nucleosomes (A) and H3K56ac nucleosomes (B), and at the pause location SHL(-2) for wild-type nucleosomes (C) and H3K56ac nucleosomes (D). The pause duration in the nucleosome entry region is reduced by 4.0 folds upon H3K56 acetylation (A and B) while the pause duration at SHL(-2) is not affected (C and D). The first columns of (A) and (B) start from 100 sec which is the measurement start time. The errors indicate fitting errors.

2.4.3. H3K56ac has no effect on elongation rate

To investigate whether H3K56ac alters the transcription elongation rate in the nucleosome, we measured the transition times between two major pauses, SHL(-6) or (-5) (HF) to SHL(-1) (LF). Nucleosomes showing a single step transition from the HF to the LF state were filtered out because we cannot distinguish fast elongation from fluorophore photobleaching. The transition time distribution represents the elongation time distribution and follows a single exponential decay function (Fig. 2-6). We removed the events that are too fast to be precisely measured (0-1 sec columns in figure 2-6). The elongation rates in both wild-type and H3K56ac nucleosomes are the same within error (0.96 ± 0.04 and 0.89 ± 0.04 sec, respectively), indicating that H3K56ac has no effect on the elongation rate (Fig. 2-6). As the HF state is a pause at SHL(-6) or (-5), we can estimate the elongation rate in each case. The elongation rate through the wild-type nucleosome is 52 ± 3 and 42 ± 2 nt/s when we assume that the HF state is a pause at SHL(-6) and (-5), respectively. As SHL(-5) is the dominant pause location between the two, we conclude that the elongation rate is most likely 42 ± 2 nt/s. The rate through the H3K56 acetylated nucleosome is 45 ± 2 nt/s. In other words, wild-type nucleosomes take 24 ± 1 ms to transcribe one nucleotide while H3K56ac nucleosomes need 22 ± 1 ms. These values are consistent with previously published results (Bintu et al. 2012, Chen et al. 2019) and essentially the same within error, indicating that H3K56ac does not alter the transcription elongation rate through the nucleosome.

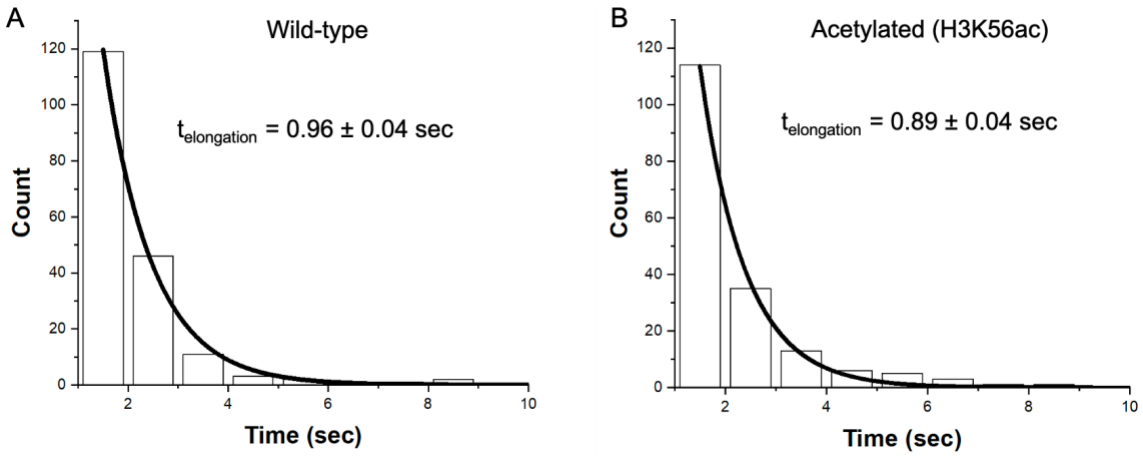

Figure **2-6**: Transcription elongation rate through the nucleosome is unaffected by H3K56ac.

Elongation times of Pol II from the nucleosome entry region to the final pause SHL(-1) for wild-type nucleosomes (A) and H3K56ac nucleosomes (B). H3K56ac did not induce any difference in the elongation rate. The first columns of the histograms start at 1 sec because we discarded single-step elongation events that belong to the histogram column 0 – 1 sec. The errors indicate fitting errors.

2.4.4. DNA rewrapping events are rare in both wild-type and acetylated nucleosomes

Next, we examined whether nucleosomal DNA rewraps as Pol II passes through the pause locations. Based on the nature of the nucleosome structure, we postulated that nucleosomal DNA would not rewrap spontaneously in the absence of other factors such as histone chaperone (Belotserkovskaya et al. 2003a, Kulaeva, Hsieh and Studitsky 2010, Hsieh et al. 2013, Kulaeva and Studitsky 2010, Kulaeva et al. 2013). Pol II has also been suggested to function as histone chaperone (Kulaeva et al. 2009, Chang et al. 2014). DNA rewrapping after Pol II passage can be identified by an increasing FRET transition from the LF or MF state to the MF or HF state. We counted these nucleosomes with and without H3K56ac. Our data indicates that rewrapping events occurred in 3.6 $\pm$ 1.9 % (23 out of 641, the error is the standard error of binomial distributions) of

the wild-type nucleosomes and 4.4 ± 2.0 % (38 out of 862) of the H3K56ac nucleosomes. These values are identical within error, indicating no effect of H3K56ac on the efficiency of nucleosome reassembly that is already low in the wild-type nucleosome. These values also confirm that spontaneous nucleosome reassembly during Pol II translocation in real-time is very inefficient although this conclusion does not rule out that nucleosomes may reassemble by the aid of another factor (e.g. histone chaperone) after Pol II runs off completely.

2.4.5. Nap1 has no effect on the nucleosome dynamics during transcription elongation by Pol II

We investigated the roles of the histone chaperone Nap1 in regulating the nucleosome dynamics during Pol II transcription. Nap1 competes against DNA for histone binding. Therefore, unlike H3K56ac that facilitates spontaneous nucleosome dynamics, Nap1 may play a direct enzymatic role in regulating DNA-histone interactions during transcription. First, we explored whether Nap1 affects the pause dynamics in the nucleosome entry region (Fig. 2-7 A). The result indicates that the entry pause duration in the presence of Nap1 is 1277 ± 381 sec which is the same within error as the pause duration in the absence of Nap1, 1104 ± 211 sec (Fig. 2-5 A). We also analyzed the transcription elongation rate in the presence of Nap1 (Fig. 2-7 B). By measuring the transition times between two major pauses (HF to LF), we found that the elongation rate is 1.18 ± 0.19 sec which is the same within error as the rate in the absence of Nap1 (Fig. 2-6 A). Thus, the results indicate that Nap1 has no effect on either the pause dynamics or the transcription elongation rate.

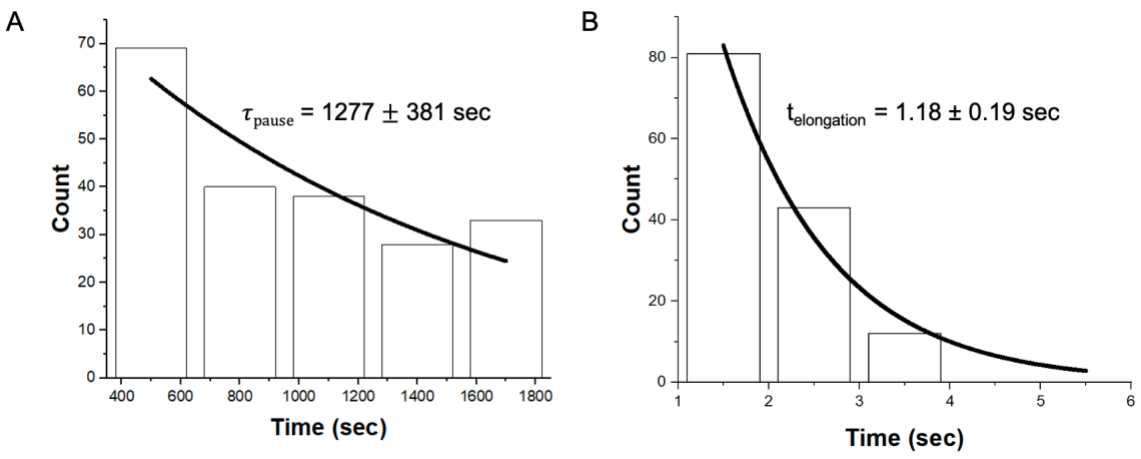

Figure **2-7**: Transcription elongation kinetics through the nucleosome is unaffected by Nap1.

Distributions of the pause durations of Pol II in the nucleosome entry region (A) and of the elongation rates (B) in the presence of 600 nM Nap1. The first columns start at non-zero values because the measurement in (A) started at 300 sec and the single time-point transitions in (B) were discarded. The errors indicate fitting errors.

Next, we examined whether Nap1 facilitates nucleosome reassembly during Pol II progression. We counted the nucleosomes with DNA rewrapping, which can be identified by an increasing FRET transition from the LF or MF state to the MF or HF state. Our data shows that rewrapping events occurred in 2.3 ± 1.5 % (6 out of 260) of the nucleosomes in the presence of Nap1. This result indicates that Nap1 does not promote nucleosome reassembly during Pol II progression in real time although this conclusion does not rule out a possibility that Nap1 can mediate nucleosome reassembly after Pol II runs off completely.

2.4.6. Three-color smFRET confirms inefficient nucleosome reassembly during transcription

We looked further into the recovery of the nucleosome during transcription by Pol II in real time with three-color smFRET. Nucleosome recovery has been suggested to proceed through two mechanisms: one involves dissociation and reassociation of one H2A-H2B dimer while the other involves displacement of the entire histone octamer (Kulaeva et al. 2009, Hsieh et al. 2013, Kulaeva et al. 2010, Kulaeva and Studitsky 2010, Kulaeva et al. 2013, Belotserkovskaya et al. 2003a). As the 601 sequence is an extremely strong nucleosome positioning sequence (Lowary and Widom 1998), the first mechanism is more likely applicable. We employed a three-color smFRET system to monitor the DNA dynamics and histone H2A-H2B dynamics simultaneously (Fig. 2-8 A). The nucleosomal DNA was labeled with a FRET pair (Cy3 and Cy5) at the same locations as in figure 2-3 to report DNA unwrapping and rewrapping. A T112C mutant of H2B was labeled with Cy5.5 to introduce a second FRET acceptor to report histone H2A-H2B dissociation and association. According to the relative intensities from the three fluorophores, we can identify the nucleosomes fully intact, DNA unwrapped, and/or one or both H2A-H2B displaced (see Fig. 2-9 for further details).

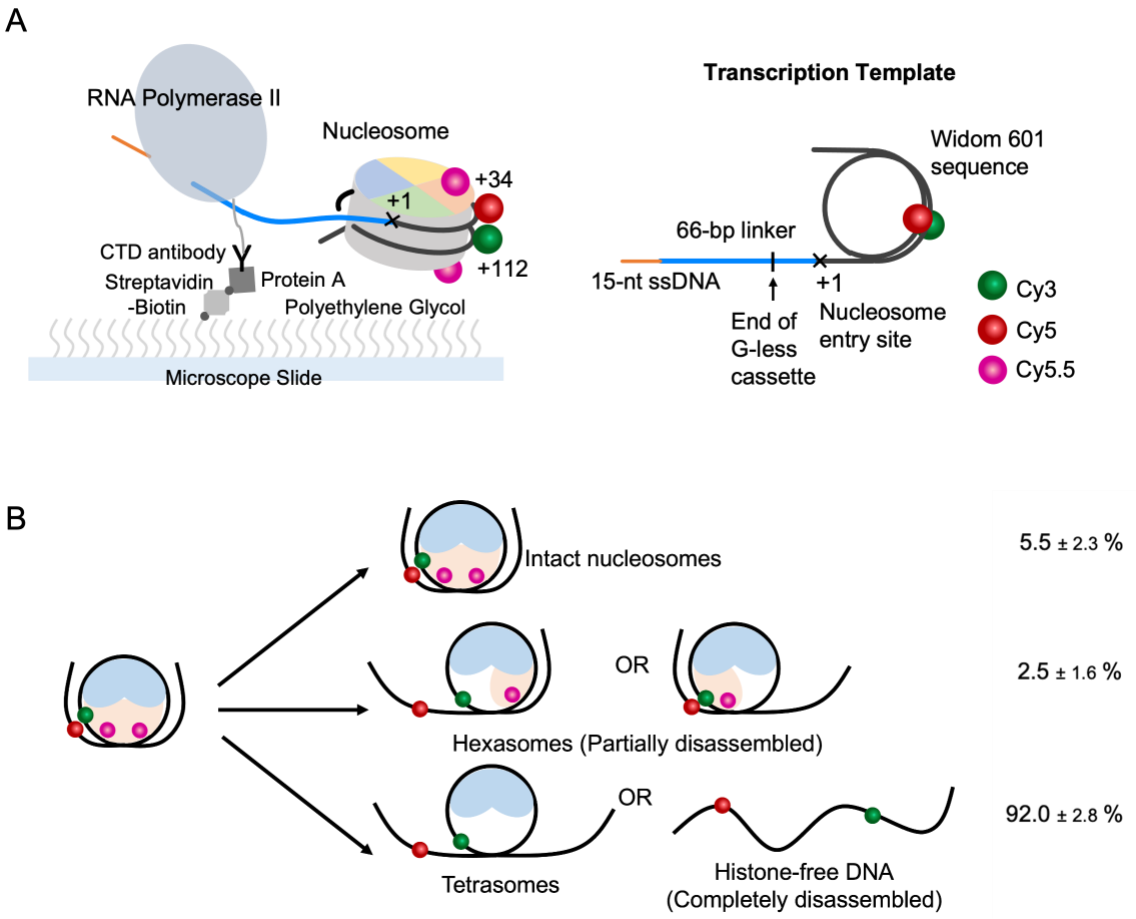

Figure **2-8**: A three-color smFRET experimental system reports both DNA and H2A-H2B dynamics during and after transcription by Pol II .

(A) Nucleosomal DNA is labeled with a FRET pair, Cy3 and Cy5, at the +112th and +34th nucleotides from the entry site, to report DNA wrapping and unwrapping during transcription. H2B T112C is labeled with Cy5.5 maleimide to introduce a second acceptor fluorophore that reports histone H2A-H2B dissociation and reassociation. (B) Schematics show the fate of nucleosomes after transcription. See figure 2-9 for intensity changes of the three fluorophores induced by DNA and H2A-H2B dynamics during transcription. The vast majority of the nucleosomes are either fully or partially disassembled after transcription.

In order to avoid premature photobleaching of Cy5.5 before Pol II passage, we imaged the fluorescence only for 500 ms every 7.5 seconds during a 3-minute time period (see further

details in Materials and Methods). Our imaging scheme enabled us to monitor the nucleosome dynamics without premature photobleaching of the majority of the fluorophores. After Pol II passage, we counted the population of intact nucleosomes and intermediates (Figs. 2-8 and 2-9). Our data indicates that most 601 nucleosomes are left with DNA unwrapped and H2A-H2B displaced upon Pol II passage. Only 5.5 ± 2.3 % (47 out of 857) of the nucleosomes are kept intact or reassembled, confirming the result from the two-color smFRET measurements based on DNA re-wrapping (3.6 $\pm$ 1.9 %). We also found some partially reassembled nucleosomes that show the intensity trajectories of hexasome-like intermediates formed by one dimer reassociation after both dimers were displaced (Figs. 2-8 and 2-9). These particles account for 2.5 ± 1.6 % (21 out of 857) of the nucleosomes. Therefore, the efficiency of at least one H2A-H2B dimer retained or re-associated is 8.0 ± 2.8 %. Overall, our results indicate that most nucleosomes are left disassembled with unwrapped DNA and both H2A-H2B dimers displaced during transcription. It is noteworthy that the majority (>93 %) of H2A-H2B dimers displaced from the nucleosome still remains in the elongation complex "locally" as they show Cy5.5 within the complex that does not FRET with Cy3 or Cy5 (Fig. 2-9). This may be explained by the re-positioning of the dimer along the DNA. H2A-H2B binds DNA in the absence of the tetramer. Alternatively, it was proposed that electrostatic interactions between negatively-charged surfaces on Pol II can retain histones in the elongation complex (Kulaeva et al. 2009, Chang et al. 2014).

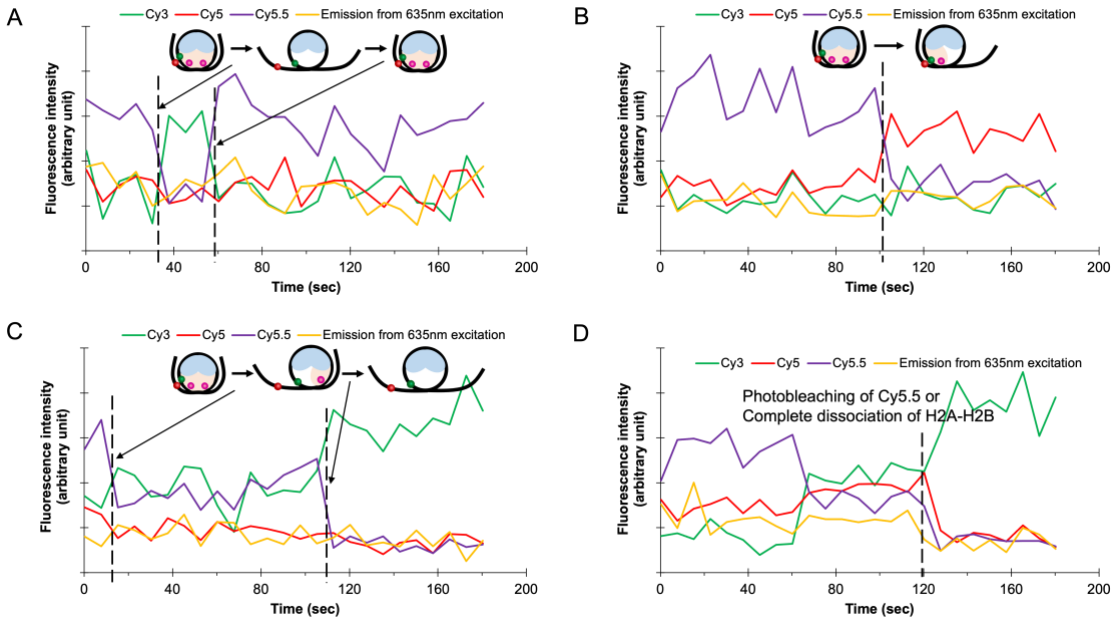

Figure **2-9**: Sample time trajectories of Cy3, Cy5, and Cy5.5 fluorescence intensities represent the nucleosome dynamics during transcription.

Nucleosomal DNA was labeled with a FRET pair, Cy3 and Cy5, at the +112th and +34th nucleotides from the entry site, respectively. H2B T112C was labeled with Cy5.5, forming a three-way FRET system. Data was collected right after adding the imaging buffer to start transcription elongation. The nucleosomes were illuminated with alternating excitation of a 532 nm laser for 750 ms, followed by a 635 nm laser for 750 ms in every 7.5 sec time window. In each 7.5 sec time window, intensities of the fluorophores were recorded for 2 frames x 250 ms/frame. Dynamic changes in the FRET intensities collected from the 532 nm excitation were extracted (marked in green, red and purple respectively for Cy3, Cy5, and Cy5.5 in panels A-D). The intensity of Cy5.5 from 635 nm excitation was extracted and plotted together with the other intensities (yellow lines in panels A-D). In so doing, the yellow line was synchronized to the other lines by shifting it 2 time-points ahead. As such, the yellow intensity at any given time point represents the intensity 500 ms ahead of time. The intensity time trajectories were used to identify DNA unwrapping and H2A-H2B dissociation events. When Cy5.5 is photobleached, concomitant drops in Cy5 and Cy5.5 intensities in both laser excitations were observed (D). The concomitancy may have a gap of a single time-point as the yellow line had been shifted for synchronization. Both H2A-H2B dimers were labeled in our experiments and the distance between the Cy5.5 labeled at the distal dimer and Cy3 is shorter than that between Cy3 and Cy5. Therefore, an intact nucleosome was identified by a significantly higher Cy5.5 intensity than Cy3 and Cy5 intensities because Cy5.5 is more likely to get most of the energy transferred from Cy3 (see the early time region in A). In some cases, increased Cy3 and decreased Cy5.5 were observed, indicating H2A-H2B displacement and DNA unwrapping, resulting in a disassembled nucleosome (see ~32 sec

time point in A). In 47 out of 857 total nucleosomes, the disassembly signal was followed by the opposite intensity changes, indicating re-association of H2A-H2B and rewrapping of DNA, which results in nucleosome re-assembly (see >58 sec time window in A). In case of nucleosome intermediates (hexasome or a similar structure), decreased Cy5.5 intensity was observed as one H2A-H2B was displaced (see ~101 sec time point in B). Extinction of Cy5 and Cy5.5 without photobleaching (no change in the intensities detected with 635 nm excitation) indicates dissembled nucleosomes (tetramer or histone-free DNA) (see two-step H2A-H2B displacement in C at ~12 and 110 sec time points). No change in the emission from 635 nm excitation (yellow line) in panels A-C means no photobleaching of Cy5.5, indicating that H2A-H2B still remains in the complex after displaced from the nucleosome. Panel D shows an example of a signature for Cy5.5 photobleaching or complete dissociation of H2A-H2B from the elongation complex (decrease in both the purple and yellow lines).

2.5. Discussion

Our single-molecule FRET experimental systems enabled us to monitor the DNA motions and H2A-H2B dynamics in the nucleosome during transcription elongation in real-time in a time-resolved manner (Lee et al. 2019a). Based on the measurements, we investigated the roles of histone-DNA interactions in regulating the Pol II transcription elongation kinetics and examined the nucleosome structural changes. It has been suggested that Pol II does not actively dissociate nucleosomal DNA from the histone core due to the act of transcription (Hodges et al. 2009, Bintu et al. 2012). These papers reported the frequency of transcription pauses in the presence and absence of a nucleosome based on a dual-trap optical tweezers setup where the transcription template is stretched through Pol II. According to the measurements, the pause frequency is increased significantly in the presence of a nucleosome, which cannot be explained if Pol II can actively break through a DNA-histone interface. Instead, Pol II gets stalled when it encounters a roadblock such as a strong DNA-histone interface (Johnson and Chamberlin 1994, Komissarova and Kashlev 1997, Wang et al. 2009, Jin et al. 2010, Cheung and Cramer 2011,

Lisica et al. 2016). Fluctuations in DNA-histone interactions that occasionally induce a large histone-DNA gap would open a path for a paused Pol II to resume. Our results suggest that spontaneous opening of histone-DNA interfaces heavily impacts the efficiency of transcription by facilitating resumption of a paused Pol II. In the first set of experiments, we addressed the role of H3K56 acetylation in the progression of Pol II through the nucleosome. It has been established that H3K56 acetylation facilitates spontaneous DNA opening in the nucleosome entry region where K56 is located (Kim et al. 2015, Lee and Lee 2019). Consistent with this, we found that H3K56 acetylation dramatically shortens the pause duration in the entry region of the nucleosome by 4.0 folds. As H3K56 acetylation removes a positive charge on the αN helix and consequently weakens histone interaction with DNA termini, it will increase the frequency of spontaneous DNA opening and the size of opening on average. The frequency of opening increases by 50 % according to our previous report (Kim et al. 2015). This is a considerable impact although it cannot account for the 4.0-fold increase we observed here. This remarkable increase can be explained by the following mechanism as we proposed (Lee and Lee 2019). The 50 % increase in the opening frequency is for openings with all possible sizes while the opening required for Pol II escape should be very large and rare. These rare large opening events make up the tailing edge of an approximate gaussian distribution as we modeled (Fig. 2-10) (Lee and Lee 2019). This tailing edge decays dramatically as the opening size gets larger. Conversely, the tailing edge rises dramatically by shifting the entire distribution to the larger side. When the entire gaussian distribution shifts toward the larger side upon H3K56 acetylation, therefore, the frequency of tailing edge events (i.e. rare large opening events) will increase dramatically (Fig. 2-10). The remarkable 4.0-fold increase in the escape rate of paused Pol II strongly supports that paused Pol II requires rare large DNA opening ahead of it in order to escape. The frequency of such rare events can be significantly increased by a small increase in the average opening. Without invoking any unknown or mysterious source, this mechanism can explain how spontaneous

nucleosome dynamics can play a major role in regulating the efficiency of nucleosomal transcription. This effect is significant because the overall efficiency of nucleosomal transcription is determined mainly by pause durations that last for tens to hundreds of seconds while the elongation rate is very fast at tens of milliseconds per nucleotide.

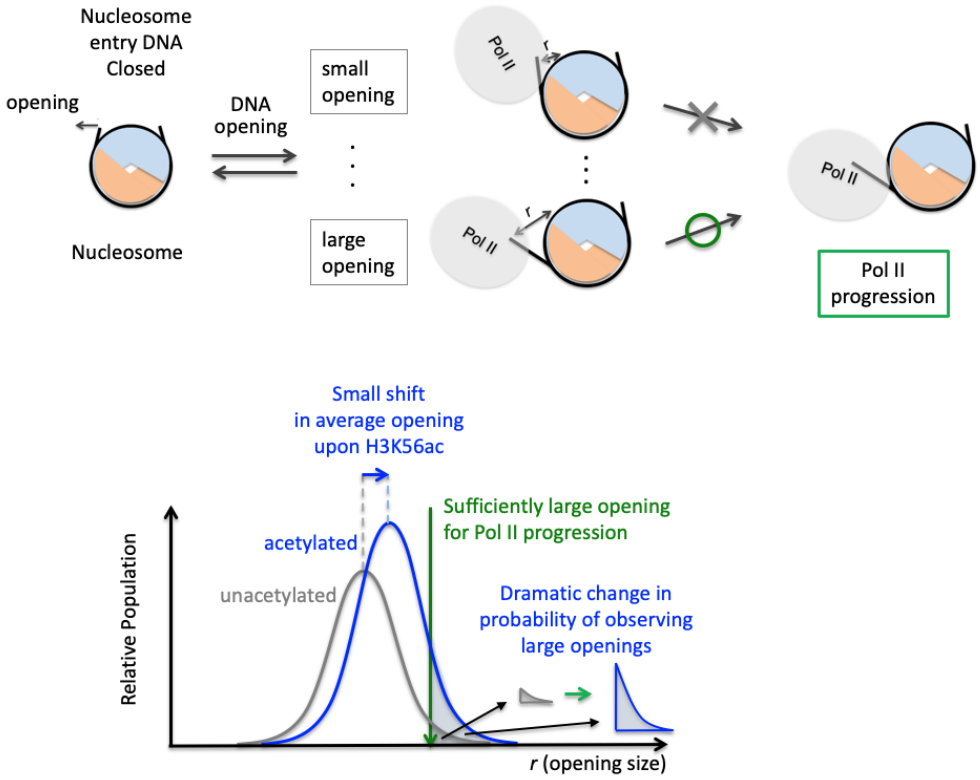

Figure **2-10**: How a small change in the average nucleosome opening size can amplify the rate of rare large openings.

The probability distribution of the DNA opening size in the nucleosome entry region can be approximated with a Gaussian distribution (e.g. the two curves on the chart). See reference 30 for further details on this modeling. A small increase in the average opening size of DNA upon H3K56ac will shift the entire distribution to the right (indicated by the blue arrow in the chart). This small shift can result in a dramatic impact on the probability of observing rare large openings that allow for paused Pol II to progress (indicated by the green arrow, change in the shaded areas under the two curves). The ratio of the shaded areas before and after the acetylation represents the decrease in the pause duration, which can be very large with a small shift in the average opening size of the nucleosome.

Previous reports suggest that nucleosomes reassemble upon Pol II passage in moderately transcribed genes (Kulaeva et al. 2009, Hsieh et al. 2013, Kulaeva et al. 2010, Kulaeva and Studitsky 2010, Kulaeva et al. 2013, Belotserkovskaya et al. 2003a). Our results indicate that only <5 % of the nucleosomes reassemble during Pol II progression in real-time. The three-color single molecule FRET measurements report the same level of nucleosome reassembly and 8.0 ± 2.8 % histone H2A-H2B (one or both) recovery during transcription. These results indicate that most nucleosomes do not reassemble during transcription in real time. One major difference between our experimental system and the previously reported ones is that our system inherently filters out nucleosomal changes unrelated to Pol II progression. Any change in the nucleosome after Pol II run-off is not reported in our system because the nucleosome would have already left the Pol II. Therefore, our results indicate that Pol II mediates nucleosome reassembly very inefficiently during transcription. This conclusion does not rule out nucleosome reassembly after Pol II runs off completely, most likely utilizing a plethora of chromatin assembly factors and ATP-dependent chromatin remodeling complexes. According to our three-color measurements, the majority (>93%, 857 out of 915 nucleosomes) of the H2A-H2B dimers displaced during Pol II progression are still observed within the elongation complex. Therefore, it is feasible that Pol II or an unwrapped portion of the nucleosomal DNA harbors H2A-H2B during elongation and helps reassemble the nucleosome after Pol II passes. Further investigations remain in order to test whether extended DNA at the exit side of the nucleosome would make Pol II stay longer with the nucleosome and facilitate nucleosome reassembly. Of note, extended DNA may induce technical problems such as heterogeneity in nucleosome positioning which will require a major redesign of the experimental system.

Among the disassembled nucleosomes detected during transcription, some were identified as hexasomes. Structural and biochemical studies have established that hexasomes can survive transcription (Kireeva et al. 2002, Belotserkovskaya et al. 2003a, Hsieh et al. 2013,

Kulaeva and Studitsky 2010, Kulaeva et al. 2010). While our system allows us to detect hexasome generation during transcription, it is not designed to monitor any further changes of the hexasomes. Future studies can be designed to investigate the transcription pathways through hexasomes.

Histone chaperones mediate assembly and disassembly of the nucleosome and have been hypothesized that they may affect the kinetics of nucleosomal transcription (Akey and Luger 2003, Park and Luger 2006, Park and Luger 2008, Lorch et al. 2006, De Koning et al. 2007, Hsieh et al. 2013). In order to investigate the roles of a generic histone chaperone Nap1 in regulating nucleosome dynamics during transcription, we carried out smFRET measurements in the presence of Nap1. Our results indicate that Nap1 has no effects on the pause dynamics, the elongation rate, and the nucleosome reassembly efficiency during transcription. This result is consistent with ensemble biochemical studies that indicated Nap1 on its own did not affect Pol II progression through the nucleosome (Kuryan et al. 2012). Instead, Nap1 only had an effect in the presence of the ATP-dependent chromatin remodeling complex RSC.

It might not be surprising that Nap1 failed to have an effect. Structural studies of Pol II on the nucleosome and its intermediates shed some light on possible explanations. In the paused state at SHL(-6), nucleosomal DNA is completely wrapped around the histone core (Bilokapic et al. 2018). Nap1 cannot bind H2A-H2B in fully wrapped nucleosome(Andrews et al. 2010), and therefore cannot impact on the SHL(-6) pause dynamics. Even in the paused state at SHL(-5) where only ~15 base pairs of DNA gets unwrapped (Bilokapic et al. 2018), the interactions between DNA and H2A-H2B are mostly preserved (Bilokapic et al. 2018, Hall et al. 2009, Arimura et al. 2012). Moreover, the nucleosome and histone surfaces around the H2A-H2B region are sterically hindered by Pol II in the SHL(-5) pause, which will inhibit the action of Nap1. The next paused state at SHL(-2), albeit rare to form, may be shortened by Nap1 because a large surface area of H2A-H2B is exposed that can be a good target for Nap1 action.

Unfortunately, we could not measure the pause duration at SHL(-2) in the presence of Nap1 because of the too small number of pauses observed at this location. This result may indicate that Nap1 does significantly shorten the duration of SHL(-2) pauses, resulting in extremely rare pauses observable. Regardless, the effect of Nap1 at this pause location should be minimal because it is already a very weak pause location.

We did not observe any change in the number of reassembled nucleosomes during Pol II progression in the presence of Nap1 despite its widely accepted function of nucleosome assembly (Andrews et al. 2010, McBryant et al. 2003, Vlijm et al. 2012, Aguilar-Gurrieri et al. 2016). As is mentioned above, our measurements record nucleosomal changes only during Pol II progression because the nucleosome will dissociate from Pol II after Pol II runs off. Therefore, our result indicate that Nap1 does not mediate nucleosome reassembly during transcription in real time although it does not rule out that Nap1 may promote nucleosome reassembly after Pol II passes through the nucleosome.

In conclusion, our results suggest that Pol II progression through a nucleosome is enabled by spontaneous opening of DNA-histone interfaces and that Pol II or histone chaperone does not mediate nucleosome disassembly or reassembly very efficiently during transcription in real time. The role of H3K56ac in facilitating transcription elongation is to shorten the pause duration in the entry region of the nucleosome, which is likely by accelerating the spontaneous opening of the DNA-histone interface in this region.

Chapter 3

The Effects of Histone H2B Ubiquitylations on the Nucleosome Structure and Internucleosomal Interactions

This chapter is adapted with permission from reference (Sengupta et al. 2022). Copyright 2022 Biochemistry.

3.1. Abstract

Eukaryotic gene compaction takes place at multiple levels to package DNA to chromatin and chromosomes. Two of the most fundamental levels of DNA packaging are at the nucleosome and dinucleosome stacks. The nucleosome is the basic gene packing unit and is composed of DNA wrapped around a histone core. Nucleosomes stack with one another for further compaction of DNA. The first stacking step leads to dinucleosome formation, which is driven by internucleosomal interactions between various parts of two nucleosomes. Histone proteins are rich targets for post-translational modifications, some of which affect the structure of the nucleosome and the interactions between nucleosomes. These effects are often implicated in the regulation of various genomic transactions. In particular, histone H2B ubiquitylation has been associated with facilitated transcription and hexasome formation. Here, we employed semi-synthetically ubiquitylated histone H2B and single-molecule FRET to investigate the effects of H2B ubiquitylations at lysine 34 (H2BK34) and lysine 120 (H2BK120) on the structure of the nucleosome and the interactions between two nucleosomes. Our results suggest that H2BK34 ubiquitylation widens the DNA gyre gap in the nucleosome and stabilizes long- and short-range

internucleosomal interactions while H2BK120 ubiquitylation does not affect the nucleosome structure or internucleosomal interactions. These results suggest potential roles for H2B ubiquitylations in facilitated transcription and hexasome formation while maintaining the structural integrity of chromatin.

3.2. Introduction

The nucleosome is the basic gene packing unit in eukaryotes. A nucleosome core particle is composed of ~147 bp DNA wrapped around the octameric histone protein core. The histone core comprises two H2A-H2B dimers and one $(H3\text{-}H4)_2$ tetramer (Luger et al. 1997a). This octamer is rich with arginine and lysine, which are positively charged at a neutral pH and interact strongly with the phosphate backbone of DNA, driving the formation of nucleosome core particles. Stable sub-nucleosome particles such as the hexasome comprising one H2A-H2B and one $(H3\text{-}H4)_2$ can be formed during transcription, DNA replication and repair (Arimura et al. 2012). Nucleosomes are linked in an array format in chromatin. Efficient compaction of nucleosome arrays to maximize space utilization of the nucleus depends much on internucleosomal interactions (Stehr et al. 2008, Bendandi et al. 2020, Krajewski 2016). The most fundamental level of internucleosomal compaction is at dinucleosomes where two nucleosomes combine to form a stack. Structures of dinucleosome stacks have been observed through theoretical models and experimental analyses. X-ray crystallography, negative stain electron microscopy (EM), and cryo-EM resulted in images of stacked nucleosomes (Finch et al. 1977, Vasudevan, Chua and Davey 2010, Scheffer et al. 2012). Nucleosome stacking has also been reported by single-molecule measurements (Meng, Andresen and van Noort 2015, Kaczmarczyk et al. 2017, Cui and Bustamante 2000, Li et al. 2016, Lee, Wei and Lee 2011, Dhall et al. 2014). An *in-silico* study suggested that internucleosomal interactions

exist between a transcription start site and a termination site (Chen et al. 2018b). Another theoretical study supports that internucleosomal interactions are predominantly contributed by the N-terminal tail domains of the histone proteins, especially H4 tails (Kulaeva et al. 2012). These interactions are important for long-range communications between regulatory elements (Kulaeva et al. 2012). Dinucleosome stacks can also form after chromatin remodeling of dinucleosome arrays although in most cases these dinucleosome stacks contain one nucleosome and one hexasome (Kato et al. 2017).

Post-translational modifications to histones such as acetylation, methylation, ubiquitylation, SUMOylation, and phosphorylation often affect the structure, dynamics, and functions of nucleosomes (Lee 2019, Bowman and Poirier 2015b, Smith and Shilatifard 2010). These modifications can change the local structures of the nucleosome, which may lead to an altered charge distribution on the surfaces of histones and the nucleosome. These changes directly influence the stability of the nucleosome, chromatin condensation, or the recruitment of enzymes to perform various genome transactions including transcription, chromatin remodeling, DNA replication and repair ,(Delage and Dashwood 2008, Wilkins et al. 2014, Cavalieri 2021). For instance, acetylation and phosphorylation of lysine neutralize the positive charge or add a negative charge, thereby weakening DNA-histone interactions, which compromises the stability of the nucleosome and the efficiency of chromatin condensation (Bannister and Kouzarides 2011). We previously reported the effects of histone acetylation and SUMOylation on destabilizing nucleosomal DNA wrapping, inhibiting dinucleosome formation, and destabilizing dinucleosome stacks using single-molecule FRET (smFRET) (Lee et al. 2011, Dhall et al. 2014). Here, we employed similar smFRET approaches to investigate the effects of histone ubiquitylations at H2BK34 and H2BK120 on the structure of the nucleosome, the rate of dinucleosome formation, and the stability of dinucleosome stacks. Ubiquitin is a 76-residue protein and protein ubiquitylation has been associated with regulating various biological processes (Swatek and

Komander 2016, Cai et al. 2018, Cao and Yan 2012). Histone ubiquitylations at H2B have been identified at H2BK34 and H2BK120 that are directly coupled to facilitated transcription and Dot1L-induced H3K79 methylations (Valencia-Sánchez et al. 2019, Fleming et al. 2008). The incorporation of bulky ubiquitin groups into the nucleosome may alter the DNA-histone interactions as was suggested for H2BK34 ubiquitylated nucleosomes (Li et al. 2017, Krajewski et al. 2018, Krajewski 2020b). H2B ubiquitylations may also affect internucleosomal interactions and subsequently chromatin condensation by modifying the global and local structures of the nucleosome (Fierz et al. 2011, Lee et al. 2019b). Using semi-synthetically ubiquitylated histone H2B and smFRET, we show that H2BK34 ubiquitylation (H2K34ub) widens the DNA gyre gap in the nucleosome, facilitates dinucleosome formation, and stabilizes dinucleosome stacks whereas H2BK120 ubiquitylation (H2BK120ub) does not have any significant impact on these properties. These results provide the mechanisms for the effects of H2B ubiquitylations on facilitated transcription and hexasome formation while maintaining the structural integrity of chromatin.

3.3. Materials and Methods

3.3.1. Nucleosomal DNA construction and labeling

The Widom 601 nucleosome positioning sequence was used for nucleosomal DNA construction. Five oligonucleotides (three for forward and two for reverse strands) were purchased (Integrated DNA Technologies, Coralville, IA). One of the DNA fragments contains a 20 nucleotide-long linker one end of which is labeled with biotin. For structural measurements of nucleosomes, the thymine bases at the 34^{th} and 112^{th} nucleotides counted from the nucleosome entry, and for dinucleosome stacking measurements, at the 60^{th} and 129^{th} nucleotides were modified

with an NH_2 functionalized C6 linker for fluorophore labeling (Integrated DNA Technologies). The sequences of all the oligonucleotides are provided in Table. 3-1.

Table **3-1**: Sequences of the oligonucleotides to construct nucleosomal DNA.

Oligonucleotide name	**Description**
F1_bio (biotinylated)	/5Biosg/CAACGAAATC CTCCGAGAGG ATCGAGAATC CCGGTGCCGA GGCCGCTCAA
F1	CTCCGAGAGG ATCGAGAATC CCGGTGCCGA GGCCGCTCAA
F2_34 (structural measurement)	/5Phos/ TTGG /iAmMC6T/CGTAGACAG CTCTAGCACC GCTTAAACGC ACGTACGCGC TGTCCCCCGC GTTTTAACCG CCAAGGGGAT TAC
F2_60 (stacking measurement)	/5Phos/ TTGGTCGTAG ACAGCTCTAG CACCGCTTA/iUniAmM/ ACGCACGTAC GCGCTGTCCC CCGCGTTTTA ACCGCCAAGG GGATTAC
F3_112 (structural measurement)	/5Phos/ TCC C/iAmMC6T/AGTCTCCA GGCACGTGTC AGATATATAC ATCCGAT
F3_129 (stacking measurement)	/5Phos/ TCC CTAGTCTCCA GGCACGTG/iAmMC6T/C AGATATATAC ATCCGAT
R1	ATCGGATGTA TATATCTGAC ACGTGCCTGG AGACTAGGGA GTAATCCCCT TGGCGGTTAA AACGCGGGG
R2	/5Phos/G ACAGCGCGTA CGTGCGTTTA AGCGGTGCTA GAGCTGTCTA CGACCAATTG AGCGGCCTCG GCACCGGGAT TCTCGAT

The site specifically modified oligonucleotides were labeled using NHS-ester functionalized Cy3 and Cy5 (GE Healthcare). Briefly, oligonucleotides were dissolved in deionized water (100 nM) and the dye-NHS-ester was dissolved in 20 µl dimethyl sulfoxide (DMSO). The dye solution was then added to the oligonucleotide solution (5:1 dye: oligonucleotide ratio) slowly with constant mixing. The reaction was continued overnight with gentle but constant agitation. The

labeled oligonucleotides were purified using Illustra NAP-5 columns (Cytiva). Three different sets of DNA containing the Widom 601 sequence were prepared by annealing and ligating the corresponding fragments (Table. 3-2).

Table **3-2**: Description of DNA constructs for structural (DNA_{str}) and dinucleosome stacking (DNA_{cy3} and DNA_{cy5}) measurements.

Name	**Description**	**Combination of oligos**
DNA_{str}	Cy3-Cy5 labeled DNA for structural measurement	F1_bio + F2_34-Cy5 + F3_112-Cy3 + R1 + R3
DNA_{cy3}	Cy3 labeled DNA for stacking measurement	F1_bio + F2_60 + F3_129-Cy3 + R1 + R2
DNA_{cy5}	Cy5 labeled DNA for stacking measurement	F1 + F2_60-Cy5 + F3_129 + R1 + R2

3.3.2. Mutation, expression, and purification of histone proteins

Wild-type, unmodified histones H2A (UniProt accession ID: P0C0S8), H2B (P33778), H3.2 (Q71DI3), and H4 (P62805) were expressed in *E. coli*, purified from inclusion bodies, and assembled into octamers as previously described (Luger et al. 1999a, Spangler et al. 2022). Human H2BK120ub with a ubiquitin (UniPro accession ID: P62975) G76A substitution was prepared by expressed protein ligation and assembled into octamers with wild-type human H2A, H3.2, and H4 histones as previously described (Anderson et al. 2019a). Human H2BK34ub was prepared by dichloroacetone crosslinking of an H2BK34C mutant protein and a ubiquitin G76C mutant protein as previously described (Anderson et al. 2019a). Briefly, human H2B(K34C) was cloned by site-directed mutagenesis. Following expression in *E. coli* and purification from inclusion bodies, H2BK34C was reconstituted into an H2A-H2BK34C dimer with wild-type unmodified H2A and purified by ion exchange chromatography using a Source S resin (GE Healthcare). A strep-6xHis

tagged ubiquitin G76C mutant protein was purified as previously described (Anderson et al. 2019a). The H2A-H2BK34C dimer and tagged ubiquitin G76C were crosslinked with dichloroacetone, refolded into a histone dimer, and purified by metal affinity chromatography using Cobalt resin (ABT). The strep-6xHis tag was cleaved from ubiquitin using TEV protease and the resulting H2A-H2BK34ub dimer was purified by ion exchange chromatography using a Source S resin. The H2BK34ub octamer was refolded as described for other octamers using the H2A-H2BK34ub dimer and an unmodified, wild-type H3.2-H4 tetramer in a 2:1 ratio and purified by size exclusion chromatography using a Superdex 200 increase 10/300 column (GE Healthcare). The histones were analyzed with SDS-PAGE to confirm ubiquitylation (Fig. 3-1).

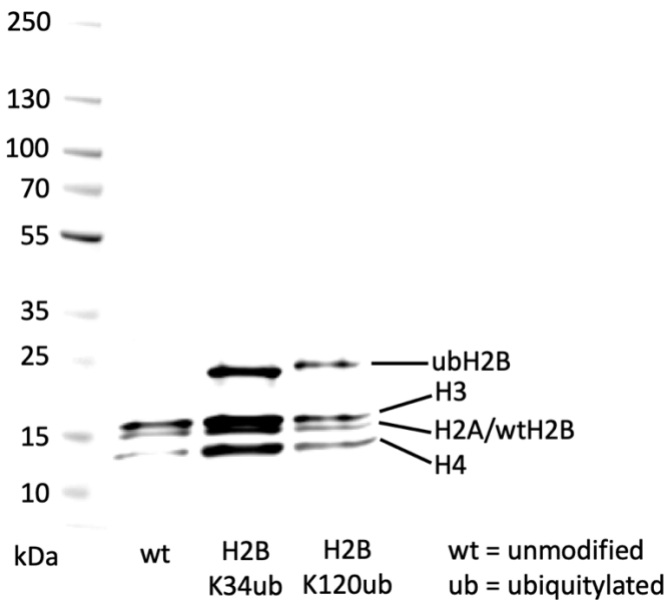

Figure **3-1**: SDS-PAGE gel image to confirm histone H2B ubiquitylation.

From left to right: marker, unmodified histones, H2BK34ub histones, and H2BK120ub histones.

3.3.3. Nucleosome reconstitution

We prepared three different sets of nucleosomes each with unmodified and H2BK34ub- and H2B120ub-modified histones (Table. 3-3). The first three-nucleosome set is for the structural measurements and contains DNA labeled with a FRET pair (Fig. 3-3 A). For dinucleosome stacking measurements, six different nucleosomes were prepared. One three-nucleosome set is labeled with Cy3 and biotin at DNA (unmodified, H2BK34ub and H2BK120ub) and the other with Cy5 only (unmodified, H2BK34ub and H2BK120ub). Nucleosomes were reconstituted by a stepwise salt dialysis method (Dhall et al. 2014). Briefly, DNA and histones were mixed and dialyzed for 1 hour each against a series of TE buffer (10 mM Tris-HCl, 1 mM EDTA, pH 8.0) solutions containing 850 mM, 650 mM, 500 mM, 300 mM, and 10 mM NaCl, respectively. A DNA to histone ratio of 1:1.2 was found to be optimal. After the final dialysis step, the solution was kept at 55 ^{o}C for 1 hour. The quality of the nucleosomes was confirmed using native gel electrophoresis (Fig. 3-2). We used the crush-and-soak native PAGE gel purification method to get pure nucleosomes devoid of any free DNA. The concentration of the nucleosomes was measured from their absorbances at 260 nm and 280 nm.

Table **3-3**: Description of nucleosomes for structural and dinucleosome stacking measurements.

A total of 9 different nucleosomes were assembled using different combinations of DNA and histone octamers.

Name	**Description**
Cy3-Cy5-labeled unmodified nucleosome	DNA_{str} + unmodified histone octamer
Cy3-Cy5-labeled H2BK34ub nucleosome	DNA_{str} + H2BK34ub histone octamer
Cy3-Cy5-labeled H2BK120ub nucleosome	DNA_{str} + H2BK120ub histone octamer
Cy3-labeled unmodified nucleosome	DNA_{cy3} + unmodified histone octamer
Cy5-labeled unmodified nucleosome	DNA_{cy5} + unmodified histone octamer
Cy3-labeled H2BK34ub nucleosome	DNA_{cy3} + H2BK34ub histone octamer
Cy5-labeled H2BK34ub nucleosome	DNA_{cy5} + H2BK34ub histone octamer
Cy3-labeled H2BK120ub nucleosome	DNA_{cy3} + H2BK120ub histone octamer
Cy5-labeled H2BK120ub nucleosome	DNA_{cy5} + H2BK120ub histone octamer

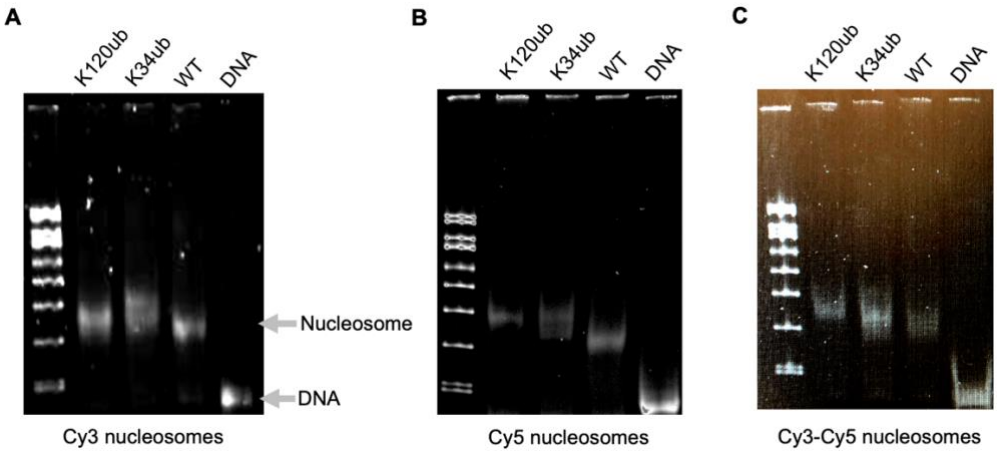

Figure **3-2**: Native PAGE gel images of the nucleosomes.

(A) Cy3-labeled nucleosomes and nucleosomal DNA: DNA marker, H2BK120ub nucleosome, H2BK34ub nucleosome, unmodified nucleosome (WT), and nucleosomal DNA from left to right, (B) Cy5-labeled nucleosomes and nucleosomal DNA: DNA marker, H2BK120ub nucleosome, H2BK34ub nucleosome, unmodified nucleosome (WT), and nucleosomal DNA from left to right, (C) Cy3/Cy5-labeled nucleosomes and nucleosomal DNA: DNA marker, H2BK120ub nucleosome, H2BK34ub nucleosome, unmodified nucleosome (WT), and nucleosomal DNA from left to right.

3.3.4. smFRET sample preparation and measurement

Microscope slides were cleaned, and surface functionalized with polyethylene glycol (PEG) as previously publishedB(Lee et al. 2019b). Briefly, microscope slides with 5 pairs of holes (10 holes in total, Finkenbeiner, Waltham, MA) aligned to construct five fluidic channels were cleaned thoroughly using a series of organic solvents and a highly oxidizing Nochromix® (Godax Laboratories, inc.) solution. The surface was PEGylated using an acetonitrile solution of PEG and biotin-PEG (99:1 ratio, Laysan Bio Inc., Arab, AL). Fluidic channels were constructed on the slide where the nucleosomes would be surface-immobilized.

As the first step of smFRET measurements, 40 µl 0.1 mg/ml streptavidin solution in 1x phosphate buffered saline was injected into the channel. 15 min after the streptavidin injection, a 0.1 mg/ml solution of bovine serum albumin (BSA, 40 µl) was used to wash the unbound streptavidin and to passivate the surface to minimize nonspecific binding of the nucleosomes. For structural measurements, a 50 µl Tris-HCl (pH 8.0, 10 mM) solution containing 2 mM $MgCl_2$, 50 mM NaCl, 0.05% Tween-20 and 0.1 nM nucleosomes was injected and incubated for 5 min followed by washing with the imaging buffer (2 mM $MgCl_2$, 50 mM NaCl, 0.05 % Tween-20, 4 mM protocatechuic acid (PCA) and 0.4 units/ml protocatechuate dioxygenase (PCD). Fluorescence images of the surface immobilized nucleosomes (Fig. 3-3 B) on a prism coupled TIR microscope custom-built based on a commercial microscope (Nikon TE2000) were taken as a time series, a collection of which forms a movie file. Each image integrated the fluorescence signals for 100 ms and was taken every 100 ms until most of the fluorophores were photobleached. FRET efficiencies for each surface-immobilized nucleosome were estimated using $E_{FRET} = I_{Cy5}/(I_{Cy3} + I_{Cy5})$ on each frame of the movie, where I is fluorescence intensity.

For dinucleosome stacking measurements, a 50 µl Tris-HCl (pH 8.0) solution containing 2 mM $MgCl_2$, 50 mM NaCl and 0.1 nM Cy3-labeled nucleosome was injected and incubated for 5 min. After 5 min, a 0.1 mg/ml BSA solution containing 4 mM PCA and 0.4 units/ml PCD was injected to wash unbound nucleosomes. Finally, a 10 nM solution of Cy5-labeled nucleosomes in the imaging buffer was injected to the channel. The imaging buffer contains 10 mM Tris-HCl, 8 mM PCA and 0.8 unit/ml PCD, 1 mM Trolox, 2 mM $MgCl_2$, and 50 mM NaCl. After the final injection (for both structural and stacking measurements), 10 min was given for PCD-PCA to react and exhaust the oxygen in the channel. The slide was then placed on the microscope. Multiple fluorescence movies were recorded in each channel over the period of 30 min. A FRET-on state is identified visually by examining the intensity time trajectories of the FRET pair from each

nucleosome when the FRET acceptor intensity increases with a concomitant decrease in the FRET donor intensity.

3.4. Results

3.4.1. H2BK34 ubiquitylation widens the DNA gyre gap in the nucleosome

To investigate the effects of H2B ubiquitylations on the nucleosome structure and dinucleosome formation, we semi-synthetically ubiquitylated histone H2B and assembled nucleosomes with unmodified, H2BK34ub- and H2BK120ub-modified histones (see methods and figures 3-1 and 3-2). For smFRET measurements of the structural effect, we labeled the 34^{th} and 112^{th} nucleotides of the nucleosomal DNA respectively with fluorophores Cy3 and Cy5 (Fig. 3-3 A). According to a crystal structure of a nucleosome core particle reconstituted with the Widom 601 DNA sequence (PDB ID: 3LZ0), these residues come in close proximity when the DNA wraps around the histone core, resulting in a distance of 25.3 Å between the C5 positions of the thymine bases where Cy3 and Cy5 are labeled via an amine modification linker. Therefore, the Cy3 and Cy5 fluorophores will form a FRET pair and yield a high FRET efficiency in an intact nucleosome (>90 % with their förster radius of 54 Å (Kujirai et al. 2018)) (Fig. 3-3 A). We measured the FRET efficiencies from the nucleosomes reconstituted with the unmodified, H2BK34ub-, and H2BK120ub-modified histone core. According to our data, the average FRET efficiency from the unmodified nucleosome is 0.92 ± 0.01, validating the design of our experimental system (Fig. 3-4 A). The average FRET efficiencies from the H2BK34ub- and H2BK120ub-modified nucleosomes are 0.77 ± 0.01 and 0.91 ± 0.01, respectively (Fig. 3-4 BC). The significantly lower FRET efficiency from the H2BK34ub nucleosome supports the hypothesis of the ubiquitin molecules

protruding through the gap between the DNA gyres, consequently widening it (Li et al. 2017, Chu et al. 2019). The FRET efficiency from the H2BK120ub nucleosome is identical within error to that from the unmodified nucleosome, suggesting no change in the DNA gyre structure as the ubiquitin molecules in H2BK120ub nucleosomes will likely sit on the lateral surface of the histone core (Worden et al. 2019).

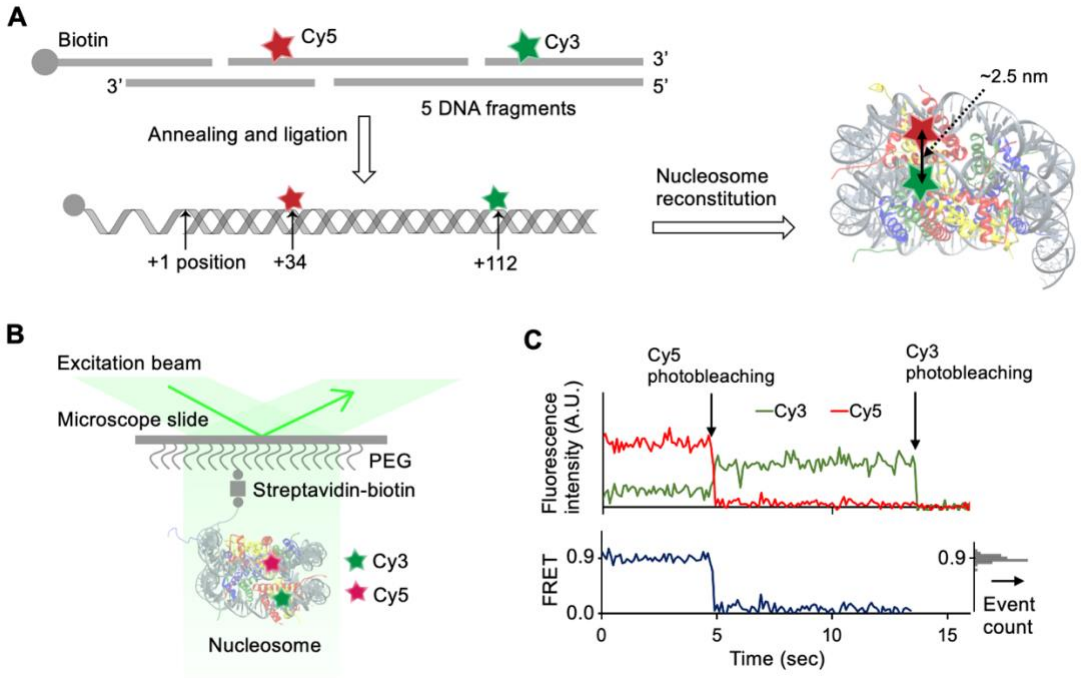

Figure **3-3**: Experimental scheme to monitor the effect of histone H2B ubiquitylations on the nucleosome structure.

(A) Five DNA oligonucleotides are ligated to construct the nucleosomal DNA. A FRET pair (Cy3 and Cy5, förster radius = 5.4 nm) labeled at the 34th and 112th nucleotides reports the gap between the DNA gyres in the nucleosome (PDB ID: 3LZ0). (B) Surface-immobilized nucleosomes are excited by an evanescent field generated with a laser beam at 532 nm to produce a FRET signal. (C) Representative fluorescence intensity and FRET traces from a nucleosome particle. A much higher acceptor emission (Cy5, red) than donor emission (Cy3, green) indicates an intact nucleosome. The fluorophores photobleach after some time as is shown with the arrows. A histogram representing the FRET efficiency distribution from a single nucleosome particle is shown on the right side of the lower panel.

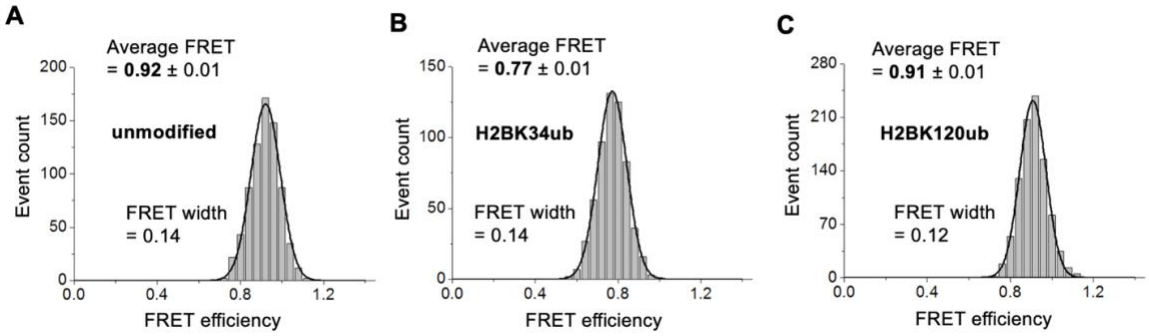

Figure **3-4**: FRET efficiency histograms from (A) unmodified, (B) H2BK34ub, and (C) H2BK120ub nucleosomes.

Solid black lines represent fitting with a gaussian distribution function. The average FRET efficiencies from the fitting are 0.92 ± 0.01, 0.77 ± 0.01, and 0.91 ± 0.01 for unmodified, H2BK34ub, and H2BK120ub nucleosomes, respectively. The significantly lower average FRET efficiency from H2BK34ub nucleosomes indicates a relaxed structure of the nucleosome. Data were collected by Bhaswati Sengupta and analyzed by both Bhaswati Sengupta and Mai Huynh.

3.4.2. Long-range internucleosomal interactions are facilitated by H2BK34 ubiquitylation

Next, we measured the formation frequency of dinucleosome stacks. We immobilized the Cy3-labeled nucleosomes on a microscope slide surface and injected Cy5-labeled nucleosomes to let them form dinucleosome stacks spontaneously, transiently, and repeatedly (Fig. 3-5 A), generating smFRET signals. No FRET signal is detected with surface-immobilized Cy3-labeled nucleosomal DNA and freely diffusing Cy5-labeled nucleosomal DNA during the same period of observation. The dinucleosome stacks may have various geometries among which we can detect a subset yielding a detectable FRET signal (Fig. 3-5 C). As the collisions between two nucleosomes must be via random trajectories and the dinucleosome structures are also likely random, the subset

contains randomized samples that should properly represent the dynamics of dinucleosome formation in general.

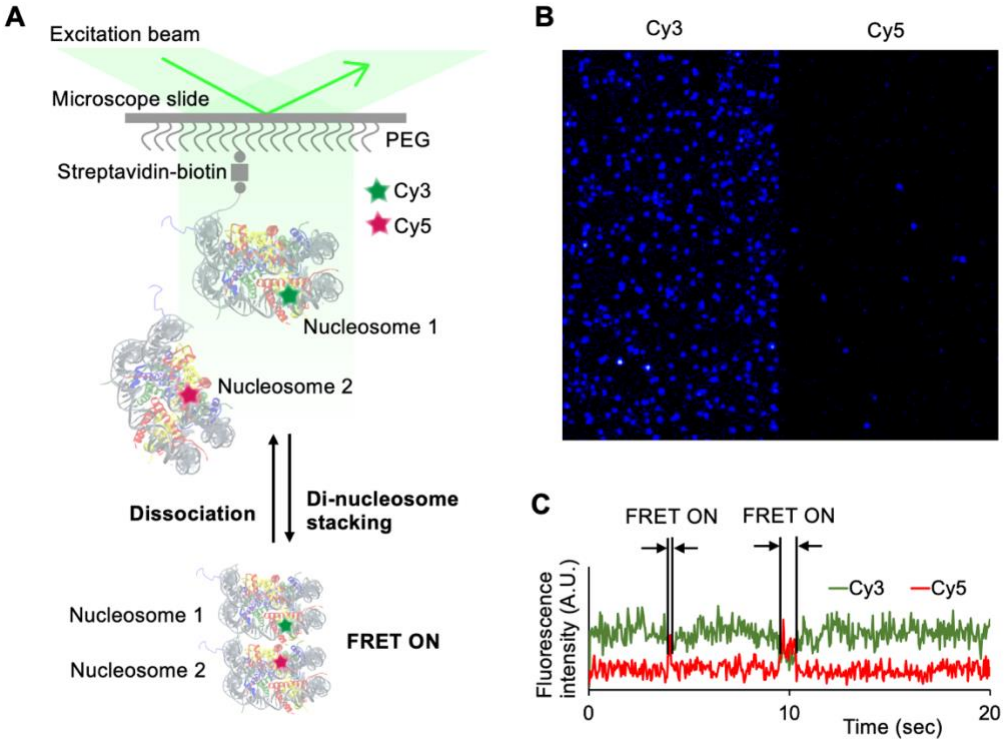

Figure **3-5**: Experimental scheme to investigate dinucleosome stack formation.

(A) Two nucleosomal DNA constructs each labeled with Cy3 or Cy5 were used to reconstitute nucleosomes that will report a FRET signal when a dinucleosome stack is formed. The Cy3 labeled nucleosomes are surface-immobilized while the Cy5 labeled nucleosomes are freely diffusing in solution. (B) An example of a movie frame shows surface-immobilized Cy3-labeled nucleosomes. The fluorescence signal is divided into two spectral regions respectively for Cy3 and Cy5 and imaged on a camera side-by-side. (C) Representative fluorescence intensity traces show transiently formed dinucleosome stacks. "FRET ON" indicates dinucleosome formation and subsequent dissociation.

The dinucleosome formation frequency was calculated as follows. We recorded fluorescence movies each with ~300 surface-immobilized Cy3 nucleosomes (Fig. 3-5 B). The

duration of each movie was 2 min. For each channel, 15 movies were collected giving us a total observation time of 30 min. For unmodified and H2BK34ub nucleosomes a total of 6 datasets were recorded, giving us a total observation time of 3 hours, whereas for H2BK120ub a total of 8 datasets were recorded, giving us a total observation time of 4 hours. Out of these numbers, we computed the total observation times of one surface-immobilized nucleosome that are 844, 870, and 1114 hours respectively for unmodified, H2BK34ub, and H2BK120ub nucleosomes with 10 nM Cy5-nucleosomes freely diffusing in solution (Fig. 3-6 A). We visually identified the "FRET ON" events resulting from dinucleosome stack formation (Fig. 3-5 C) and counted the total number of the stacking events. The criteria to identify a FRET event were FRET efficiency >0.3 with anti-correlated Cy3-Cy5 intensities (i.e. Cy5 increase accompanied by Cy3 decrease for the onset of a FRET event and Cy5 decrease accompanied by Cy3 increase at the end of a FRET event). Dividing the total number of stacking events by the total duration of the observation and the concentration of the Cy5-nucleosomes results in the rate constant of dinucleosome formation. According to the results shown in figure 3-6 A, H2BK34ub nucleosomes show significantly higher dinucleosome formation frequency ($7.91 \pm 0.51 \times 10^3$ $M^{-1}s^{-1}$) than unmodified ($4.28 \pm 0.36 \times 10^3$ $M^{-1}s^{-1}$) and H2BK120ub ($3.86 \pm 0.30 \times 10^3$ $M^{-1}s^{-1}$) nucleosomes. The frequency of dinucleosome stacking events should not be affected by any changes in the nucleosomes if the event is driven solely by a simple collision. This is because the change(s) in a nucleosome can be sensed by the other nucleosome only after they collide and stack already. Therefore, if dinucleosome stacking frequency is affected by any nucleosomal changes, the stacking events must be mediated by long-range interactions (i.e., undetectable with the FRET pair) following or in conjunction with a simple collision. As such, we conclude that H2BK34 facilitates long-range internucleosomal interactions.

A

Dinucleosome formation	unmodified	H2BK34ub	H2BK120ub
Number of events (with 10 nM nucleosomes)	130 ± 11	248 ± 16	155 ± 12
Total observation time (hours)	844	870	1114
Formation frequency (x10^3 $M^{-1}s^{-1}$)	4.28 ± 0.36	7.91 ± 0.51	3.86 ± 0.30
$\Delta G_{stacking}$ (kJ/mol)	–20.3 ± 0.3	–23.1 ± 0.2	–19.6 ± 0.5

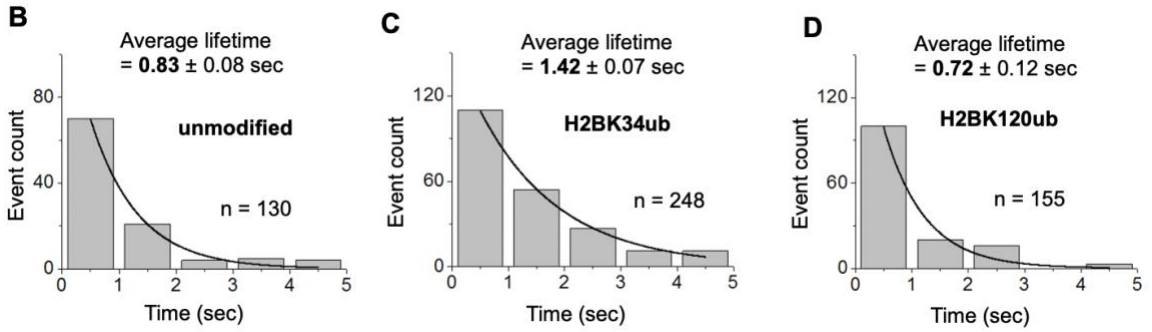

Figure **3-6**: Dinucleosome formation frequencies and stabilities.

(A) The total number of observed events of dinucleosome formation, total observation times, event frequencies, and free energy of dinucleosome formation ($\Delta G_{stacking}$) with the associated binomial errors for unmodified, H2BK34ub, and H2BK120ub nucleosomes. The calculation of $\Delta G_{stacking}$ also used the dinucleosome stabilities shown in the histograms of the durations of dinucleosome stacks in (B) unmodified, (C) H2BK34ub, and (D) H2BK120ub cases. The sample sizes are denoted by 'n'. Solid black lines indicate fitting with a single exponential decay function whose time constant is the average lifetime of the dinucleosomes. The considerably longer dinucleosome lifetime of H2BK34ub indicates strengthened internucleosomal interactions once dinucleosomes form. Data were collected by Bhaswati Sengupta and analyzed by Mai Huynh.

3.4.3. Short-range internucleosomal interactions are strengthened by H2BK34 ubiquitylation

Lastly, we measured the lifetimes of dinucleosomes by measuring the durations of the FRET events (Fig. 3-5 C). We constructed the histograms of the FRET durations and fit them with a single-exponential decay function to get the average lifetimes of dinucleosome stacks in the three

nucleosome cases (Fig. 3-6 B-D). For the unmodified, H2BK34ub, and H2BK120ub nucleosomes, the average lifetimes of the dinucleosomes are 0.82 ± 0.08 sec, 1.42 ± 0.07 sec, and 0.72 ± 0.12 sec, respectively, showing significantly more stable dinucleosomes with H2BK34ub. As the stability of dinucleosomes should be governed largely by short-range internucleosomal interactions, we conclude that H2BK34ub strengthens short-range internucleosomal interactions.

As we have both dinucleosome formation and dissociation (= 1/lifetime) rates, we can compute the equilibrium constant (i.e., K = dinucleosome formation rate × lifetime) and the free energy change of dinucleosome formation at 25 ^{o}C which is our experimental condition ($\Delta G_{stacking} = -RT\ lnK$) (Fig. 3-6 A). According to the results, the thermodynamic stability of dinucleosomes relative to nucleosomes is the same within error between the unmodified and H2BK120ub nucleosomes while it is significantly higher with H2BK34ub nucleosomes ($\Delta\Delta G_{stacking} = -2.8 \pm 0.4$ kJ/mol between H2BK34ub and unmodified nucleosomes). The difference is larger than the thermal energy at 25 ^{o}C which is 2.5 kJ/mol (= RT, where R is the gas constant and T is temperature), indicating that H2BK34ub significantly facilitates nucleosome stacking thermodynamically as well.

3.5. Discussion

We found a significant decrease in the FRET efficiency of the H2BK34ub nucleosome (to 0.77 ± 0.01 from 0.92 ± 0.01 of the unmodified nucleosome), which corresponds to a considerable increase in the distance between the FRET donor and the acceptor. Given the location of the fluorophores (Fig. 3-3 A), this increase may be attributed to inter-gyre gap widening or DNA unwrapping. The decreased FRET efficiency is still very high compared to a stable mid-range FRET (~0.5) observed from a DNA unwrapped state in the DNA-(H2A-H2B) region as we

previously reported during transcription elongation (Kim et al. 2015, Huynh et al. 2020). Therefore, we conclude that the FRET decrease is likely due to the widening of the gap between the DNA gyres in the H2BK34ub nucleosome. This is in line with the cryo-EM structures of nucleosomes reconstituted with H2BK34ub, suggesting that the ubiquitin moieties may protrude between the DNA gyres (Li et al. 2017, Chu et al. 2019). This protrusion would destabilize DNA-histone contacts in the DNA-(H2A-H2B) region and make the nucleosome conformationally more dynamic than unmodified nucleosomes, facilitating genome transactions in the nucleosome (Krajewski et al. 2018, Krajewski 2019, Krajewski 2018). Expedited hexasome generation from H2BK34ub nucleosomes by histone chaperone Nap1 supports this mechanism (Krajewski et al. 2018, Machida et al. , Li et al. 2017, Krajewski 2020b, Krajewski 2020a). A similar effect was observed with H2BK120ub albeit to a much lesser extent (Krajewski et al. 2018, Krajewski 2018, Krajewski 2020b), possibly because the ubiquitin is far from the DNA-histone contact region and likely sits on the lateral surface of the histone core (Krajewski 2019).

Long-range internucleosomal interactions are mediated by histone tails (Zheng and Hayes 2003). For instance, Chen *et al.* showed interactions between H4 tail R17-R23 residues and the H2A-H2B surface of neighboring nucleosomes (Chen et al. 2017). Although dinucleosome formation is a thermodynamically favorable process, the formation frequency is low as long-range internucleosomal interactions are weak (Lee et al. 2011, Dhall et al. 2014). According to our results, H2BK34ub elevates the rate of dinucleosome formation (to $7.91 \pm 0.51 \times 10^3$ $M^{-1}s^{-1}$ from $4.28 \pm 0.36 \times 10^3$ $M^{-1}s^{-1}$ for unmodified nucleosomes). Possible scenarios to explain this effect are (i) ubiquitin molecules directly participate in long-range internucleosomal interactions and (ii) ubiquitin molecules relax the nucleosome structure around the DNA-(H2A-H2B) region, which may facilitate long-range internucleosomal interactions. We ruled out scenario (i) because the effect is not observed with H2BK120ub. Therefore, we conclude that the relaxed DNA-(H2A-H2B) region may contribute to long-range internucleosomal interactions between DNA and histone tails.

Relaxed structures in this region will make nucleosomes prone to partial disassembly to hexasomes as we previously reported (Huynh et al. 2020). The formation of stable dinucleosome stacks between an intact nucleosome and a hexasome has been reported upon nucleosome remodeling (Kato et al. 2017).

Once a dinucleosome stack is formed, it spontaneously disassembles after a short period of time (~ 1 sec). The average lifetime of dinucleosomes before they dissociate is significantly longer with H2BK34ub (1.42 ± 0.07 sec compared to 0.83 ± 0.08 sec for unmodified nucleosomes), indicating that shorter-range internucleosomal interactions are also strengthened by H2BK34ub. The effect is likely due to the relaxed nucleosome structure around the DNA-(H2A-H2B) contact region. Based on our analysis of the dinucleosome formation rate and stability, we found significantly lower $\Delta G_{stacking}$ with H2BK34ub, demonstrating that H2BK34ub facilitates internucleosomal compaction both kinetically and thermodynamically. We do not observe any significant changes in the frequency of dinucleosome formation or the stability of dinucleosomes with H2BK120ub. It has been suggested that the ubiquitin molecules in nucleosome arrays modified with H2BK120ub interact with each other in an internucleosomal fashion to impede the condensation of the arrays (Debelouchina, Gerecht and Muir 2017a). These two effects (i.e. short-range internucleosomal ub-ub interactions and impeded internucleosomal compaction) would cancel each other in our experimental system, which may explain no effects of H2BK120ub on the short-range internucleosomal interactions.

Histone H2B ubiquitylations are implicated in facilitated transcription and hexasome formation (Fierz et al. 2011, Fleming et al. 2008, Krajewski et al. 2018). Our results suggest that the direct effects are likely from H2BK34ub inducing favorable changes in the nucleosome structure (Krajewski 2019, Krajewski 2020a) and that indirect effects are expected from H2BK120 mainly recruiting histone methyltransferase Dot1L (Anderson et al. 2019a, Valencia-Sánchez et al.

2019, Zhang and Kutateladze 2019, Worden and Wolberger 2019). The results with H2BK34ub add a support to the hypothesis that bulky polypeptide PTMs can directly program stably-altered dynamic chromatin structures that differ from canonical nucleosomes (Krajewski 2019, Krajewski 2020a). Interestingly, we also observe strengthened long- and short-range internucleosomal interactions with H2BK34ub that will facilitate chromatin compaction and help maintaining the structural integrity of chromatin. On the basis of these results, we suggest that the ubiquitin molecules in H2BK34ub nucleosomes protrude between the DNA gyres and relax the DNA-(H2A-H2B) contact region, thereby destabilizing the nucleosome. Such destabilization would play dual roles. First, it would facilitate nucleosomal processes such as transcription elongation and hexasome formation (Krajewski et al. 2018, Fleming et al. 2008, Fierz et al. 2011). Second, it would strengthen internucleosomal interactions between DNA and histone tails and help stabilize the chromatin structure (Wright and Kao 2015). In conclusion, H2BK34ub likely exerts direct effects on the nucleosome structure and dynamics, which would facilitate genome transactions while helping maintain the structural integrity of chromatin.

Chapter 4

The Effects of Histone H2B ubiquitylations and H3K79me$_3$ on Transcription Elongation

This chapter is adapted with permission from (Huynh et al. 2023). Copyright 2023 American Chemical Society.

4.1. Abstract

Histone modifications often mediate gene regulation by altering the global and local stability of the nucleosome, the basic gene packing unit of eukaryotes. We employed single-molecule FRET to investigate the effects of histone H2B ubiquitylations at K34 (H2BK34ub) and K120 (H2BK120ub) and H3K79 trimethylation (H3K79me$_3$) on the kinetics of transcription elongation by RNA Polymerase II (Pol II). Pol II pauses at several locations within the nucleosome for a few seconds to minutes, which governs the overall efficiency of transcription. We found that H2B ubiquitylations suppress pauses and shorten the pause durations near the nucleosome entry while H3K79me$_3$ shortens the pause durations and increases the rate of RNA elongation near the center of the nucleosome. We also found that H2BK34ub facilitates partial rewrapping of the nucleosome upon Pol II passage. These observations suggest that H2B ubiquitylations facilitate transcription elongation and help maintain the chromatin structure by inducing and stabilizing nucleosome intermediates and that H3K79me$_3$ facilitates Pol II progression possibly by destabilizing the local structure of the nucleosome. Our results provide the mechanisms of how these modifications coupled by a network of regulatory proteins facilitate

transcription in two different regions of the nucleosome and help maintain the chromatin structure during active transcription.

4.2. Introduction

The nucleosome is the most basic gene packaging unit in eukaryotes that contains ~147 base-pair (bp) DNA wrapping around a histone protein core made of two H2A-H2B dimers and one $(H3\text{-}H4)_2$ tetramer (Kornberg 1974, Luger et al. 1997a). Histone proteins are targets for various post-translational modifications (PTMs) such as acetylation, methylation, phosphorylation, and ubiquitylation (Bowman and Poirier 2015a, Rothbart and Strahl 2014, Fuchs, Laribee and Strahl 2009, Mersfelder and Parthun 2006). Many histone PTMs play gene regulatory roles by mediating the interactions among the nucleosome, transcription factors, chromatin remodelers, and other various enzymes or by altering the global and local structure and stability of the nucleosome (Cosgrove and Wolberger 2005, Cosgrove et al. 2004, Bannister and Kouzarides 2011). Lysine methylations and ubiquitylations can have either activating or repressive roles depending on their locations (Simon et al. 2011, Zentner and Henikoff 2013, Xu et al. 2005, Black et al. 2012, Weake and Workman 2008, Pagé et al. 2019). Ubiquitylations of H2B at K34 and K120 have been associated with enhanced processivity of RNA Polymerase II (Pol II) (Wu et al. 2014). These two modifications are coupled in the same network of protein interactions where the MOF-MSL and RNF/20/40 complexes ubiquitylate H2B K34 and K120, respectively, in an inter-dependent manner through interactions with a general transcription elongation factor Paf1C (Wu et al. 2014). An *in vitro* study has found that H2BK34 ubiquitylation (H2BK34ub) destabilizes H2A-H2B dimer association with the nucleosome, thus facilitating hexasome formation by histone chaperone Nap1 (Krajewski et al. 2018, Krajewski 2019, Krajewski 2022). Recent cryo-EM studies of H2BK34

nucleosomes reported that the ubiquitin moieties protrude the DNA gyre gap in the nucleosome and distort the DNA near the nucleosome entry region, thereby destabilizing the nucleosome and facilitating the binding of a histone methyltransferase Dot1L (Li et al. 2017, Ai et al. 2022). However, no report is currently available to show how such effects of H2BK34ub directly regulate the kinetics of transcription elongation by Pol II. An important feature of the transcription kinetics through the nucleosome is that Pol II faces numerous kinetic barriers. These barriers are imposed by strong DNA-histone interactions which induce pauses of Pol II. These pauses can last for a few seconds to minutes and thus govern the overall efficiency of transcription since the actual elongation rate of RNA is very fast at 40 – 50 nucleotides per second (Bintu et al. 2012, Chen et al. 2019). K120 is another target for ubiquitylation at H2B. While ubiquitylation at H2BK120 (H2BK120ub) exhibits only a moderate impact on nucleosome stability, it has been studied more actively for its role in recruiting Dot1L to methylate histone H3 at K79, which has been coupled to active transcription (Krajewski et al. 2018, Fierz et al. 2011, Fierz et al. 2012, Chatterjee et al. 2010, Valencia-Sánchez et al. 2019, Jang et al. 2019, Zhang and Kutateladze 2019, Anderson et al. 2019b, Worden et al. 2019, Ljungman et al. 2019). Trimethylation at H3 K79 ($H3K79me_3$) promotes transcription *in vitro* and is associated with highly active genes (Schübeler et al. 2004, Wang et al. 2008, Ljungman et al. 2019) although there has not been any report showing how $H3K79me_3$ alters the transcription kinetics through the nucleosome. A structural study hinted at a possible role for dimethylated H3K79 ($H3K79me_2$) inducing a rearrangement of the local histone surface while no change was observed in the global structure of the nucleosome (Lu et al. 2008).

Here, we investigated the effects of H2BK34ub, H2BK120ub, $H3K79me_3$, and $H3K79me_3$/H2BK120ub on the kinetics of transcription elongation by Pol II through the nucleosome and the status of DNA rewrapping after Pol II passage. We employed semi-synthetic approaches to introduce these modifications and a highly refined *in vitro* transcription system where we used single-molecule FRET (smFRET) to monitor the nucleosome dynamics during and after

Pol II passage in real-time in a time-resolved manner. Our approaches and system enabled investigations of transcription kinetics at the nucleosome level without any interference from unknown or ambiguous factors, which will help interpret the previous and future *in vivo* results in depth. Our results indicate that H2B ubiquitylations and H3K79me$_3$ accelerate transcription via two different mechanisms. H2B ubiquitylations facilitate transcription by suppressing pauses at the nucleosome entry and shortening the entry pause durations while H3K79me$_3$ shortens the pause durations and increases the rate of elongation toward the internal region of the nucleosome. We also found that H2BK34ub results in a significantly increased population of nucleosome intermediates with partially rewrapped DNA upon Pol II passage. These results provide the mechanisms of how H2BK34ub, H2BK120ub, and H3K79me$_3$ that are coupled by a network of regulatory proteins facilitate transcription in two different regions of the nucleosome and how H2BK34ub may help keep the structural integrity of chromatin during active transcription.

4.3. Materials and Methods

4.3.1. Histone Preparation

Human histone proteins H3, H4, and H3 C110A K79C were purchased from the Histone Source (Colorado State University, Fort Collins, CO). Plasmids containing wild type human histone proteins H2A and H2B were kindly provided by Dr. Song Tan (Pennsylvania State University, University Park, PA). Plasmids expressing human H2B mutants with either K34C or K120C mutation were generated via site-directed mutagenesis. Histone H3 with K79 trimethylation was prepared following published protocols (Simon et al. 2007). Briefly, histone protein H3 with K79C mutation was dissolved in alkylation buffer (1 M HEPES, 10 mM D/L-methionine, 4 M

guanidium−HCl, 20 mM DTT) and incubated for 1 h at 37 °C. Then, 100 mg of (2-bromoethyl) trimethylammonium bromide was added to the reaction mixture, followed by heating at 50 °C with occasional stirring for 2.5 h. A 10 μL aliquot of 1 M DTT was then added, and the reaction was allowed to proceed for another 2.5 h. Excess β-mercaptoethanol (BME) was added to the reaction mixture to quench the reaction. The reaction results in the product trimethylated aminoethylcysteine which has the β carbon of the trimethylated lysine side chain replaced with a sulfur (i.e., the methyl group linkage replaced with a thioether linkage). This mimetic has been shown to reproduce biochemical activities of H3K79me$_3$ (Simon et al. 2007). We will call this mimetic H3K79me$_3$ for simplicity. The product was analyzed with mass spectrometry to confirm its modification and purity (Fig. 4-1). Histone H2B with K34 or K120 ubiquitylation was prepared following published protocols (Long, Furgason and Yao 2014a, Murawska et al. 2020). A plasmid expressing His-TEV-ubiquitin G76C was acquired from Addgene (Watertown, MA) and the protein was purified using Talon beads (Takara Bio Inc., Japan) following published protocols (Long et al. 2014a, Murawska et al. 2020). Briefly, ubiquitin and histone H2B were both dissolved in 50 mM Tris-HCl (pH 8.6) and 6M Urea. They were then mixed with the molar ratio of two histone proteins per one ubiquitin followed by the addition of TCEP to 5 mM and dichloroacetone. The reaction results in a nonhydrolyzable ubiquitylated histone H2B mimetic which has been used for biochemical and structural studies of H2B ubiquitylated nucleosomes (Long et al. 2014a, Murawska et al. 2020). We call these H2B ubiquitylation mimetics H2BK34ub and H2BK120ub for simplicity. SDS-PAGE was used to confirm the product (Fig. 4-2).

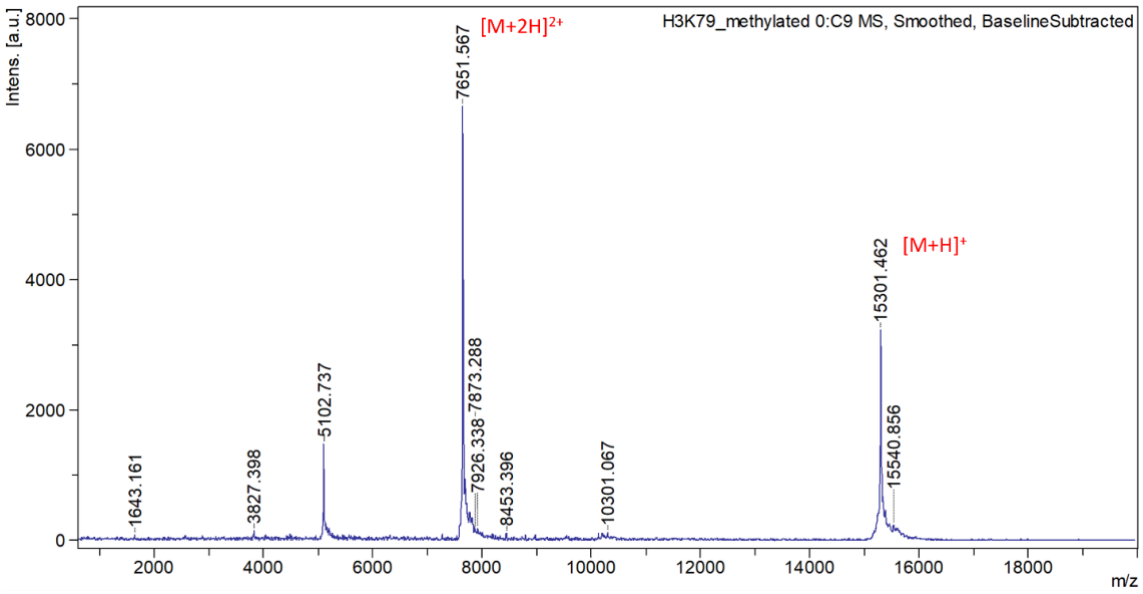

Figure **4-1**: Mass-spectrometric analysis confirms proper H3K79 trimethylation.

The peak at 15301.4 m/z denotes the trimethylated H3 monomer (calculated molecular weight: 15299.7 Da)

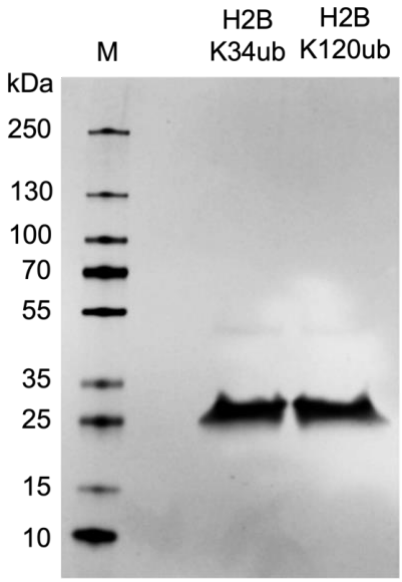

Figure **4-2**: SDS page analysis confirms histone H2B ubiquitylations.

The molar masses for H2B and ubiquitin are 14 kDa and 9 kDa, respectively.

4.3.2. DNA Preparation

Nine DNA fragments (see Table. 4-1 for sequences) were purchased (Integrated DNA Technologies, Coralville, IA). The fragments were annealed and ligated to form nucleosomal DNA containing the Widom 601 sequence (Lowary and Widom 1998). The EC-42 strands (see Table. 4-1 for sequences) with a 9-nt mismatch followed by a G-less cassette were ligated to the nucleosome entry site. The +34 and +112 nucleotides counted from the nucleosome entry site were labeled with NHS-ester functionalized Atto647N and Cy3 via the amine-functionalized C6 linkers coupled to the thymine bases (Integrated DNA Technologies, Coralville, IA). Another FRET pair was used where the +57 and +138 nucleotides counted from the nucleosome entry site were labeled with the same FRET pair, NHS-ester functionalized Atto647N and Cy3.

Table **4-1**: Sequences of DNA oligos used to generate the transcription template containing a Widom 601 nucleosome positioning sequence.

"iAmMC6T" denotes the modification of thymine with C6 amine linker (Integrated DNA Technologies, Coralville, IA) for fluorophore labeling. The EC template region contains a 9-nucleotide mismatch that mimics a transcription bubble ahead of the nucleosome.

DNA fragment	Sequence (5' – 3')
F1	/5Phos/GCAG ATC GAG AAT CCC GGT GCC GAG GCC GCT CAA
F2	/5Phos/ TTGG /iAmMC6T/CGT AGA CAG CTC TAG CAC CGC TTA AAC GCA CGT ACG CGC TGT CCC CCG CGT TTT AAC CGC CAA GGG GAT TAC
F2_alternate	/5Phos/TTG GTC GTA GAC AGC TCT AGC ACC GCT /iAmMC6T/ AAA CGC ACG TAC GCG CTG TCC CCC GCG TTT TAA CCG CCA AGG GGA TTA C
F3	/5Phos/ TCC C/iAmMC6T/AGT CTC CAG GCA CGT GTC AGA TAT ATA CAT CCG AT
F3_alternate	/5Phos/TCC CTA GTC TCC AGG CAC GTG TCA GAT ATA /iAmMC6T/ ACA TCC GAT
F4	/5Phos/GCG GCC GCG TAT AGG GTC CAT CAC ATA AGG GAT GAA CTC GGT GTG AAG AAT CAT GCT TTC CTT GGT CAT T/3Bio/
R0	AAT GAC CAA GGA AAG CAT GAT TCT TCA CAC CGA GTT CAT CCC TTA TGT GAT GGA CC
R1	/5Phos/CTA TAC GCG GCC GCA TCG GAT GTA TAT ATC TGA CAC GTG CCT GGA GAC TAG GGA GTA ATC CCC TTG GCG GTT AAA ACG CGG GG
R2	/5Phos/GAC AGC GCG TAC GTG CGT TTA AGC GGT GCT AGA GCT GTC TAC GAC CAA TTG AGC GGC CTC GGC ACC GGG ATT CTC GAT
EC Template	/5Phos/CTG CGC CAC CGC GGT CTA GAG GAT CCC CGG GAG TGG AAT GAG AAA TGA GTG TGA AGA GCT AAT TGA CTG ACG TAA GC
EC Non-Template	GCT TAC GTC AGT CTG GCC ATC TTT CAC ACT CAT TTC TCA TTC CAC TCC CGG GGA TCC TCT AGA CCG CGG TGG C

4.3.3. Nucleosome Reconstitution

Histone proteins were mixed in stoichiometric amounts and eluted through a HiLoad 16/600 Superdex 200pg column (GE Healthcare) to produce H2A-H2B dimers and $(H3\text{-}H4)_2$ tetramers separately (Luger et al. 1999a). Nucleosomes were reconstituted by dialyzing a stoichiometric mixture of histones and DNA in a dialysis device (Slide-A-Lyzer MINI Dialysis Device, 7K MWCO, Thermo Fisher Scientific) against 1X TE (pH 8.0) buffer with stepwise dilution of salt at 850, 650, 500, 300, and 2.5 mM NaCl (Luger et al. 1999a, Luger et al. 1999b). In total, five sets of nucleosomes were assembled: nucleosomes with no modification (wild type), H2BK34ub, H2BK120ub, $H3K79me_3$ and $H3K79me_3$/H2BK120Kub. All assembled transcription templates containing the nucleosome were gel-purified by the crush and soak method and confirmed by native PAGE (Fig. 4-3).

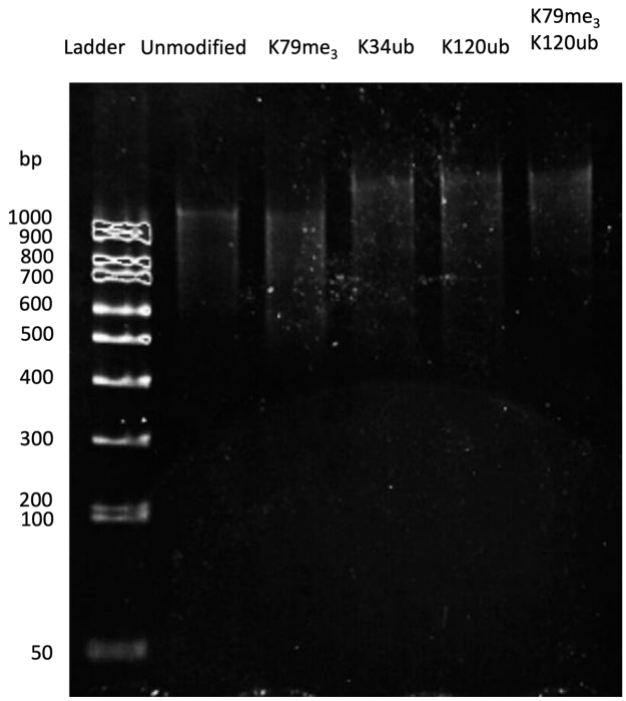

Figure **4-3**: Native PAGE analyses confirm the assembly of the transcription templates containing the nucleosomes with the modifications marked on the top of the gel.

4.3.4. Pol II and TFIIS Purification

Yeast Pol II was purified from *Saccharomyces Cerevisiae* as described in a previous publication (Brooks Crickard and Reese 2019). Briefly, yeast cells expressing Pol II with a TAP tag at Rpb4 were grown in YPD media with 20 μg/mL adenine sulfate. Yeast cells were harvested by centrifugation at 6,000 g and stored at –80 ºC in Lysis buffer (250 mM Tris-HCl pH 7.5, 5 mM EDTA, 50 μM $ZnCl_2$, 50 % glycerol, 5 % DMSO, 4 mM leupeptin, 5 mM pepstatin A, 2 mM aprotinin, 2 mM benzamidine, 10 mM DTT). Yeast cells were then thawed, lysed by homogenizer (EmulsiFlex-C3, AVESTIN, Canada), and centrifuged at 6000 g to collect the supernatant. The supernatant was centrifuged at 20,000 rpm twice for an hour and filtered through a sterilized gauze pad to remove any lipid residue. The filtered supernatant was purified with an IgG-Sepharose column followed by purification with a MonoQ column at 4 ºC. The elution fractions were collected and analyzed by SDS-PAGE to confirm the presence and purity of yeast Pol II.

A plasmid to express His-tagged TFIIS was kindly provided by Dr. Joseph Reese (Pennsylvania State University, University Park, PA). His-tagged TFIIS was expressed in *BL21(DE3)pLysS* cells in 2-YT media with 100 μg/mL ampicillin. Cells were harvested by centrifugation at 6,000 g and stored at –80 ºC in Lysis buffer (20 mM Tris-HCl pH 7.5, 0.5 M NaCl, 10 mM imidazole, 10 μM $ZnCl_2$, 10 % glycerol, 1 mM PMSF, 2 mM benzamidine). Cells were then thawed, lysed by homogenizer (EmulsiFlex-C3, AVESTIN, Canada), and centrifuged at 16,000 g for 30 min to collect the supernatant. The supernatant was incubated with Talon beads (Takara Bio Inc., Japan) for an hour at 4 ºC. The beads were then washed multiple times and eluted with 150 mM imidazole. The elution was collected in 0.5 mL fractions and analyzed by SDS-PAGE.

4.3.5. Formation of Transcription Elongation Complex

The assembled transcription template was diluted in 50 µL of transcription buffer (60 mM KCl, 1 mM $MnCl_2$, 50 mM K-HEPES (pH 7.8), 0.5 mM DTT, and 10% glycerol) to 10 nM followed by the addition of 9.5 nM Pol II, 0.3 mM UpG primer, 0.1 mg/mL BSA, and 2 unit/µL RNasin RNase inhibitor. The reaction mixture was incubated for 5 min at 30 °C to allow Pol II docking on the 9-nt DNA bubble. To initiate transcription, a mixture of ATP, CTP, and UTP each at 1 mM was added to the Pol II-DNA complex, and then incubated for another 30 min at 30 °C. Due to the lack of GTP in the system, the elongation process is halted at the end of the G-less cassette.

4.3.6. Single-Molecule FRET Measurements

Surface Preparation for smFRET Measurements

Pre-drilled microscope quartz slides were purchased from G. Finkenbeiner Inc. (Waltham, MA). The slides were cleaned thoroughly following the published protocols (Lee et al. 2019a). Briefly, the slides were immersed in acetone, dichloromethane, and methanol in series and sonicated for 15 min each. They were then subjected to KOH etching and finally dipped in a Nochromix® (Alconox, White Plains, NY) solution in concentrated sulfuric acid. Finally, they were dried using nitrogen, then coated with 1:50 biotin-PEG-silane (Laysan Bio Inc., Arab, AL) and PEG-silane (Laysan Bio Inc., Arab, AL). Five flow channels were constructed on the slide.

Nucleosome Dynamics during Transcription Elongation by Pol II

A streptavidin solution (40 µL, 0.1 mg/mL) was injected into a channel constructed on a microscope slide and incubated for 15 mins for biotin-streptavidin conjugation. After 15 minutes, unbound streptavidin was removed by washing with 40 µL wash buffer (10 mM NaCl and 10 mM K-HEPES, pH 7.8). A diluted transcription mixture (~1 nM final nucleosome concentration) was

injected into the channel and incubated for 5 minutes for the nucleosomes to conjugate to streptavidin on the surface. After 5 minutes the unbound nucleosomes were washed with wash buffer containing protocatechuic acid (10 mM, MilliporeSigma, MA) and protocatechuate 3,4-dioxygenase (1 unit/uL, MilliporeSigma, MA). The slide was then placed on an smFRET microscope which is custom-built on a commercial inverted microscope (Nikon TE2000, Japan). Right before recording the fluorescence images, the imaging buffer (a complete set of NTP at 0.4 mM, 30 nM TFIIS, 1 unit/mL PCD, 10 mM PCA, and 1 mM Trolox in the transcription buffer, 30 µl) was injected into the channel. The fluorescence images were collected every 200 ms integrating 200 ms fluorescence signal on two spectral channels to separate the FRET acceptor signal (Atto647N, 635 nm) from that of the donor (Cy3, 532 nm) using an EMCCD (Ixon Ultra, Andor Technology, Ireland). Each stack of fluorescence images forms a movie file that was recorded for 3 minutes. To make sure that any change in the FRET efficiency was not due to Atto647N photo-bleaching, we switched on a red laser (632nm, CrystaLaser, Reno NV) to excite the acceptor directly at the end of each movie, and only those points with an acceptor signal were subject to further analysis. A total of 5 movies (15 minutes total) were collected from each channel. The time traces of fluorescence intensities from each pair of Cy3 and Atto647N were extracted from the fluorescence images.

Nucleosome unwrapping and rewrapping during and after Transcription by Pol II

The transcription reaction mixture was injected into a channel and incubated for 5 min at room temperature. The imaging buffer was then added to wash unbound nucleosomes and resume the transcription process. Immediately after the addition of the imaging buffer, three consecutive fluorescence images were recorded every 4.5 sec with 532 nm laser excitation followed by another three images with 635 nm laser excitation. All images were taken with 150 ms signal integration. The signal from 635 nm excitation is used to verify no photobleaching or blinking of Atto647N. Each stack of fluorescence images that forms a movie file was taken for 3 minutes. Under our

excitation conditions, the vast majority of Atto647N was not photobleached or blinking during imaging (Huynh et al. 2020). Ten movies from different spots were recorded and analyzed. For each of all five sets of nucleosomes, at least 5 independent measurements were made.

4.3.7. Transcription Efficiency Assay

The transcription elongation complex was generated as mentioned above except Cy3-UTP was used in the NTP mix to resume transcription at the end of the G-less cassette. The transcription reaction were incubated for 30 minutes at 30 ^{o}C and subsequently terminated by 2X stop buffer (30 mM Tris-HCl pH 8.0, 100 mM NaCl, 5 mM EDTA, and 1% SDS). The resulting transcription reaction was incubated with Proteinase K for 30 min at 37 ^{o}C to release RNA from the elongation complex, and then with streptavidin agarose beads for 1 hour to pull down biotinylated DNA. RNA was extracted with PCIAA (Phenol:Chloroform:Isoamyl alcohol) and precipitated with chilled ethanol and 4μg glycogen. Solid RNA was then dissolved in RNA loading buffer (5 mM EDTA in formamide), heated at 65 ^{o}C for at least 10 min, and loaded to 8% urea gel. Fluorescent gel images were taken with Typhoon (GE Healthcare) and analyzed with ImageJ for intensities.

4.4. Results

4.4.1. A single-molecule FRET system reports nucleosome dynamics during transcription

Previous studies have established that Pol II pauses at several DNA-histone contact points during transcription through the nucleosome (Crickard et al. 2017, Kujirai et al. 2018, Hodges et al. 2009, Kwak and Lis 2013, Jonkers et al. 2014). Using smFRET, we investigated the pause frequency, durations, and the elongation rate between pauses to reveal the effects of H2BK34ub,

H2BK120ub, and H3K79me$_3$ (Fig. 4-4 A). The fluorophores were labeled at the 34th and 112th nucleotides of the non-template strand of the nucleosomal DNA counted from the entry site, reporting DNA unwrapping and rewrapping during and after the Pol II passage. The FRET pair locations are designed to give a high-FRET efficiency when DNA is properly wrapped and to show stepwise FRET decreases as DNA unwraps during Pol II passage (Fig. 4-4 B). Without Pol II or NTP, no such FRET changes are observed for 15 minutes. We monitored the changes in FRET during Pol II passage revealing three stable states with visually distinct FRET efficiencies (Fig. 4-4 B). These stable FRET states correspond to the paused states of the elongation complex at various locations in the nucleosome (Fig. 4-5 A-D).

We named the three stable FRET states high-, mid-, and low-FRET state (Fig. 4-4 B). We assigned the high-FRET state to the early pauses at superhelical location (SHL) (-6) and (-5), the mid-FRET to the mid pauses at SHL (-2), and the low-FRET to the late pauses at SHL (-1) according to the estimated FRET efficiencies from the nucleosome structures with paused Pol II (Fig. 4-5 A-D) (Kujirai et al. 2018). Of note, only a small number of traces show the mid-FRET state, which is consistent with a previously published report that SHL(-2) is a minor swift pause (Kujirai et al. 2018).

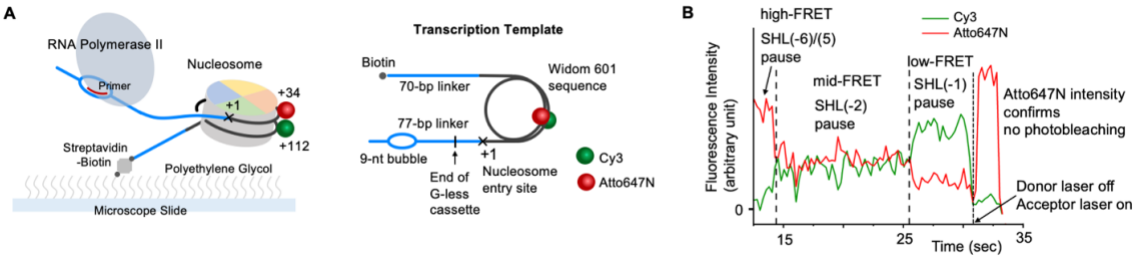

Figure **4-4**: An smFRET experimental setup shows detailed nucleosome dynamics during transcription elongation by Pol II.

(A) The structure of the transcription template containing a 601 nucleosome sequence and surface immobilization scheme to monitor smFRET signals from the nucleosome. A FRET pair (Cy3 and

Atto647N for donor and acceptor, respectively) was labeled at the nucleosomal DNA, reporting the nucleosome dynamics during Pol II progression. (B) An example showing the intensity traces of the FRET donor (Cy3, green) and the acceptor (Atto647N, red) during Pol II progression through the nucleosome. A high-FRET state indicates a pause event at SHL(-6) or SHL(-5), a mid-FRET state indicates a pause event at SHL(-2), and a low-FRET state indicates a pause event at SHL(-1) according to the structural analysis with the FRET pair locations (Fig. 4-5).

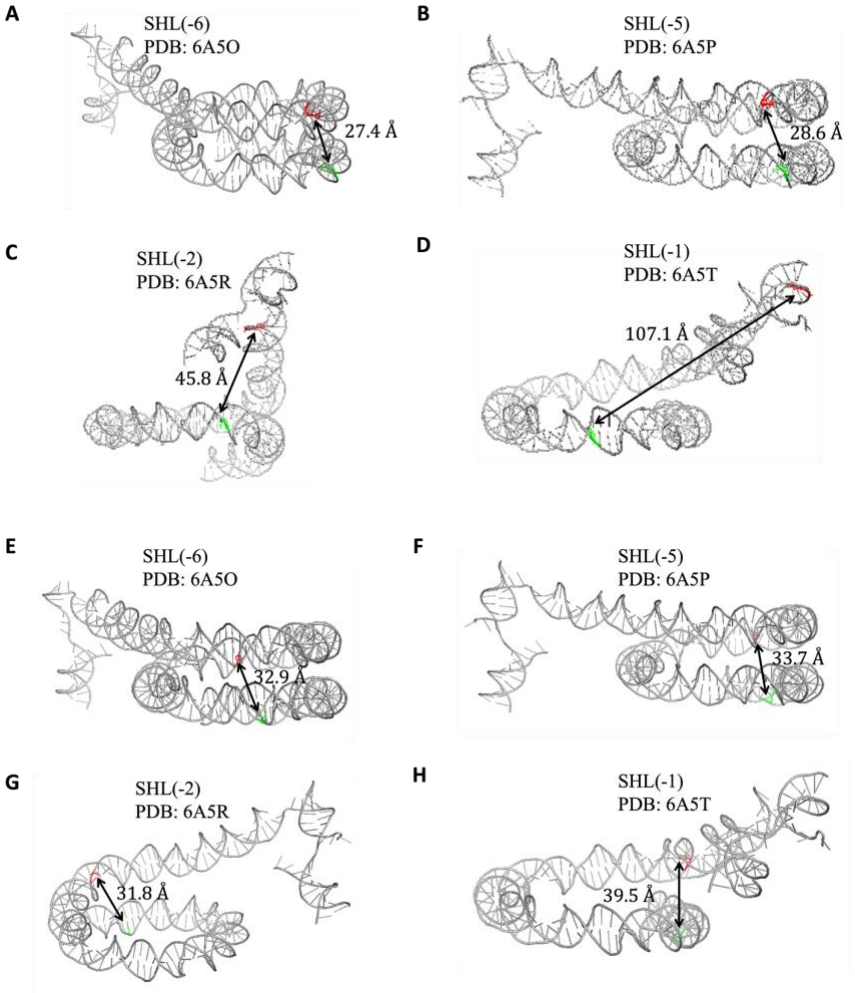

Figure **4-5**: FRET distance estimation from cryo-EM structures for two FRET pairs used in our measurements.

(A-D) The distances between the FRET donor and acceptor were estimated by measuring the distances between the two carbon atoms of the methyl groups at the 5'C atoms of the thymine

bases at the $+34^{th}$ and $+112^{th}$ nucleotides in the pauses at SHL(-6), SHL(-5), SHL(2), and SHL(-1) (PDB 6A5O, 6A5P, 6A5R, 6A5T). (E-H) The distances between the FRET donor and acceptor in the alternate FRET pair (at the $+57^{th}$ and $+138^{th}$ nucleotides) were estimated using the same method.

4.4.2. Ubiquitylated nucleosomes suppress early pauses and shorten the pause duration

We counted the number of nucleosomes showing the early pauses at SHL(-6) and SHL(-5) in the first 2 minutes after the NTP addition for Pol II progression. The early pause frequency was measured by dividing the number of nucleosomes starting with a high-FRET state by the number of total Cy3 fluorescence spots. The Cy3 spots include nucleosomes that have not been initiated for transcription, are being transcribed, and have been done with transcription. Assuming that the initiation efficiency is constant across all templates, the fraction of nucleosomes showing high FRET represents the pause density or frequency. Our results indicate that the pause frequency in the cases of H2K34ub, H2BK120ub, and H3K79me_3/H2BK120ub nucleosomes is lower than that in the unmodified case (Fig. 4-6). These results suggest that H2K34ub and H2BK120ub facilitate transcription by suppressing early pauses. Of note, the extent of the effect is a lot more significant with H2K34ub.

A

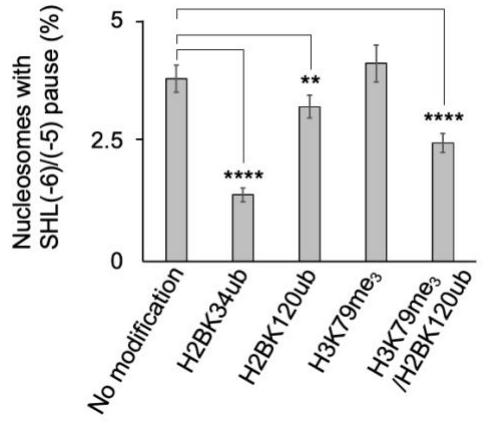

B

	Nucleosomes with SHL(-6)/(-5) pause (%)	
No modification	3.8 ± 0.3	(n = 4642)
H2BK34ub	1.4 ± 0.1	(n = 6811)
H2BK120ub	3.2 ± 0.2	(n = 5259)
$H3K79me_3$	4.1 ± 0.4	(n = 2775)
H2BK120ub /$H3K79me_3$	2.5 ± 0.2	(n = 5943)

Figure **4-6**: H2B ubiquitylations show a significantly reduced frequency of pauses at SHL(-6)/(-5).

(A) The fractions of nucleosomes showing a high-FRET state out of all nucleosomes immobilized on the surface reveal that H2B ubiquitylations suppress early pauses at SHL(-6)/(-5). (B) Numerical data for the histogram shown in A. The errors are the standard errors for binomial distributions with the given sample sizes. The binomial distribution *p*-values are <0.0001, 0.010, 0.82, and <0.0001 for H2BK34ub, H2BK120ub, $H3K79me_3$, and H2BK120ub/$H3K79me_3$, respectively. The number of asterisks designates the level of significance in the difference. Data were analyzed by Mai Huynh.

Next, we measured the pause durations which are the durations of the high-FRET states. The FRET duration histograms fit well to a single exponential decay whose time constant is the average pause duration (Fig. 4-7). Note that the histogram starts at 30 sec time point which is typically the time spent on reactant injection, flow-channel mounting, and microscope focusing. The high-FRET pause duration corresponding to the SHL(-6)/(-5) pause duration is significantly shorter in the cases of the ubiquitylated nucleosomes (13.7 ± 1.8, 16.7 ± 1.6, and 16.8 ± 1.9 sec respectively for H2BK34ub, H2BK120ub, $H3K79me_3$/H2BK120ub) than in the cases of the unmodified (22.8 ± 1.9 sec) or $H3K79me_3$ nucleosomes (22.5 ± 2.5 sec) (Fig. 4-7). It has been reported based on *in vivo* and *in vitro* studies that ubiquitylated nucleosomes promote Pol II processivity and facilitate

hexasome generation by Nap1 (Krajewski et al. 2018, Wu et al. 2014). As hexasome generation by Nap1 takes place near the DNA-(H2A-H2B) contact region, H2B ubiquitylations may destabilize the nucleosome in the entry region where SHL(-6)/(-5) are located. Therefore, our results suggest that the facilitated transcription upon H2B ubiquitylation is due to suppressed pauses and shortened pause durations in the SHL(-6)/(-5) region.

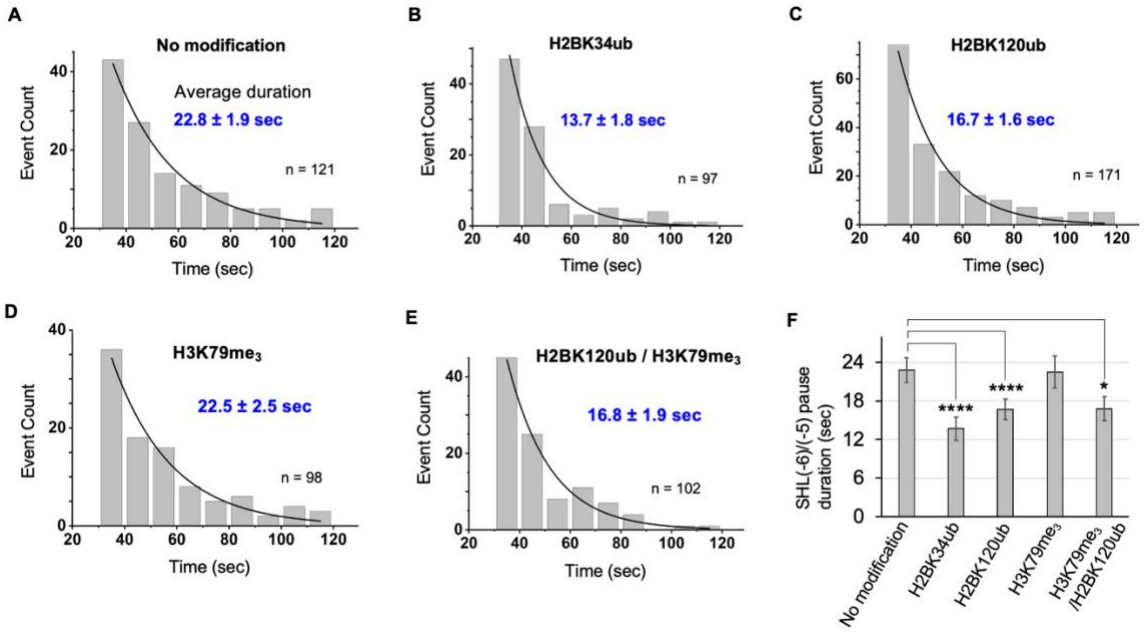

Figure **4-7**: Histone H2B ubiquitylations shorten the duration of the early pauses at SHL(-6) and SHL(-5).

The high-FRET state duration or lifetime histograms are shown for (A) unmodified, (B) H2BK34ub, (C) H2BK120ub, (D) H3K79me$_3$, and (E) H2BK120ub/H3K79me$_3$ nucleosomes. The sample size n for each case is shown in each chart. The average and error values are from the fitting with an exponential decay function. (F) Summary of the pause durations showing shortened pause durations by H2BK34ub and K120ub. The one-sided exponential distribution *p*-values (power = 0.8) are <0.0001, <0.0001, 0.760 and 0.015 for H2BK34ub, H2BK120ub, H3K79me$_3$, and H2BK120ub/H3K79me$_3$, respectively. The number of asterisks designates the level of significance in the shortened pause duration. Data were collected by Bhaswati Sengupta and analyzed by Mai Huynh.

4.4.3. Nucleosomes with H3K79me$_3$ show increased transcription rates and reduced pause durations in the SHL(-2)/(-1) region

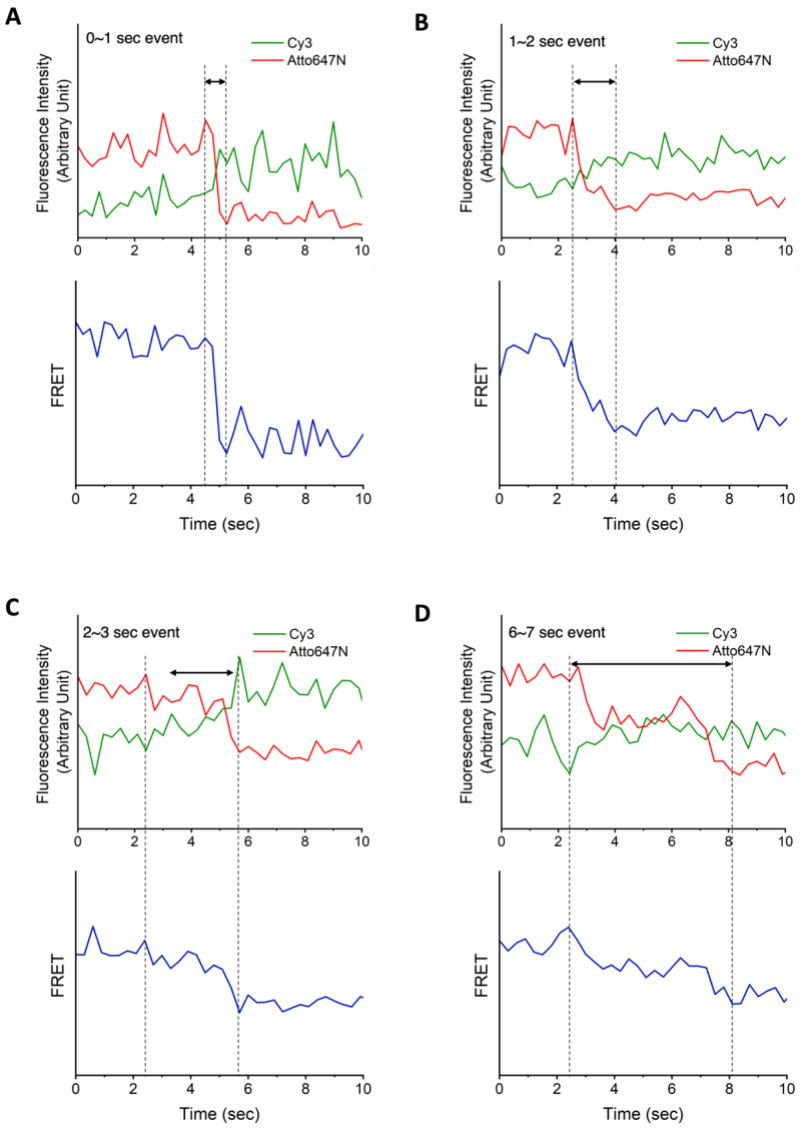

Figure **4-8**: Sample FRET trajectories showing various times of transcription elongation.

Green and red line denote Cy3 and Atto647N intensities, respectively. Blue lines represent the changes in the FRET efficiencies. (A-D) The elongation times are indicated by the arrows between the two dashed lines.

To investigate the effects of H3K79me$_3$ on transcription, we measured the elongation times between pauses. We identified FRET transitions from a high- to a low-FRET state between which elongation takes place (Fig. 4-8, Fig. 4-9 A). The transition time windows include pauses at SHL(-2) which are often short-lived (Fig. 4-8). The histograms of the width of the transition time windows are well fit with a single exponential decay function (Fig. 4-9). According to the results, the H3K79me$_3$ nucleosomes show a faster elongation rate (0.83 ± 0.06 and 0.70 ± 0.04 sec or 48 ± 3 and 57 ± 3 nucleotides per second (nt/sec), respectively for H3K79me$_3$ and H3K79me$_3$/H2BK120ub nucleosomes) than the other nucleosomes (1.15 ± 0.12, 1.01 ± 0.17, and 1.04 ± 0.15 sec or 35 ± 4, 40 ± 7, and 38 ± 6 nt/sec, respectively for unmodified, H2BK34ub, and H2BK120ub nucleosomes) (Fig. 4-9 B-F). To estimate the rates in nt/sec, we assume that the early pauses are mostly at SHL(-5) as pauses at SHL(-6) are much weaker (Kujirai et al. 2018, Kireeva et al. 2005, Gaykalova et al. 2015). With the low-FRET pauses at SHL(-1), the elongation time is for transcribing 40 nucleotides. The results suggest that H3K79me$_3$ facilitates transcription by elevating the elongation rate from the entry to the SHL(-1) region. As no change in the global nucleosome structure has been identified in the H3K79me$_2$ nucleosome structure (Lu et al. 2008), we suggest that this effect may be due to local changes induced by H3K79me$_3$ that would be similar to those by H3K79me$_2$. Such changes may affect the conformational flexibility of the nucleosome near this region, which could weaken the already swift SHL(-2) pauses and facilitate Pol II passage. This suggestion led to a hypothesis that H3K79me$_3$ may shorten SHL(-2)/(-1) pause durations. To test this hypothesis, we moved the FRET pair locations near SHL(-2) at the 57th and 138th nucleotides and repeated smFRET measurements for the unmodified and the H3K79me$_3$ nucleosomes (Fig. 4-10 A). We observed two stable FRET states – high- and low-FRET states (Fig. 4-10 B). All pauses from SHL(-6) to SHL(-1) should show a high-FRET state according to the structural analysis (Fig. 4-5 E-H). As the elongation rate is very fast compared to the pause durations, the moment of a transition from a high- to a low-FRET state should be the moment when

Pol II passes through SHL(-1) at the observation time resolution of 200 ms. Accordingly, the high-FRET duration should be a convolution of all pause durations from SHL(-6) to SHL(-1). A change in the high-FRET duration should indicate a change in the pause duration at SHL(-2)/(-1) since H3K79me$_3$ does not induce any change in the pause durations at SHL(-6)/(-5). The distribution of the high-FRET duration clearly shows significantly shorter pauses for the H3K79me$_3$ nucleosomes (Fig. 4-10, 47.2 sec on average) than the unmodified nucleosomes (Fig. 4C, 56.3 sec on average), validating our hypothesis on the shortened pause durations at SHL(-2)/(-1) by H3K79me$_3$. These results show that H3K79me$_3$ facilitates Pol II passage through the nucleosome by shortening the durations of pauses at SHL(-2)/(-1), thereby elevating the rate of elongation up to SHL (-1).

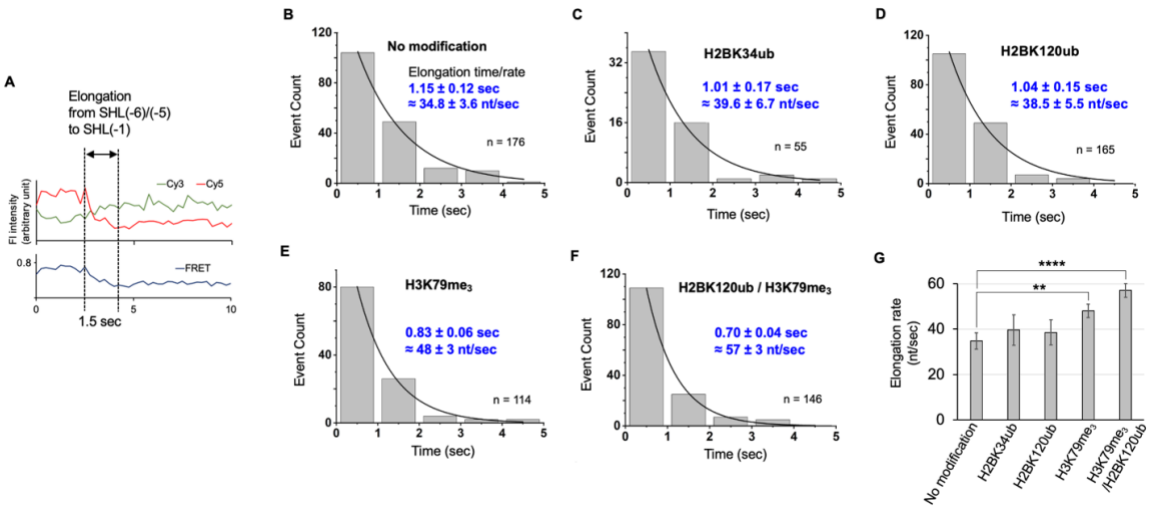

Figure **4-9**: H3K79me$_3$ increases the rate of transcription elongation .

(A) An example of fluorescence intensity traces demonstrating the elongation phase of transcription from SHL(-6)/(-5) to SHL(-1) that is indicated by a FRET transition from a high- to a low-FRET state. Elongation time histograms are shown for (B) unmodified, (C) H2BK34ub, (D) H2BK120ub, (E) H3K79me$_3$, and (F) H2BK120ub/H3K79me$_3$ nucleosomes. The sample size n for each case is shown in each chart. The elongation time and error are from fitting each histogram with an exponential decay function. The elongation rate is estimated by assuming that early pauses are mostly at SHL(-5) and consequently the measured time is to elongate 40 nucleotides. (G) Summary of the results show that H3K79me$_3$ increases the elongation rate. The one-sided exponential distribution *p*-values (power = 0.8) are 0.447, 0.324, 0.006, and <0.0001

for H2BK34ub, H2BK120ub, H3K79me$_3$, and H2BK120ub/H3K79me$_3$, respectively. The number of asterisks designates the level of significance in the increase. Data were collected by Bhaswati Sengupta and analyzed by Mai Huynh.

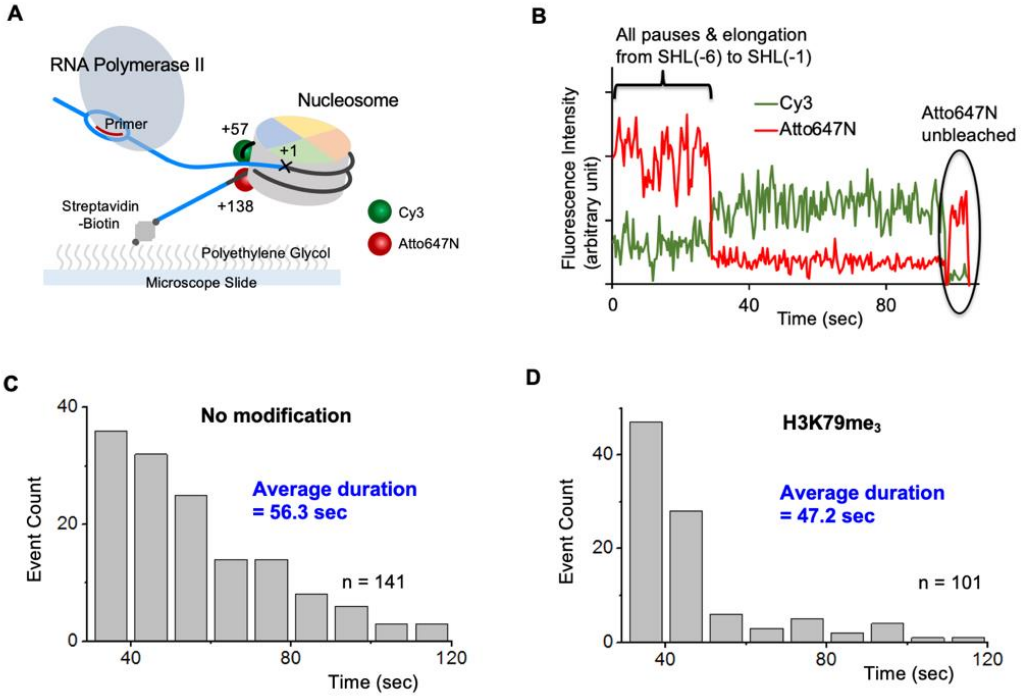

Figure **4-10**: H3K79me$_3$ shortens late pauses at SHL(-2)/(-1).

(A) Experimental setup with new FRET pair locations to investigate the late pause dynamics at SHL(-2)/(-1). According to the structural analysis with the FRET locations (Fig. 4-5), a high-FRET state is expected until Pol II passes through SHL(-1). (B) An example of fluorescence intensity traces shows an abrupt transition from a high- to a low-FRET state indicating Pol II progression through SHL(-1). High-FRET state duration histograms are shown for (C) unmodified and (D) H3K79me$_3$ modified nucleosomes. The average durations were calculated directly from the durations and their counts. These durations represent the convoluted durations of pauses from SHL(-6) to SHL(-1). A significantly shorter duration is shown in D, indicating that H3K79me$_3$ shortens the late pause durations at SHL(-2)/(1) as no change was observed in the early pause durations (Fig. 4-7). Data were collected by Bhaswati Sengupta and analyzed by Mai Huynh.

4.4.4. *In vitro* transcription assay confirms facilitated transcription

We performed an *in vitro* transcription assay where fluorescent RNA products from transcription for 30 min were extracted and analyzed on a urea gel in all five cases of the nucleosomes (Fig. 4-11 A). Three different levels of signal integration time were used to visualize the three different regions of the gel (Fig. 4-11 B). Higher amounts of RNA products are evident in all of the modified nucleosome cases, confirming facilitated transcription whose mechanisms were revealed by the smFRET measurements (Fig. 4-11 BC). The change is insignificant in the case of H2BK120ub as the effect was only weak in the single-molecule measurements as well. The assay also showed a considerably large amount of RNA products from H3K79me$_3$/H2BK120ub nucleosomes as the result should be the sum of the effects from H3K79me$_3$ which affects the SHL(-2)/(-1) region and H2BK120ub which affects the SHL(-6)/(-5) region.

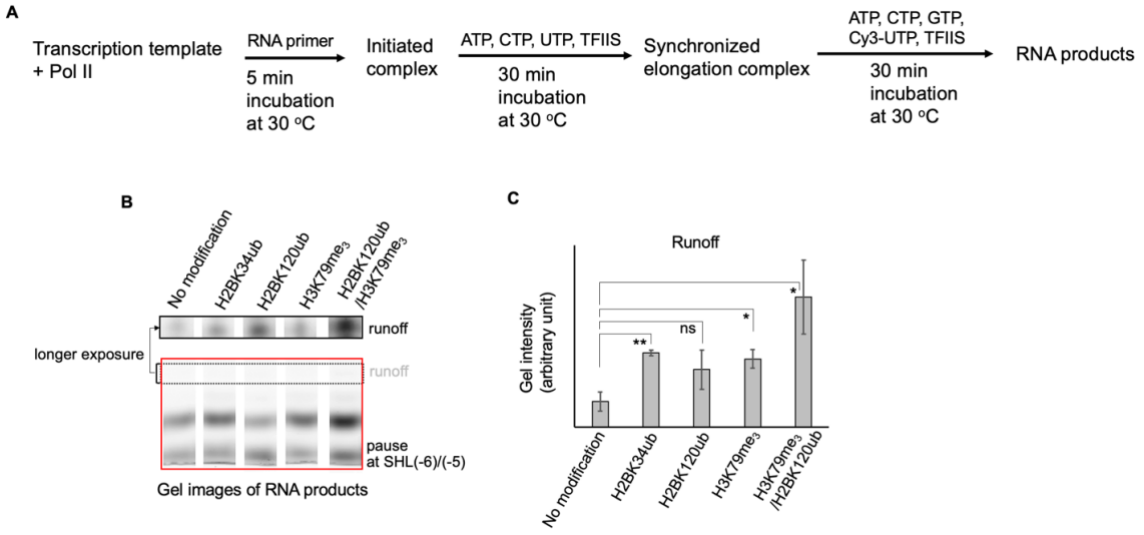

Figure **4-11**: An *in vitro* transcription assay confirms that H2B ubiquitylations and H3K79me$_3$ increases transcription efficiency.

(A) The experimental scheme for the *in vitro* transcription assay utilizing fluorescent UTP labeled with Cy3. (B) Gel images of the RNA product incorporated by Cy3-UTP. The entire gel image is shown in the red box. Four bands are apparent. The lowest band should contain the RNA products

up to the earliest pauses at SHL(-6)/(-5) as the synchronized elongation complex at the end of the G-less cassette contains no fluorescent nucleotides. The highest band should represent the runoff product. Two different signal integration/exposure times were used to image the gels more clearly in the runoff region. The black dotted-box region shows the longest RNA product on the full gel (red box). The black dotted-box region with a longer exposure time is shown in the black solid-box (runoff). (C) The amounts of the runoff products measured from the intensities of the runoff bands shown in B indicate significantly increased efficiency of transcription elongation in all of the modified nucleosomes except for the H2BK120ub case. The error bars are standard deviations from duplicate measurements. The one-sided *p*-values in the cases of H2BK34ub, H2BK120ub, H3K79me$_3$, and H2BK120ub/H3K79me$_3$, are 0.010, 0.089, 0.023, and 0.030, respectively. The number of asterisks designates the level of significance in the increased RNA production and "ns" stands for "not significant". Data were collected and analyzed by Mai Huynh.

4.4.5. H2K34ub facilitates partial DNA rewrapping upon Pol II passage

Nucleosome recovery after transcription is vital to maintaining the chromatin structure for proper gene regulation . Here, we investigated the fate of the nucleosome in the entry proximal DNA-(H2A-H2B) region after Pol II passage with the FRET pair depicted in figure 4-4 A. We modified the smFRET measurement scheme to avoid premature photobleaching of fluorophores and ensure that a FRET change is due to nucleosome dynamics rather than Atto647N blinking. In the modified scheme, fluorophores were imaged for a cycle of 1.05 sec every 4.5 sec for a total of 3 min. Each imaging cycle is made of a 450 ms period of donor excitation at 532 nm followed by a 150 ms dark period and another 450 ms period of weak acceptor excitation at 635 nm (Fig. 4-12 A). The two signals from 532 nm excitation (i.e. Cy3 signal and Atto647N signal via FRET) and the signal from 635 nm excitation (i.e. Atto647N signal from direct excitation) are plotted together at a single time point (Fig. 4-12 BC). We excluded traces that show a sign of Atto647N photobleaching or blinking (i.e. extinction of Atto647N signal from the direct 635 nm excitation cycle) from further analysis. A FRET transition from a high- to a lower FRET state indicates DNA unwrapping (Fig. 4-12 BC). Upon Pol II passage, nucleosomes may rewrap DNA completely to a

high-FRET state (Fig. 4-12 B). We counted the number of nucleosomes showing the signature of complete and stable nucleosome rewrapping after unwrapping and calculated the fraction of such nucleosomes (Fig. 4-12 D). The fractions are 14.9 ± 3.6, 19.7 ± 4.0, 18.2 ± 3.9, 14.4 ± 3.5, and 19.3 ± 3.9 % for the unmodified, H2BK34ub, H2BK120ub, H3K79me$_3$, and H3K79me$_3$/H2BK120ub nucleosomes, respectively, indicating no significant difference. In addition to the signature of complete DNA rewrapping, we also observed a FRET transition from a low- to a higher FRET state which does not recover fully to the high-FRET level where DNA unwrapping started (Fig. 4-12 C). This state indicates DNA rewrapping to an intermediate state, which we call partial rewrapping of DNA. We counted such nucleosomes and calculated the fractions (Fig. 4-12 E). The fractions are 14.3 ± 3.5, 36.7 ± 4.0, 16.8 ± 4.8, 20.2 ± 3.7, and 24.0 ± 4.3 % for the unmodified, H2BK34ub, H2BK120ub, H3K79me$_3$, and H3K79me$_3$/H2BK120ub nucleosomes, respectively, indicating a significant increase in partial DNA rewrapping by H2BK34ub. The sum of the full and partial DNA rewrapping fractions are 29.2 ± 5.0, 56.4 ± 6.0, 35.0 ± 5.3, 34.6 ± 5.3, and 43.2 ± 5.8 % for the unmodified, H2BK34ub, H2BK120ub, H3K79me$_3$, and H3K79me$_3$/H2BK120ub nucleosomes, respectively, indicating that more than half of H2BK34ub nucleosomes have partially or fully rewrapped DNA upon Pol II passage. Structural studies have suggested that ubiquitin may have stable nonspecific interactions with DNA and may also interact with histone proteins via its acidic regions (Debelouchina, Gerecht and Muir 2017b, Landré et al. 2017, Li et al. 2017). Therefore, the interactions between the ubiquitin and the nucleosome can help the nucleosome retain the ubiquitylated H2A-H2B dimer within the complex, which may help reassembly of the nucleosome. As H2BK120ub nucleosomes displayed no significantly increased rewrapping, we suggest that this effect depends on the location of ubiquitin. As the two ubiquitin molecules in H2BK34ub nucleosomes may protrude between the two gyres of the nucleosomal DNA, they may contact DNA readily to assist H2A-H2B retention and DNA rewrapping while the ubiquitin molecules in

H2BK120ub nucleosomes are farther away from histone-DNA interfaces to interact effectively with DNA.

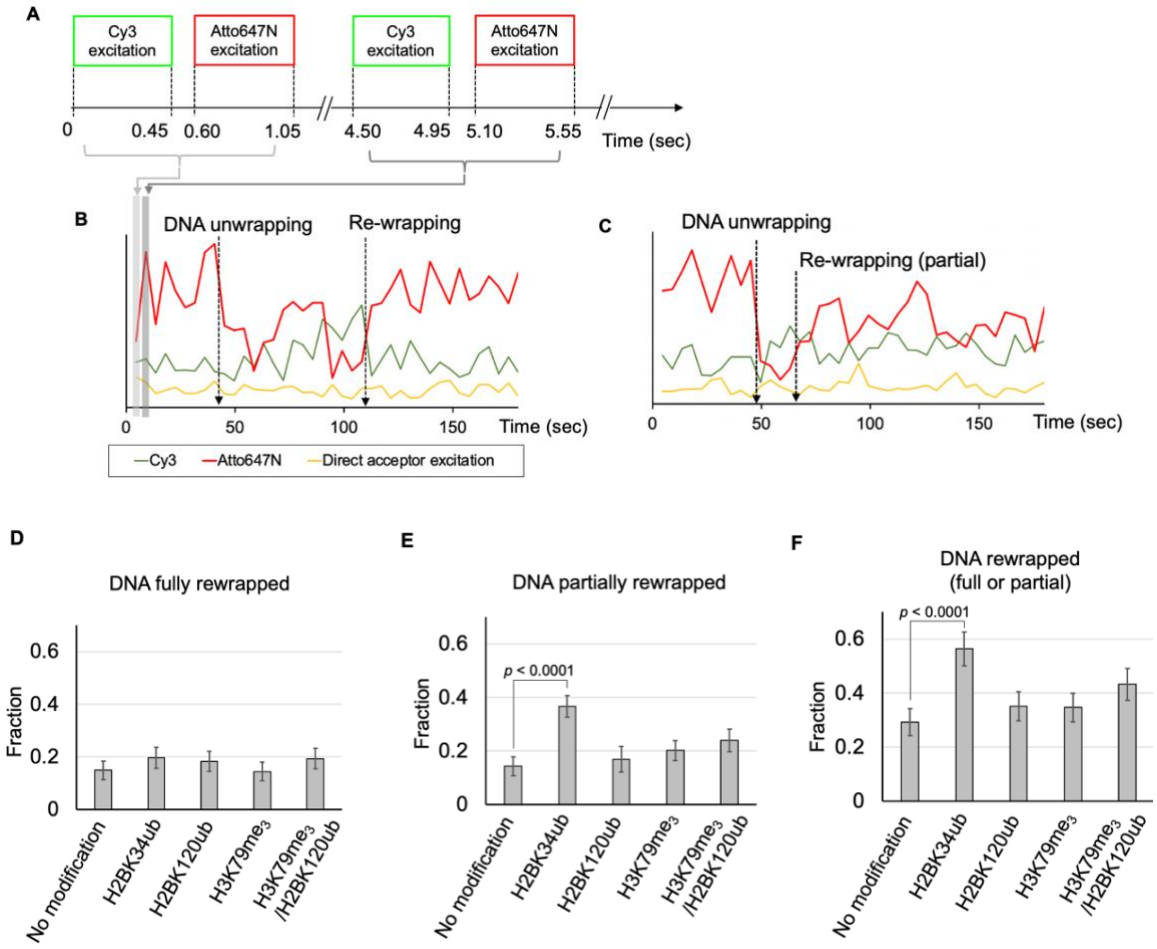

Figure **4-12**: H2BK34ub facilitates partial DNA rewrapping upon Pol II passage .

(A) The intermittent FRET excitation scheme to investigate the status of the nucleosomal DNA unwrapping and rewrapping without photobleaching of the fluorophores and interference from Atto647N blinking for 3 minutes. (B) An example of fluorescence intensity traces shows the signatures of DNA unwrapping and rewrapping. A high-FRET state in the beginning indicates the intact nucleosome before transcription. Some FRET dynamics follow as Pol II progresses through the nucleosome. The complex reaches a high-FRET state at around ~110 sec time point, suggesting complete DNA rewrapping. (C) An example of fluorescence intensity traces shows the signatures of DNA unwrapping and partial rewrapping. Upon Pol II progression coinciding with some FRET dynamics in the ~50 – 65 sec window, the complex reaches a state with fluctuations between mid- to high- FRET, which is not the completely rewrapped state, suggesting partial DNA rewrapping.

(D) The fractions of the nucleosomes showing the signature of DNA rewrapping are constant among all nucleosomes investigated. The fractions are 14.9 ± 3.6, 19.7 ± 4.0, 18.2 ± 3.9, 14.4 ± 3.5, and 19.3 ± 3.9 % for the unmodified, H2BK34ub, H2BK120ub, H3K79me$_3$, and H3K79me$_3$/H2BK120ub nucleosomes, respectively. (E) The fraction of the nucleosomes showing the signature of partial DNA rewrapping is significantly higher with H2BK34ub. The fractions are 14.3 ± 3.5, 36.7 ± 4.0, 16.8 ± 4.8, 20.2 ± 3.7, and 24.0 ± 4.3 % for the unmodified, H2BK34ub, H2BK120ub, H3K79me$_3$, and H3K79me$_3$/H2BK120ub nucleosomes, respectively. The one-sided binomial distribution *p*-value for a higher fraction with H2BK34ub is <0.0001. (F) The sum of the fractions in D and E show the fractions of the nucleosomes with full or partial DNA rewrapping upon Pol II passage. The fractions are 29.2 ± 5.0, 56.4 ± 6.0, 35.0 ± 5.3, 34.6 ± 5.3, and 43.2 ± 5.8 % for the unmodified, H2BK34ub, H2BK120ub, H3K79me$_3$, and H3K79me$_3$/H2BK120ub nucleosomes, respectively. The sample sizes are 167, 259, 214, 105, and 192 nucleosomes that do not show any sign of blinking or photobleaching for 3 minutes after transcription start for the unmodified, H2BK34ub, H2BK120ub, H3K79me$_3$, and H3K79me$_3$/H2BK120ub nucleosomes, respectively. The one-sided binomial distribution *p*-value for a higher fraction with H2BK34ub is <0.0001. All the errors shown in D-F are the standard errors for binomial distributions with the given sample sizes. Data were collected and analyzed by Mai Huynh.

4.5. Discussion

Histone proteins are rich targets for various PTMs that are often associated with gene regulation. Some mimetics of these PTMs have been implemented with semi-synthetic methods to construct highly-refined *in vitro* experimental systems. For example, histone methylations via aminoethylation of cystine have been published to successfully reproduce their biochemical functions (Hintzen et al. 2020, Lu et al. 2008, Shoaib et al. 2021). A disulfide coupling approach for ubiquitylation has also been published to reproduce the functions of ubiquitylated histones (Valencia-Sánchez et al. 2019, Murawska et al. 2020, Ai et al. 2022). We employed these approaches and a highly refined *in vitro* transcription system to construct a tractable single-molecule transcription system to investigate the effects of histone H2B ubiquitylations and H3K79me$_3$ on the kinetics of transcription elongation through the nucleosome and the status of DNA wrapping during and after transcription (Lee et al. 2019a).

Pol II pauses at various locations within the nucleosome during transcription (Kireeva et al. 2005, Gaykalova et al. 2015, Kujirai et al. 2018). Out of these pause locations, we focus on the first four - SHL(-6), (-5), (-2), and (-1) among which SHL(-5) and (-1) induce major pauses while SHL(-6) and (-2) induce weaker minor pauses (Kujirai et al. 2018). Pauses are a major determinant of transcription elongation kinetics as they last for a few seconds to minutes while the rate of elongation is typically in the range of 40 – 50 nt/sec (Bintu et al. 2012, Chen et al. 2019).

Our results indicate that H2BK34ub facilitates transcription by suppressing pauses and shortening their durations at SHL(-6) and (-5) and that H2BK120ub also has the same effects but only to a moderate extent. These differential extents between H2BK34ub and K120ub are in good agreements with their differential efficiencies for Nap1-induced hexasome formation (Krajewski et al. 2018). It was only recent when H2BK34ub started getting attention while H2BK120ub has been actively investigated for a longer time for its role in recruiting Dot1L to methylate H3K79. The recent attention to H2BK34ub was triggered by the finding that H2BK34ub is coupled to H2BK120ub in a network of direct protein interactions. The interactions involve a general transcription elongation factor Paf1C and the two ubiquitin ligase complexes MOF-MSL and RNF20/40 for ubiquitylating H2BK34 and H2BK120, respectively, which eventually promote Pol II processivity *in vivo* (Wu et al. 2014). Since then, it has been shown that H2BK34ub nucleosomes have the ubiquitin moieties protrude between the two gyres of the nucleosomal DNA, weakening the structural integrity of the nucleosome and distorting DNA toward the entry region of the nucleosome (Li et al. 2017, Ai et al. 2022). These results suggest that the effects of H2BK34ub on transcription kinetics can be the major mechanisms of facilitated transcription by H2B ubiquitylations. The effects are likely due to localized perturbations of the nucleosome structure near the DNA-(H2A-H2B) contact region, which has been validated by our recent structural study based on smFRET (Sengupta et al. 2022). We suspect that the weaker effects of H2BK120ub is due to its non-ideal location to affect DNA-histone interactions.

An important regulatory role for H2BK120ub is to recruit Dot1L and methylate H3K79. H3K79 methylations are enriched in active genes and its mis-regulation is a hallmark of many cancers (Bernt et al. 2011, Zhang et al. 2014). H3K79 methylations facilitate transcription *in vitro* and H3K79me$_2$ alters the local histone surface without inducing any significant changes to the global structure of the nucleosome (Yang et al. 2016, Barski et al. 2007, Ljungman et al. 2019, Lu et al. 2008). The addition of methyl groups to H3K79 makes this location sterically bulky and can disrupt the weak hydrogen bonding between the lysine and the L2 loop of histone H4 (Lu et al. 2008). This change makes a hydrophobic pocket lined by H3L82 and H4V70 more solvent accessible (Lu et al. 2008), which may result in more flexible conformations around the H3K79 region. Such increased conformational flexibility would positively impact on the transcription efficiency. The shortened SHL(-2)/(-1) pause durations by H3K79me$_3$ are in line with this mechanism. We suspect that the increased rate of elongation by H3K79me$_3$ is likely due to shortened SHL(-2) pauses. As we included SHL(-2) pause durations in elongation time measurements, the shortened SHL(-2) pauses by H3K79me$_3$ would result in an increased elongation rate. Overall, our results support that the increased flexibility around the (H3-H4)$_2$ tetramer region facilitate transcription elongation by shortening the durations of SHL(-2)/(-1) pauses and subsequently elevating the rate of transcription elongation through this region, providing the physical mechanism of facilitated transcription by H3K79me$_3$.

Another notable finding is that the effects exerted by H2BK120ub and H3K79me$_3$ add up to facilitate transcription to the highest extent among all 5 nucleosomes that we examined (Fig. 4-11). According to our results and the previous studies, the mechanisms of these two modifications are localized in two different regions of the nucleosome – H2BK120ub near the SHL(-6)/(-5) region and H3K79me$_3$ near the SHL(-2)/(-1) region. As such, the total effects would be the sum of their individual effects. Considering that H3K79me$_3$ is induced by H2BK120ub recruiting Dot1L and these two modifications impact on the nucleosome structure in two different regions, we suggest

that these two modifications may work together to contribute significantly to facilitated transcription *in vivo*. It is noteworthy that a previous research reported heightened nucleosome barriers around SHL(-2)/(-1) by H2BK120ub alone (Chen et al. 2019). Combined with our results, it is implied that the effect of H3K79me$_3$ overwrites that of H2BK120ub around SHL(-2)/(-1). Considering that the end result of H2BK120ub is H3K79me$_3$ upon transcription activation, we suggest that H2BK120ub helps maintaining the structure of the nucleosome around SHL(-2)/(-1) and induces H3K79me$_3$ upon transcription activation to greatly facilitate transcription through the nucleosome.

A histone methyltransferase Dot1L mediates the crosstalk between H2BK120ub and H3K79me$_3$ and is known to affect the structure of the nucleosome upon binding even in its inactive form (Anderson et al. 2019a, Jang et al. 2019, Zhang and Kutateladze 2019). This effect of Dot1L might contribute to the mechanism of how Dot1L is coupled to facilitated chromatin remodeling (Alvarez et al. 2021). It will be an important future study to investigate how Dot1L binding to H2B ubiquitylated nucleosomes modulates the overall structure and stability of the nucleosome during transcription.

An important focus on the nucleosome dynamics during transcription is how the nucleosome maintains its structural integrity. A previous study suggested that H2A-H2B dimers are displaced or dissociated transiently and return to their original positions to reassemble the nucleosome during transcription elongation (Schwabish and Struhl 2004). Our results show that ~30 % of the nucleosomes partially or fully rewrap the DNA around the entry proximal H2A-H2B contact region after Pol II passage and that H2BK34ub significantly facilitates partial rewrapping of DNA. This effect of H2BK34ub suggests its role for stabilizing nucleosome intermediates during transcription. The effect might be due to the favorable location of the ubiquitin to interact with DNA as stable interactions between ubiquitin and DNA have been suggested previously (Debelouchina et al. 2017b, Landré et al. 2017, Li et al. 2017). Combining the effects of H2BK34ub, H2BK120ub, and

H3K79me$_3$ all of which are in the same regulatory network, our results suggest that these modifications induce and stabilize nucleosome intermediates during transcription. These dual roles would facilitate transcription elongation through the nucleosome while helping maintain the chromatin structure to ensure proper gene regulation.

Chapter 5

Conclusions and Future Directions

5.1. Conclusion

The majority of my research projects involve the use of highly refined tractable single-molecule systems to investigate the effects of various histone modifications (histone H3 acetylation, histone H2B ubiquitylations, and H3K79 tri-methylation) and histone chaperones (Nap1 and FACT) on transcription through the nucleosome by RNA polymerase II (Pol II). By employing two- and three-color single-molecule FRET techniques, I was able to track the DNA and histone movements in real time during Pol II transcription. Single-molecule observations demonstrated that these histone modifications had a direct effect on the transcription kinetics, with increased transcription efficiency seen in histone H3K56 acetylation, histone H2BK34 ubiquitylation, H3K79 tri-methylation, and the combination of histone H2BK120 ubiquitylation and H3K79 tri-methylation .

5.2. Implications for future studies

The research presented in this dissertation has shown that single molecule FRET is a reliable technique for learning about dynamics and conformational changes within nucleosomes. We have thoroughly examined the functions of specific histone post-translational modifications during Pol II transcription. To get deeper understanding of the mechanisms by which histone

post-translational modifications regulate the nucleosome structure in transcription beyond DNA unwrapping/rewrapping dynamics, certain changes to the current system can be implemented. In this section, I would like to introduce a few remaining unanswered questions and possible future directions.

5.2.1. The role of histone post-translational modifications in nucleosome recovery

In Chapter 4, our findings show that H2BK34ub and H2BK120ub both enhance transcription, although the effect is less pronounced with H2BK120ub. Additionally, we see that around one-third of the nucleosomes partially or fully rewrap the DNA around the entry proximal H2A-H2B contact region after Pol II passage and that H2BK34ub significantly facilitates partial rewrapping of DNA while this effect is absent in H2BK120ub. These variations between H2BK34ub and K120ub are consistent with their differential efficiencies for Nap1-induced hexasome formation (Krajewski et al. 2018). However, these results raise a question as to how only H2BK34ub is capable of facilitating nucleosome recovery. Some structural studies have suggested that ubiquitin has stable nonspecific interactions with DNA and may also interact with histone proteins via its acidic patches (Debelouchina et al. 2017a, Landré et al. 2017). Therefore, the interactions between the ubiquitin and the nucleosome can help the nucleosome retain displaced H2A-H2B dimer within the complex, which subsequently facilitates rewrapping of the nucleosomal DNA around the H2A-H2B dimer-DNA contact region. However, as mentioned previously, H2BK120ub nucleosomes displayed no increased rewrapping, suggesting that this effect may depend on the location of ubiquitin. As the two ubiquitin molecules in H2BK34ub nucleosomes protrude between the two gyres of the nucleosomal DNA (Li et al. 2017, Ai et al. 2022), they may readily contact DNA to assist H2A-H2B retention and DNA rewrapping while the ubiquitin molecules in H2BK120ub

nucleosomes are further away from histone-DNA interfaces and more difficult to engage with DNA. Interestingly, we also observed an increased rewrapping in the H3K79me$_3$/H2BK120ub nucleosomes in contrast to these two single mutants. This observation raises a possibility that H2BK120ub may have the capability to hold the H2A-H2B dimer within the complex and in conjunction with H3K79me$_3$, promote DNA rewrapping.

In order to examine the aforementioned notions, examination of the histone protein positions during and after transcription may be crucial in understanding the mechanism of nucleosome recovery and potential intermediates. Building on our two-color study, which used a FRET pair at two DNA positions, we may use a third acceptor at H2B T112C to create a second FRET pair to track changes in the structural organization of the nucleosome between DNA and H2A-H2B dimer(s) in transcription. This three-color system made up of these two fluorophores on DNA and a third one on H2B T112C (Fig. 5-1 A) can be used to monitor the motions of both DNA and histone H2A-H2B dimers during transcription. By tracking the locations of histone H2A-H2B dimers in all stages of transcription, we should be able to determine whether ubiquitin has the ability to retain histone H2A-H2B dimers in the elongation complex after transcription or if there are other pathways that cause the transiently dissociated or relocated histone dimers to return to their original positions and reassemble the nucleosome.

In addition to H2B ubiquitylations, our results demostrate that H3K79 methylations facilitate transcription elongation by shortening SHL(-2)/(-1) pauses and, as a result, increasing the rate of transcription elongation across this region. We attribute this effect to the increased flexibility around the (H3-H4)$_2$ tetramer region. To test this notion, a FRET pair between +57 and +138 DNA locations and a second acceptor at H4E63C can be used in a three-color measurement. This three-color system may capture the nucleosome structural changes that occur between DNA and (H3-H4)$_2$ tetramer (Fig. 5-1 B).

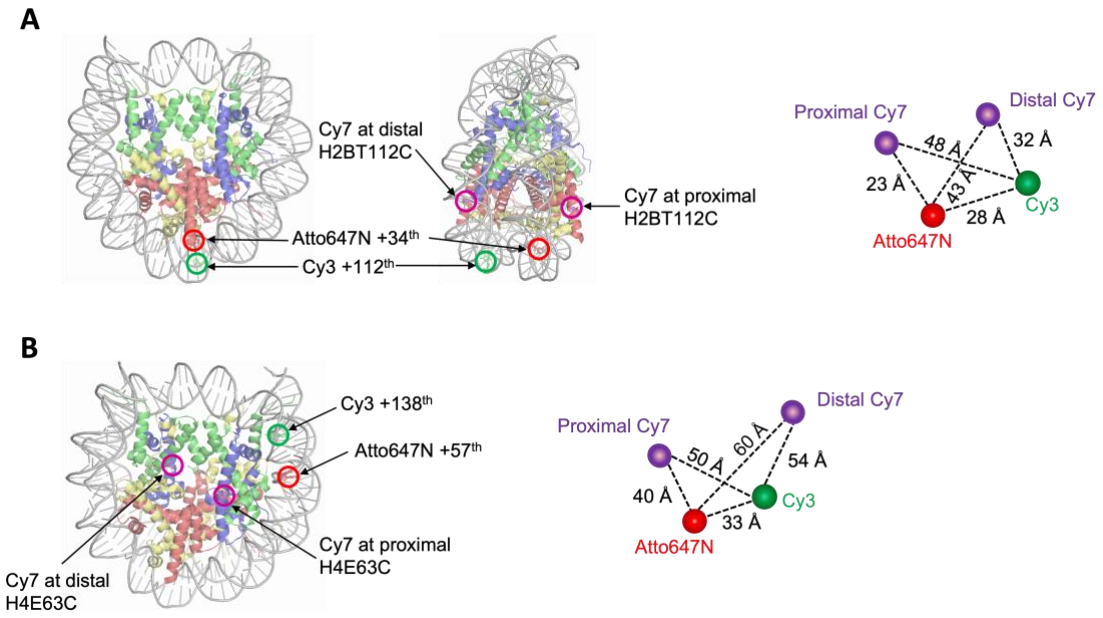

Figure **5-1**: Schematics outlining the labeling schemes in three-color smFRET measurements.

H2BT112C is labeled with Cy7 in (A) to study the DNA-histone H2A-H2B dimer contacts while H4E63C is labeled with Cy7 in (B) to study DNA-histone $(H3\text{-}H4)_2$ tetramer interactions. FRET distance estimations from cryo-EM structures for two FRET pairs are also noted in case of intact nucleosomes.

5.2.2. Histone chaperone FACT: a potential future project

How the nucleosome maintains its structural integrity during transcription is a crucial area of study for nucleosome dynamics because it plays a pivotal role in maintaining transcription fidelity. Defects in nucleosome recovery can lead to aberrant transcription (Kaplan, Laprade and Winston 2003, Mason and Struhl 2003, Cheung et al. 2008, Nielsen et al. 2019, Chen et al. 2020). During transcription by Pol II, the nucleosome undergoes structural rearrangements to facilitate DNA opening which often leads to partially unwrapped nucleosomes. This raises the question of whether the nucleosome can restore on its own or if additional chromatin factors are required.

Previous *in vitro* studies on the nucleosome during transcription showed that most nucleosomes has at least one H2A-H2B dimer displaced or the whole octamer evicted (Kireeva et al. 2002, Bintu et al. 2011, Hsieh et al. 2013, Cole et al. 2014). However, *in vivo* studies showed contradictory results that most nucleosome remain intact after transcription (Lee et al. 2004, Ramachandran, Ahmad and Henikoff 2017). Therefore, the assistance of chromatin remodelers and histone chaperones has been proposed to facilitate the process of nucleosome recovery (Bondarenko et al. 2006, Clapier et al. 2017, Lai and Pugh 2017, Gurova et al. 2018, Formosa and Winston 2020, Zhou, Liu and Luger 2020).

One potential candidate for our future study is FACT (FAcilitates Chromatin Transcription) because it is among one of the most commonly studied histone chaperones. FACT is a widely conserved histone chaperone among different species that can promote both nucleosome assembly and disassembly during different phases of biological processes (Keller and Lu 2002, Xin et al. 2009, Valieva et al. 2016, Gurova et al. 2018, Hauer and Gasser 2017, Lai and Pugh 2017, Talbert and Henikoff 2017, Serra-Cardona and Zhang 2018, Liu et al. 2020, Zhou et al. 2020). FACT is thought to facilitate nucleosome disassembly by diminishing the nucleosome barrier to Pol II, thus inducing transcription (Belotserkovskaya et al. 2003a, Schwabish and Struhl 2004, Takahata, Yu and Stillman 2009, Hsieh et al. 2013, Shakya et al. 2015, Chen et al. 2018a). However, there are previous reports suggesting that FACT binding occurs after DNA region consisted of around 30 base pairs (bp) at the nucleosome entry site gets loosened (Mayanagi et al. 2019, Ehara et al. 2022). Even though transcription can lead to destabilized nucleosome structure, reports also found that this process is reversible, and FACT can function to reassemble nucleosome (Belotserkovskaya et al. 2003b, Winkler et al. 2011, Formosa 2013, Valieva et al. 2016, Valieva et al. 2017, Wang et al. 2018). Previous structural reports have found that FACT domains have extensive contacts with both DNA and H2A-H2B dimer (Kemble et al. 2015, Wang et al. 2018, Mayanagi et al. 2019, Liu et al. 2020). FACT exerts its effects by binding to histone surfaces

exposed by nucleosome unwrapping either by contacting free H2A-H2B dimer following dimer eviction or forming complexes with partially unwrapped nucleosome induced by nucleosome spontaneous breathing, then tethering histone and DNA components together to restore a canonical nucleosome (Belotserkovskaya et al. 2003a, Xin et al. 2009, Hsieh et al. 2013, Tsunaka et al. 2016, Wang et al. 2018, Mayanagi et al. 2019).

For our future project, we can investigate the effects of FACT on nucleosome recovery after transcription. We can utilize both two-color and three-color single-molecule FRET (smFRET) systems to determine successful DNA rewrapping efficiency and monitor histone protein locations throughout transcription process, thereby gaining more insights into the mechanisms FACT adopts to modulate the nucleosome structure through transcription.

In particular, a FRET pair at +34 and +112 DNA locations for a two-color study, and another additional acceptor at H2B T112C for a three-color study can be utilized to monitor the nucleosome structural alterations that occur between DNA and H2A-H2B dimer(s) following transcription. From a two-color study, an increased population of nucleosomes exhibiting DNA rewrapping signatures after Pol II progression is expected. A three-color system made up of these two fluorophores and a third one on H2B T112C (Fig. 5-1 A) can be used to monitor nucleosome reassembly, thus giving us insights into how FACT regulates histone H2A-H2B dimer-DNA interactions during transcription. From our three-color study, increased nucleosome recovery in the presence of FACT is anticipated. With the increased nucleosome recovery, we can imply that FACT can restore and stabilize H2A-H2B dimer-DNA contacts following transcription, either by retaining the original histone H2A-H2B dimer in the elongation complex or recruiting histone H2A-H2B dimer in the solution for subsequent histone H2A-H2B dimer deposit to the transcribed DNA.

Additionally, a FRET pair between +57 and +138 DNA locations for a two-color analysis and another extra acceptor at H4E63C can be employed in a three-color analysis to evaluate the nucleosome structural changes that occur after transcription between DNA and $(H3\text{-}H4)_2$ tetramer

(Fig. 5-1 B). We expect that most histone $(H3\text{-}H4)_2$ tetramer remain either intact or nearby in the elongation complex, and ready for reassembly after Pol II progression. However, another interesting possibility, which has been brought up by a recent cryo-EM paper, is that nucleosomes may get reorganized during transcription process to form stable intact nucleosome at a different DNA position (Ehara et al. 2022). These rearranged nucleosome states, if they exist, should be visible in our three-color analysis. From these possible data from both two-color and three-color studies on two different FRET pairs, we are hoping to design future studies where we can look at the processes of FACT in conjunction with other transcription factors in nucleosome recovery or reorganization, as well as obtaining the kinetics data from them.

Appendix A

General methods

This chapter describes a list of comprehensive protocols that are briefly mentioned in chapters 2-4. This chapter has detailed protocols of transcription template design and construction, oligonucleotide labeling, histone post-translational modifications and labeling, nucleosome reconstition, and single molecule FRET setup.

A.1. Nucleosomal DNA construction

We employ a high affinity 601-nucleosome positioning sequence (Lowary and Widom 1998), which has been widely employed in nucleosome research due to its high strength in nucleosome positioning. The complete 601 sequence is constructed by annealing and ligating oligonucleotides between 34 and 78 nucleotides by their complementary overhangs at the ends (Huynh et al. 2020, Lee et al. 2019a, Crickard et al. 2017).

In order to create a FRET pair in the nucleosome, either two DNA fragments or one DNA fragment and the histone core are each labeled with a fluorophore. The histone-DNA interaction points of interest can be used to construct the fluorophore labeling spots. We utilize NHS-ester functionalized dyes via the amine-functionalized C6 linkers coupled to the thymine bases (Integrated DNA Technologies, Coralville, IA) for DNA labeling and maleimide functionalized dyes via thiol-maleimide conjugation for histone labeling.

Since the 601 sequence contains a lot of thymine bases, the nucleosome can be labeled at almost any location of interest for DNA-histone interactions. It is desirable to label a thymine

base that is not in direct contact with the histone core. For example, a FRET acceptor (e.g., Atto647N or Cy5) at the +34th nucleotide counting from the nucleosome entry and a FRET donor (e.g., Cy3) at the +112th nucleotide work well to study DNA unwinding and rewinding around a histone H2A-H2B dimer-DNA contact region. It is also possible to analyze the DNA unwrapping and rewrapping around the histone $(H3\text{-}H4)_2$ tetramer-DNA interaction region by labeling a nucleosome at the +58th and +137th nucleotides instead. A nucleosome can additionally be labeled with a second acceptor (for example, Cy5.5 or Cy7) on the histone core (for example, H2BT112C) to track histone locations during histone exchange or histone displacement by transcription by Pol II.

A.1.1. Oligonucleotide labeling

DNA oligonucleotides should be labeled before annealing and ligation to construct the nucleosomal DNA or the transcription template. NHS-ester-functionalized Cy3 (GE Healthcare or Lumiprobe) and Atto647N (Sigma-Aldrich) fluorophores are used to label the site-specifically modified oligonucleotides.

1. Dissolve NHS-ester fluorophore in dimethyl sulfoxide (DMSO) to the final concentration of 100 μg/ μL , and the oligonucleotide of interest in 0.1 M $NaHCO_3$ (pH 8.3) to the final concentration of 100 μM.
2. Mix the DNA solution with the five-molar excess dye solution in a microtube, followed by mild agitation on a slow rotisserie rotor overnight at 4 ^{o}C.
3. Purify the labeled oligonucleotide from excess dye by multiple Illustra^{TM} NAP-5 disposable columns (Cytiva) until no color is visible in the column.
4. Concentrate the labeled oligonucleotide (optional) by centrifugal concentrator (Corning® Spin-X® UF 500 μL Centrifugal Concentrator, 10K MWCO) to 100 μM.

A.1.2. Oligonucleotide annealing and ligation

1. Dissolve approximately 100 pmol of each oligonucleotides in deionized water. Measure the concentrations of all oligonucleotides using UV-Vis spectrometer at 260 nm wavelength.
2. Aliquot all template oligonucleotides (each 100 pmol) into a small clean PCR tube. Add deionized water to the final volume of 20 μL.
3. Anneal the oligonucleotides by incubating at 95°C for 5 minutes, then gradually cool to 4°C in a thermal cycler (T100 Thermo Cycler, Part #1861096, Bio-Rad Laboratories, Inc.) at a rate of 1.5°C per minute. By annealing, we create double-stranded DNA sequence by pairing the complementary strands together through their hydrogen bonding.
4. Ligate the annealed oligonucleotides by adding T4 DNA ligase (NEB, # M0202L) and incubate the reaction mixture at 16 ^{o}C for 16 hours.
5. Eliminate T4 DNA ligase by a PCR purification kit (QIAquick PCR Purification Kit, Qiagen).
6. Run native PAGE of the resulting DNA on a 12 % gel in 0.5X TBE. Purify the DNA from the gel using a crush and soak procedure. The purified DNA is resuspended in 1X TE and stored at -20 ^{o}C.

A.1.3. Nucleosome reconstitution

1. Dissolve histone (H2A, H2B, H3, or H4) in the unfolding buffer (7M Guanidinium-HCl and 20 mM Tris-HCl (pH 7.5), 1 mM DTT) to 2 mg/mL and incubate on ice for at least 30 mins.

2. Assemble histone octamer by mixing stoichiometric amounts of all four histone proteins and dialyze against the refolding buffer (2M NaCl, 10mM Tris-HCl (pH 7.5), 1mM EDTA, 5mM BME) three times for 2 hours, 4 hours, and overnight using a dialysis cassette (Thermo Fisher Scientific's Slide-A-Lyzer Dialysis Cassette, 3.5K MWCO) or SnakeSkin dialysis tubing (Thermo Fisher Scientific, 7K MWCO). Instead of a complete histone octamer, histone H2A-H2B dimers or histone $(H3\text{-}H4)_2$ tetramer can be assembled separately with the same method.
3. Purify the resulting mixture by eluting through a HiLoad 16/600 Superdex 200pg column (GE Healthcare). We collect histone complex fractions based on the absorbance at 280 nm and analyze its presence by 18% SDS-PAGE.
4. Mix stoichiometric amounts of histone complexes (octamer or dimers + tetramer) and DNA (1000 ng) into a small clean PCR tube and store in an ice bath for at least 30 mins.
5. Transfer the mixture into a mini-dialysis cup (Thermo Fisher Scientific's Slide-A-Lyzer MINI Dialysis Device, 7K MWCO) and dialyze against 1X TE (pH 8.0) buffers with stepwise salt dilution at 850, 650, 500, 300, and 2.5 mM NaCl for 1 hour.
6. Heat the collected nucleosome sample at 54 ^{o}C for 2 hours to induce correct nucleosome positioning.
7. Further purify nucleosomes if necessary (optional) using a crush and soak method from a 12 % native PAGE gel in 0.5X TBE. The nucleosome gel band is extracted and suspended in 1X TE (pH 8.0) buffer containing 2.5 mM NaCl and 1 mg/ml bovine serum albumin (BSA), followed by incubation at 4 ^{o}C overnight. The purified nucleosome is then verified by native PAGE.

A.2. Histone labeling, acetylation, methylation, and ubiquitylation

In some measurements, we use nucleosomes with a FRET pair labeled at DNA and histone. In some cases, we need to introduce chemical groups to histones in a site-specific manner (Lee and Lee 2019, Sengupta et al. 2022). The following procedures describe the protocols to carry out these tasks of histone modifications.

A.2.1. Histone labeling

1. Prepare the unfolding solution containing 7M Guanidinium-HCl and 20 mM Tris-HCl (pH 7.5). Degas for 30 mins by sonication to remove oxygen.
2. Dissolve maleimide fluorophore in dimethyl sulfoxide (DMSO) to 100 µg/ µL.
3. Dissolve the cysteine-containing target histone protein to the final concentration of 2 mg/mL in unfolding buffer with ten-fold histone molar excess of TCEP and incubate on ice for 30 mins.
4. Gently mix the unfolded histone solution with twenty-molar excess maleimide dye solution for two hours at ambient temperature and then overnight at 4 ^{o}C with slow rotation agitation.
5. Purify the labeled protein from excess dye through multiple disposable PD-10 desalting columns (Cytiva) until no color is visible in the column.
6. Concentrate the labeled protein (optional) by centrifugal filter (EMD Millipore, Amicon® Ultra-4 Centrifugal Filter Units, 3K MWCO).

A.2.2. Histone acetylation

We generate a mimetic acetylated histone protein via a radical-mediated thiol-ene reaction. An acetyl-thialysine histone is produced with a thioether linked side chain of acetylated lysine (Li et al. 2011). This method has been successfully employed to reproduce the results from chemically pure histone modifications (Li et al. 2011). The following protocol is to introduce acetylation to H3 K56. These protocols apply to other acetylations once the target acetylation site is point-mutated to cysteine.

1. Prepare the reaction solution containing 0.2 M sodium acetate (pH 4), 6 M guanidine-HCl, 7 mM L-glutathione, 50 mM N-vinylacetamide, 100 mM dimethyl sulfide, and 5 mM VA-044 (2,2′- [azobis(dimethyl methylene)]bis(2-imidazoline)-dihydrochloride).
2. Dissolve the double mutant histone H3 K56C/C110A in the reaction solution to a final concentration of 1 mM.
3. Incubate the reaction mixture for 2 hours at 70 °C. VA-044 is light-sensitive so all experiments are performed in complete darkness.
4. Dialyze the reaction mixture three times against deionized water, and then lyophilize for an additional night to collect solid acetylated H3 histone protein. The protein is stored at -80 ^{o}C.
5. To confirm successful acetylation, dissolve a small amount of acetylated H3 into 50 % acetonitrile (the final concentration of approximately 1-0.5 mg/ml is sufficient). This sample is analyzed by mass-spectrometry to confirm its presence and purity.

A.2.3. Histone ubiquitylation

Histone ubiquitylation is performed by conjugating a His-TEV-ubiquitin G76C mutant to the histone protein containing a lysine residue at the target ubiquitylation site (e.g. H2BK34C and H2BK120C) (Long, Furgason and Yao 2014b, Murawska et al. 2020). His-TEV-ubiquitin G76C-expressing plasmid is purchased from Addgene (Watertown, MA), while plasmid strains expressing histone mutants H2BK34C and H2BK120C are generated by site-directed mutagenesis and confirmed by sequencing.

Below is the procedure for ubiquitin expression and purification:

1. Ubiquitin is expressed in BL21(DE3)pLysS in 2 L 2-YT media (Thermo Fisher Scientific). The cell pellets are collected by centrifugation at 6,000 xg for 10 mins at room temperature.
2. Dissolve the cell pellets in lysis buffer (50mM Tris-HCl (pH 8), 500 mM NaCl, 10 mM imidazole, and 10 μM PMSF), lyse the suspension by homogenizer (EmulsiFlex-C3, AVESTIN, Canada), and centrifuge them at 6000 xg to collect the supernatant.
3. Purify the resulting supernatant by flowing through a self-packed Ni-NTA agarose column (Thermo Fisher Scientific), followed by three washes with the lysis buffer. Ubiquitin is then eluted in the elution buffer (50mM Tris-HCl (pH 8), 500 mM NaCl, 10 mM imidazole, and 10 μM PMSF).
4. Dialyze the collected ubiquitin against the low salt buffer (50 mM ammonium acetate (pH 4.5), 100 mM NaCl, 3 mM BME) for 2 hours, 4 hours, and overnight for the second step of purification.

5. Further purify the dialyzed sample by flowing through the HiTrap SP HP column (Cytiva) and elute with a salt gradient 0-100% of the high salt buffer (50 mM ammonium acetate (pH 4.5), 1 M NaCl, 3 mM BME). Ubiquitin is collected in fractions and analyzed by SDS-PAGE to confirm its presence and purity.
6. Dialyze purified His-TEV-ubiquitin against deionized water containing 1 mM acetic acid three times for 2 hours, 4 hours, and overnight, followed by lyophilization for storage at -80 ^{o}C.

With the prepared His-TEV-ubiquitin and cysteine-containing histone protein (e.g., H2BK34C or H2BK120C), below is the protocol to generate ubiquitylated histone:

1. Dissolve both ubiquitin and histone H2B in the reaction buffer containing 50 mM Tris-HCl (pH 8.6) and 6 M Urea.
2. A molar ratio of two histone proteins to one ubiquitin are subsequently combined with 5 mM final TCEP concentration, followed by incubation at room temperature for 30 mins.
3. Add 1,3-dichloroacetone to the reaction tube to the final concentration that is equal to 50 % of the combined concentration of ubiquitin and histone protein.
4. Incubate the reaction on ice for 16 hours before quenching by the addition of 10 mM BME final concentration. A nonhydrolyzable ubiquitylated histone mimic is produced. Ubiquitylated histones produced with this method have been employed for biochemical and structural research on histone-ubiquitylated nucleosomes.
5. Further purify the product by flowing through a self-packed HisPur Ni-NTA column (Thermo Fisher Scientific). The column is washed with two column volumes of wash buffer (0.5M NaCl, 50mM Tris-HCl (pH 8.0), 10mM BME, and 0.1mM PMSF). 10 μL TEV protease per 1mL column volume is added to the column to cleave the 6xHis tag

and elute the final product. This product contains ubiquitin, ubiquitin-ubiquitin, ubiquitylated histone. Ubiquitin and ubiquitin-ubiquitin does not interfere with the formation of H2A-H2B dimer, therefore can be separated during the histone dimer assembly step.

6. Dialyze the final product against deionized water for 2 hours, 4 hours, and overnight. The product is then lyophilized and kept at -80 ºC.
7. To verify successful ubiquitylation, we assemble ubiquitylated H2A-H2B dimers using above described steps. Ubiquitylated H2A-H2B dimers are collected in fractions and analyzed by SDS-PAGE.

A.2.4. Histone methylation

We generate a mimetic methylated histone protein via an aminoethylation reaction in which a cysteine is alkylated with an electrophilic ethylamine producing aminoethylcysteine (Simon et al. 2007).

1. Dissolve mutant histone protein (e.g. H3K79C) (5-10 mg) in the alkylation buffer (1 M HEPES, 10 mM D/L-methionine, 4 M Guanidium-HCl, and 20 mM DTT), then incubate it for an hour at 37 ºC in a water bath.
2. Add 100 mg of (2-bromoethyl) trimethylammonium bromide into the protein solution and heated at 50 ºC with intermittent stirring for 2.5 hours.
3. Add an aliquot of 10 μL 1M DTT and allow the reaction to continue for an additional 2.5 hours.
4. Add 50 μL of 14.2 M excess mercaptoethanol (BME) to quench the reaction. This reaction produces trimethylated aminoethylcysteine, which has a sulfur side chain in

place of the trimethylated lysine side chain (i.e., the methyl group linkage replaced with a thioether linkage).

5. To confirm successful methylation, dissolve a small amount of methylated H3 into 50 % acetonitrile (the final concentration of about 1-0.5 mg/ml is adequate). Mass spectrometry is used to verify the presence and purity of this material.

A.3. Single-molecule FRET setup

For smFRET measurements, we employ a prism-coupled total internal reflection (TIR) geometry built on a commercial microscope (Nikon TE2000, Japan). All lenses and mirrors used in our setup were purchased from Thor Labs Inc. and dichroic mirrors and optical filters were obtained from Chroma Technology (Bellow Falls, VT).

Our lab-constructed smFRET microscope has two excitation lasers: one green laser at 532 nm (diode-pumped solid-state, 300 mW, CrystaLaser, Reno, NV) and one red laser at 635 nm (diode, 150 mW, CrystaLaser, Reno, NV). A pair of telescopic lenses are used to create prism-coupled TIR and make the beam parallel and control the size of the beam appropriate for tight focusing at the TIR interface. The focusing lens are responsible for directing and concentrating the TIR beam through a prism (Pellin-Broca, CVI Laser Optics, PLBC-10.0-77.2, 10 mm thickness, Albuquerque, NM) on the interface between the quartz slide surface and buffer inside of the flow channel. A thin layer of microscope objective immersion oil (Cargille Labs, Cedar Grove, NJ, type FF) is deposited between the prism and the slide surface. The focusing lens located on a 3D translational stage is used to control the location and size of the illumination area.

Our lab has two imaging optical setups for two- or three-color smFRET measurements as previously published (Yue et al. 2016, Lee et al. 2015). Briefly mentioned, the imaging optic

system for the two-color smFRET setup (Fig. A-1) is made up of a width-adjustable slit, a fixed dichroic mirror (620 nm, long-pass filter), three mirrors mounted on a kinematic mount (part # KM100, Thorlabs Inc., Newton, NJ), and two relay-lenses (part # AC508-100-A, Thorlabs Inc., Newton, NJ), which are installed on a single-axis translational stage (Thorlabs Inc., XR25C, Newton, NJ).

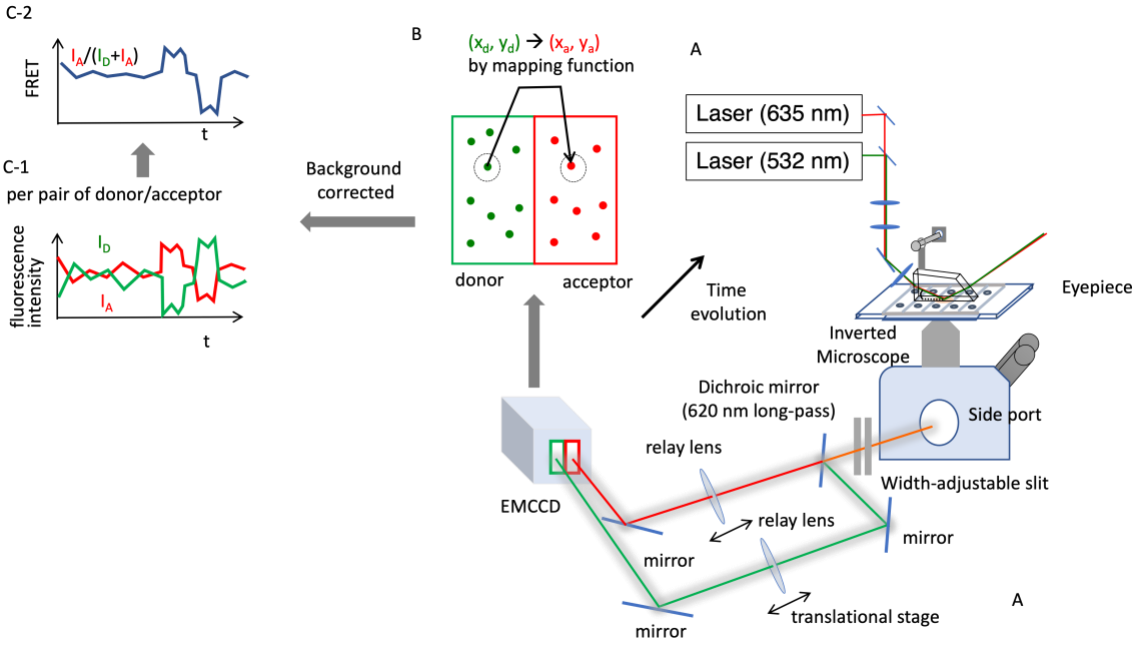

Figure **A-1**: Prism coupled total internal reflection fluorescence microscopy (TIRFM) setup.

(A) Our optical setup contains two lasers for TIRF excitation: a 532 nm green laser and a 635 nm red laser. Samples are excited at single molecule level by either laser. The donor and acceptor signals pass through optical filters before detection by an EMCCD camera. The fluorescence images are collected through an oil immersion, split into the donor and acceptor emissions and imaged side by side on the EMCCD camera. (B) The mapping function used to extract the fluorescence signals from each molecule and generate time traces containing a time series of fluorescence changes. (C) An example of a time trace extracted from a fluorescence movie. This time trace represent changes in fluorescence intensities of the donor (I_D) and the acceptor (I_A) over a certain period. The FRET efficient can be calculated based on both fluorescence intensities as demonstrated in (C-1 and C-2). This figure is adapted with permission.

References

Aguilar-Gurrieri, C., A. Larabi, V. Vinayachandran, N. A. Patel, K. Yen, R. Reja, I. O. Ebong, G. Schoehn, C. V. Robinson, B. F. Pugh & D. Panne (2016) Structural evidence for Nap1-dependent H2A-H2B deposition and nucleosome assembly. *EMBO J,* 35**,** 1465-82.

Ai, H., M. Sun, A. Liu, Z. Sun, T. Liu, L. Cao, L. Liang, Q. Qu, Z. Li, Z. Deng, Z. Tong, G. Chu, X. Tian, H. Deng, S. Zhao, J. B. Li, Z. Lou & L. Liu (2022) H2B Lys34 Ubiquitination Induces Nucleosome Distortion to Stimulate Dot1L Activity. *Nat Chem Biol,* 18**,** 972-980.

Akey, C. W. & K. Luger (2003) Histone chaperones and nucleosome assembly. *Curr Opin Struct Biol,* 13**,** 6-14.

Albrecht, C. 2008. Joseph R. Lakowicz: Principles of fluorescence spectroscopy. Springer.

Allahverdi, A., R. Yang, N. Korolev, Y. Fan, C. A. Davey, C.-F. Liu & L. Nordenskiöld (2010) The effects of histone H4 tail acetylations on cation-induced chromatin folding and self-association. *Nucleic Acids Research,* 39**,** 1680-1691.

Alvarez, N. S., P. Brachova, T. A. Fields & P. E. Fields (2021) Dot1L-dependent H3K79 methylation facilitates histone variant H2A.Z exchange at DNA double strand breaks and is required for high fidelity, homology-directed DNA repair. *bioRxiv***,** 544981.

Anderson, C. J., M. R. Baird, A. Hsu, E. H. Barbour, Y. Koyama, M. J. Borgnia & R. K. McGinty (2019a) Structural Basis for Recognition of Ubiquitylated Nucleosome by Dot1L Methyltransferase. *Cell Rep,* 26**,** 1681-1690.e5.

--- (2019b) Structural Basis for Recognition of Ubiquitylated Nucleosome by Dot1L Methyltransferase. *Cell reports,* 26**,** 1681-1690.e5.

Andrews, A. J., X. Chen, A. Zevin, L. A. Stargell & K. Luger (2010) The histone chaperone Nap1 promotes nucleosome assembly by eliminating nonnucleosomal histone DNA interactions. *Mol Cell,* 37**,** 834-42.

Andrews, A. J., G. Downing, K. Brown, Y. J. Park & K. Luger (2008) A thermodynamic model for Nap1-histone interactions. *J Biol Chem,* 283**,** 32412-8.

Arimura, Y., H. Tachiwana, T. Oda, M. Sato & H. Kurumizaka (2012) Structural Analysis of the Hexasome, Lacking One Histone H2A/H2B Dimer from the Conventional Nucleosome. *Biochemistry,* 51**,** 3302-3309.

Bannister, A. J. & T. Kouzarides (2011) Regulation of chromatin by histone modifications. *Cell Res,* 21**,** 381-95.

Barski, A., S. Cuddapah, K. Cui, T. Y. Roh, D. E. Schones, Z. Wang, G. Wei, I. Chepelev & K. Zhao (2007) High-resolution profiling of histone methylations in the human genome. *Cell,* 129**,** 823-37.

Bednar, J., V. M. Studitsky, S. A. Grigoryev, G. Felsenfeld & C. L. Woodcock (1999) The Nature of the Nucleosomal Barrier to Transcription: Direct Observation of Paused Intermediates by Electron Cryomicroscopy. *Molecular Cell,* 4**,** 377-386.

Belotserkovskaya, R., S. Oh, V. A. Bondarenko, G. Orphanides, V. M. Studitsky & D. Reinberg (2003a) FACT Facilitates Transcription-Dependent Nucleosome Alteration. *Science,* 301**,** 1090-1093.

--- (2003b) FACT facilitates transcription-dependent nucleosome alteration. *Science,* 301**,** 1090-3.

Bendandi, A., S. Dante, S. R. Zia, A. Diaspro & W. Rocchia (2020) Chromatin Compaction Multiscale Modeling: A Complex Synergy Between Theory, Simulation, and Experiment. *Front Mol Biosci,* 7**,** 15.

Berger, S. L. (2007) The complex language of chromatin regulation during transcription. *Nature,* 447**,** 407-12.

Bernt, K. M., N. Zhu, A. U. Sinha, S. Vempati, J. Faber, A. V. Krivtsov, Z. Feng, N. Punt, A. Daigle, L. Bullinger, R. M. Pollock, V. M. Richon, A. L. Kung & S. A. Armstrong (2011) MLL-rearranged leukemia is dependent on aberrant H3K79 methylation by DOT1L. *Cancer cell,* 20**,** 66-78.

Bilokapic, S., M. Strauss & M. Halic (2018) Histone octamer rearranges to adapt to DNA unwrapping. *Nature structural & molecular biology,* 25**,** 101-108.

Bintu, L., T. Ishibashi, M. Dangkulwanich, Y.-Y. Wu, L. Lubkowska, M. Kashlev & C. Bustamante (2012) Nucleosomal elements that control the topography of the barrier to transcription. *Cell,* 151**,** 738-749.

Bintu, L., M. Kopaczynska, C. Hodges, L. Lubkowska, M. Kashlev & C. Bustamante (2011) The elongation rate of RNA polymerase determines the fate of transcribed nucleosomes. *Nature Structural & Molecular Biology,* 18**,** 1394-1399.

Black, J. C., C. Van Rechem & J. R. Whetstine (2012) Histone lysine methylation dynamics: establishment, regulation, and biological impact. *Molecular cell,* 48**,** 491-507.

Blosser, T. R., J. G. Yang, M. D. Stone, G. J. Narlikar & X. Zhuang (2009) Dynamics of nucleosome remodelling by individual ACF complexes. *Nature,* 462**,** 1022-7.

Bondarenko, V. A., L. M. Steele, A. Ujvári, D. A. Gaykalova, O. I. Kulaeva, Y. S. Polikanov, D. S. Luse & V. M. Studitsky (2006) Nucleosomes can form a polar barrier to transcript elongation by RNA polymerase II. *Mol Cell,* 24**,** 469-79.

Bowman, G. & M. Poirier (2015a) Post-Translational Modifications of Histones That Influence Nucleosome Dynamics. 115**,** 2274-2295.

--- (2015b) Post-Translational Modifications of Histones That Influence Nucleosome Dynamics. *Chem Rev,* 115**,** 2274-2295.

Bowman, G. D. & M. G. Poirier (2015c) Post-Translational Modifications of Histones That Influence Nucleosome Dynamics. *Chemical Reviews,* 115**,** 2274-2295.

Brehove, M., T. Wang, J. North, Y. Luo, S. J. Dreher, J. C. Shimko, J. J. Ottesen, K. Luger & M. G. Poirier (2015) Histone core phosphorylation regulates DNA accessibility. *The Journal of biological chemistry,* 290**,** 22612-22621.

Brooks Crickard, J. & J. C. Reese (2019) Biochemical methods to characterize RNA polymerase II elongation complexes. *Methods,* 159-160**,** 70-81.

Böhm, V., A. R. Hieb, A. J. Andrews, A. Gansen, A. Rocker, K. Tóth, K. Luger & J. Langowski (2011) Nucleosome accessibility governed by the dimer/tetramer interface. *Nucleic Acids Res,* 39**,** 3093-102.

Cai, J., M. K. Culley, Y. Zhao & J. Zhao (2018) The role of ubiquitination and deubiquitination in the regulation of cell junctions. *Protein Cell,* 9**,** 754-769.

Cao, J. & Q. Yan (2012) Histone Ubiquitination and Deubiquitination in Transcription, DNA Damage Response, and Cancer. *Frontiers in Oncology,* 2.

Cavalieri, V. (2021) The Expanding Constellation of Histone Post-Translational Modifications in the Epigenetic Landscape. *Genes,* 12.

Chandrasekharan, M. B., F. Huang, Y. C. Chen & Z. W. Sun (2010) Histone H2B C-terminal helix mediates trans-histone H3K4 methylation independent of H2B ubiquitination. *Mol Cell Biol,* 30**,** 3216-32.

Chang, C.-H. & D. S. Luse (1997) The H3/H4 Tetramer Blocks Transcript Elongation by RNA Polymerase II in Vitro. *Journal of Biological Chemistry,* 272**,** 23427-23434.

Chang, H. W., O. I. Kulaeva, A. K. Shaytan, M. Kibanov, K. Kuznedelov, K. V. Severinov, M. P. Kirpichnikov, D. J. Clark & V. M. Studitsky (2014) Analysis of the mechanism of nucleosome survival during transcription. *Nucleic Acids Res,* 42**,** 1619-27.

Chatterjee, C., R. K. McGinty, B. Fierz & T. W. Muir (2010) Disulfide-directed histone ubiquitylation reveals plasticity in hDot1L activation. *Nature Chemical Biology,* 6**,** 267-269.

Chen, F., W. Zhang, D. Xie, T. Gao, Z. Dong & X. Lu (2020) Histone chaperone FACT represses retrotransposon MERVL and MERVL-derived cryptic promoters. *Nucleic Acids Res,* 48**,** 10211-10225.

Chen, P., L. Dong, M. Hu, Y. Z. Wang, X. Xiao, Z. Zhao, J. Yan, P. Y. Wang, D. Reinberg, M. Li, W. Li & G. Li (2018a) Functions of FACT in Breaking the Nucleosome and Maintaining Its Integrity at the Single-Nucleosome Level. *Mol Cell,* 71**,** 284-293.e4.

Chen, Q., R. Yang, N. Korolev, C. F. Liu & L. Nordenskiöld (2017) Regulation of Nucleosome Stacking and Chromatin Compaction by the Histone H4 N-Terminal Tail-H2A Acidic Patch Interaction. *J Mol Biol,* 429**,** 2075-2092.

Chen, W., Y. Liu, S. Zhu, G. Chen & J. J. Han (2018b) Inter-nucleosomal communication between histone modifications for nucleosome phasing. *PLoS Comput Biol,* 14**,** e1006416.

Chen, Z., R. Gabizon, A. I. Brown, A. Lee, A. Song, C. Díaz-Celis, C. D. Kaplan, E. F. Koslover, T. Yao & C. Bustamante (2019) High-resolution and high-accuracy topographic and transcriptional maps of the nucleosome barrier. *eLife,* 8**,** e48281.

Cheung, A. C. M. & P. Cramer (2011) Structural basis of RNA polymerase II backtracking, arrest and reactivation. *Nature,* 471**,** 249-253.

Cheung, V., G. Chua, N. N. Batada, C. R. Landry, S. W. Michnick, T. R. Hughes & F. Winston (2008) Chromatin- and transcription-related factors repress transcription from within coding regions throughout the Saccharomyces cerevisiae genome. *PLoS Biol,* 6**,** e277.

Chu, G.-C., M. Pan, J. Li, S. Liu, C. Zuo, Z.-B. Tong, J.-S. Bai, Q. Gong, H. Ai, J. Fan, X. Meng, Y.-C. Huang, J. Shi, H. Deng, C. Tian, Y.-M. Li & L. Liu (2019) Cysteine-Aminoethylation-Assisted Chemical Ubiquitination of Recombinant Histones. *Journal of the American Chemical Society,* 141**,** 3654-3663.

Clapier, C. R., J. Iwasa, B. R. Cairns & C. L. Peterson (2017) Mechanisms of action and regulation of ATP-dependent chromatin-remodelling complexes. *Nat Rev Mol Cell Biol,* 18**,** 407-422.

Cole, H. A., J. Ocampo, J. R. Iben, R. V. Chereji & D. J. Clark (2014) Heavy transcription of yeast genes correlates with differential loss of histone H2B relative to H4 and queued RNA polymerases. *Nucleic Acids Research,* 42**,** 12512-12522.

Cosgrove, M. S., J. D. Boeke & C. Wolberger (2004) Regulated nucleosome mobility and the histone code. *Nat Struct Mol Biol,* 11**,** 1037-43.

Cosgrove, M. S. & C. Wolberger (2005) How does the histone code work? *Biochem Cell Biol,* 83**,** 468-76.

Crickard, J. B., J. Lee, T. H. Lee & J. C. Reese (2017) The elongation factor Spt4/5 regulates RNA polymerase II transcription through the nucleosome. *Nucleic Acids Res,* 45**,** 6362-6374.

Cui, Y. & C. Bustamante (2000) Pulling a single chromatin fiber reveals the forces that maintain its higher-order structure. *Proceedings of the National Academy of Sciences,* 97**,** 127-132.

Davey, C. A., D. F. Sargent, K. Luger, A. W. Maeder & T. J. Richmond (2002) Solvent Mediated Interactions in the Structure of the Nucleosome Core Particle at 1.9Å Resolution††We dedicate this paper to the memory of Max Perutz who was particularly inspirational and supportive to T.J.R. in the early stages of this study. *Journal of Molecular Biology,* 319**,** 1097-1113.

De Koning, L., A. Corpet, J. E. Haber & G. Almouzni (2007) Histone chaperones: an escort network regulating histone traffic. *Nature Structural & Molecular Biology,* 14**,** 997-1007.

Debelouchina, G. T., K. Gerecht & T. W. Muir (2017a) Ubiquitin utilizes an acidic surface patch to alter chromatin structure. *Nat Chem Biol,* 13**,** 105-110.

--- (2017b) Ubiquitin utilizes an acidic surface patch to alter chromatin structure. *Nature chemical biology,* 13**,** 105-110.

Deindl, S., W. L. Hwang, S. K. Hota, T. R. Blosser, P. Prasad, B. Bartholomew & X. Zhuang (2013) ISWI remodelers slide nucleosomes with coordinated multi-base-pair entry steps and single-base-pair exit steps. *Cell,* 152**,** 442-52.

Delage, B. & R. H. Dashwood (2008) Dietary Manipulation of Histone Structure and Function. *Annual Review of Nutrition,* 28**,** 347-366.

Dhall, A., S. Wei, B. Fierz, C. L. Woodcock, T.-H. Lee & C. Chatterjee (2014) Sumoylated human histone H4 prevents chromatin compaction by inhibiting long-range internucleosomal interactions. *The Journal of biological chemistry,* 289**,** 33827-33837.

Ehara, H., T. Kujirai, M. Shirouzu, H. Kurumizaka & S. I. Sekine (2022) Structural basis of nucleosome disassembly and reassembly by RNAPII elongation complex with FACT. *Science,* 377**,** eabp9466.

Farnung, L., M. Ochmann, M. Engeholm & P. Cramer (2021) Structural basis of nucleosome transcription mediated by Chd1 and FACT. *Nat Struct Mol Biol,* 28**,** 382-387.

Fierz, B., C. Chatterjee, R. K. McGinty, M. Bar-Dagan, D. P. Raleigh & T. W. Muir (2011) Histone H2B ubiquitylation disrupts local and higher-order chromatin compaction. *Nat Chem Biol,* 7**,** 113-9.

Fierz, B., S. Kilic, A. R. Hieb, K. Luger & T. W. Muir (2012) Stability of nucleosomes containing homogenously ubiquitylated H2A and H2B prepared using semisynthesis. *J Am Chem Soc,* 134**,** 19548-51.

Filipovski, M., J. H. M. Soffers, S. M. Vos & L. Farnung (2022) Structural basis of nucleosome retention during transcription elongation. *Science,* 376**,** 1313-1316.

Finch, J. T., L. C. Lutter, D. Rhodes, R. S. Brown, B. Rushton, M. Levitt & A. Klug (1977) Structure of nucleosome core particles of chromatin. *Nature,* 269**,** 29-36.

Fleming, A. B., C. F. Kao, C. Hillyer, M. Pikaart & M. A. Osley (2008) H2B ubiquitylation plays a role in nucleosome dynamics during transcription elongation. *Mol Cell,* 31**,** 57-66.

Formosa, T. (2013) The role of FACT in making and breaking nucleosomes. *Biochim Biophys Acta,* 1819**,** 247-55.

Formosa, T. & F. Winston (2020) The role of FACT in managing chromatin: disruption, assembly, or repair? *Nucleic Acids Res,* 48**,** 11929-11941.

Fuchs, S. M., R. N. Laribee & B. D. Strahl (2009) Protein modifications in transcription elongation. *Biochimica et biophysica acta,* 1789**,** 26-36.

Gamarra, N., S. L. Johnson, M. J. Trnka, A. L. Burlingame & G. J. Narlikar (2018) The nucleosomal acidic patch relieves auto-inhibition by the ISWI remodeler SNF2h. *Elife,* 7.

Gansen, A., A. Valeri, F. Hauger, S. Felekyan, S. Kalinin, K. Tóth, J. Langowski & C. A. M. Seidel (2009) Nucleosome disassembly intermediates characterized by single-molecule FRET. *Proceedings of the National Academy of Sciences,* 106**,** 15308-15313.

Gaykalova, D. A., O. I. Kulaeva, O. Volokh, A. K. Shaytan, F. K. Hsieh, M. P. Kirpichnikov, O. S. Sokolova & V. M. Studitsky (2015) Structural analysis of nucleosomal barrier to transcription. *Proc Natl Acad Sci U S A,* 112**,** E5787-95.

Gurova, K., H. W. Chang, M. E. Valieva, P. Sandlesh & V. M. Studitsky (2018) Structure and function of the histone chaperone FACT - Resolving FACTual issues. *Biochim Biophys Acta Gene Regul Mech*.

Hall, M. A., A. Shundrovsky, L. Bai, R. M. Fulbright, J. T. Lis & M. D. Wang (2009) High-resolution dynamic mapping of histone-DNA interactions in a nucleosome. *Nature structural & molecular biology,* 16**,** 124-129.

Harada, B. T., W. L. Hwang, S. Deindl, N. Chatterjee, B. Bartholomew & X. Zhuang (2016) Stepwise nucleosome translocation by RSC remodeling complexes. *Elife,* 5.

Hauer, M. H. & S. M. Gasser (2017) Chromatin and nucleosome dynamics in DNA damage and repair. *Genes Dev,* 31**,** 2204-2221.

Hintzen, J. C. J., J. Poater, K. Kumar, A. H. K. Al Temimi, B. Pieters, R. S. Paton, F. M. Bickelhaupt & J. Mecinović (2020) Comparison of Molecular Recognition of Trimethyllysine and Trimethylthialysine by Epigenetic Reader Proteins. *Molecules*, 25.

Hodges, C., L. Bintu, L. Lubkowska, M. Kashlev & C. Bustamante (2009) Nucleosomal fluctuations govern the transcription dynamics of RNA polymerase II. *Science (New York, N.Y.)*, 325**,** 626-628.

Hsieh, F.-K., O. I. Kulaeva, S. S. Patel, P. N. Dyer, K. Luger, D. Reinberg & V. M. Studitsky (2013) Histone chaperone FACT action during transcription through chromatin by RNA polymerase II. *Proceedings of the National Academy of Sciences of the United States of America*, 110**,** 7654-7659.

Huynh, M. T., B. Sengupta, W. A. Krajewski & T. H. Lee (2023) Effects of Histone H2B Ubiquitylations and H3K79me(3) on Transcription Elongation. *ACS Chem Biol*.

Huynh, M. T., S. P. Yadav, J. C. Reese & T.-H. Lee (2020) Nucleosome Dynamics during Transcription Elongation. *ACS Chemical Biology*, 15**,** 3133-3142.

Ito, T., M. Bulger, R. Kobayashi & J. T. Kadonaga (1996) Drosophila NAP-1 is a core histone chaperone that functions in ATP-facilitated assembly of regularly spaced nucleosomal arrays. *Mol Cell Biol*, 16**,** 3112-24.

Izban, M. G. & D. S. Luse (1992) Factor-stimulated RNA polymerase II transcribes at physiological elongation rates on naked DNA but very poorly on chromatin templates. *Journal of Biological Chemistry*, 267**,** 13647-55.

Jang, S., C. Kang, H. S. Yang, T. Jung, H. Hebert, K. Y. Chung, S. J. Kim, S. Hohng & J. J. Song (2019) Structural basis of recognition and destabilization of the histone H2B ubiquitinated nucleosome by the DOT1L histone H3 Lys79 methyltransferase. *Genes Dev*, 33**,** 620-625.

Jin, J., L. Bai, D. S. Johnson, R. M. Fulbright, M. L. Kireeva, M. Kashlev & M. D. Wang (2010) Synergistic action of RNA polymerases in overcoming the nucleosomal barrier. *Nature structural & molecular biology*, 17**,** 745-752.

Johnson, S. L. & G. J. Narlikar (2022) ATP Hydrolysis Coordinates the Activities of Two Motors in a Dimeric Chromatin Remodeling Enzyme. *J Mol Biol*, 434**,** 167653.

Johnson, T. L. & M. J. Chamberlin (1994) Complexes of yeast RNA polymerase II and RNA are substrates for TFIIS-induced RNA cleavage. *Cell*, 77**,** 217-224.

Jonkers, I., H. Kwak & J. T. Lis (2014) Genome-wide dynamics of Pol II elongation and its interplay with promoter proximal pausing, chromatin, and exons. *eLife*, 3**,** e02407.

Joo, C., H. Balci, Y. Ishitsuka, C. Buranachai & T. Ha (2008) Advances in Single-Molecule Fluorescence Methods for Molecular Biology. *Annual Review of Biochemistry*, 77**,** 51-76.

Kaczmarczyk, A., A. Allahverdi, T. B. Brouwer, L. Nordenskiöld, N. H. Dekker & J. van Noort (2017) Single-molecule force spectroscopy on histone H4 tail-cross-linked chromatin reveals fiber folding. *Journal of Biological Chemistry*, 292**,** 17506-17513.

Kaplan, C. D., L. Laprade & F. Winston (2003) Transcription elongation factors repress transcription initiation from cryptic sites. *Science*, 301**,** 1096-9.

Kato, D., A. Osakabe, Y. Arimura, Y. Mizukami, N. Horikoshi, K. Saikusa, S. Akashi, Y. Nishimura, S. Y. Park, J. Nogami, K. Maehara, Y. Ohkawa, A. Matsumoto, H. Kono, R. Inoue, M. Sugiyama & H. Kurumizaka (2017) Crystal structure of the overlapping dinucleosome composed of hexasome and octasome. *Science*, 356**,** 205-208.

Keller, D. M. & H. Lu (2002) p53 serine 392 phosphorylation increases after UV through induction of the assembly of the CK2.hSPT16.SSRP1 complex. *J Biol Chem*, 277**,** 50206-13.

Kemble, D. J., L. L. McCullough, F. G. Whitby, T. Formosa & C. P. Hill (2015) FACT Disrupts Nucleosome Structure by Binding H2A-H2B with Conserved Peptide Motifs. *Mol Cell*, 60**,** 294-306.

Kettenberger, H., K.-J. Armache & P. Cramer (2003) Architecture of the RNA Polymerase II-TFIIS Complex and Implications for mRNA Cleavage. *Cell,* 114**,** 347-357.

--- (2004) Complete RNA Polymerase II Elongation Complex Structure and Its Interactions with NTP and TFIIS. *Molecular Cell,* 16**,** 955-965.

Kim, J., J. Lee & T. H. Lee (2015) Lysine Acetylation Facilitates Spontaneous DNA Dynamics in the Nucleosome. *J Phys Chem B,* 119**,** 15001-5.

Kim, J., S. Wei, J. Lee, H. Yue & T. H. Lee (2016) Single-Molecule Observation Reveals Spontaneous Protein Dynamics in the Nucleosome. *J Phys Chem B,* 120**,** 8925-31.

Kireeva, M. L., B. Hancock, G. H. Cremona, W. Walter, V. M. Studitsky & M. Kashlev (2005) Nature of the nucleosomal barrier to RNA polymerase II. *Mol Cell,* 18**,** 97-108.

Kireeva, M. L., W. Walter, V. Tchernajenko, V. Bondarenko, M. Kashlev & V. M. Studitsky (2002) Nucleosome remodeling induced by RNA polymerase II: loss of the H2A/H2B dimer during transcription. *Mol Cell,* 9**,** 541-52.

Komissarova, N. & M. Kashlev (1997) RNA Polymerase Switches between Inactivated and Activated States By Translocating Back and Forth along the DNA and the RNA. *Journal of Biological Chemistry,* 272**,** 15329-15338.

Kornberg, R. D. (1974) Chromatin Structure: A Repeating Unit of Histones and DNA. *Science,* 184**,** 868-871.

--- (1977) Structure of Chromatin. *Annual Review of Biochemistry,* 46**,** 931-954.

Kouzarides, T. (2007) Chromatin modifications and their function. *Cell,* 128**,** 693-705.

Krajewski, W. A. (2016) On the role of inter-nucleosomal interactions and intrinsic nucleosome dynamics in chromatin function. *Biochemistry and Biophysics Reports,* 5**,** 492-501.

--- (2018) Effects of DNA Superhelical Stress on the Stability of H2B-Ubiquitylated Nucleosomes. *J Mol Biol,* 430**,** 5002-5014.

--- (2019) Ubiquitylation: How Nucleosomes Use Histones to Evict Histones. *Trends Cell Biol,* 29**,** 689-694.

--- (2020a) “Direct” and “Indirect” Effects of Histone Modifications: Modulation of Sterical Bulk as a Novel Source of Functionality. *BioEssays,* 42**,** 1900136.

--- (2020b) The intrinsic stability of H2B-ubiquitylated nucleosomes and their in vitro assembly/disassembly by histone chaperone NAP1. *Biochimica et Biophysica Acta (BBA) - General Subjects,* 1864**,** 129497.

--- (2022) Histone Modifications, Internucleosome Dynamics, and DNA Stresses: How They Cooperate to "Functionalize" Nucleosomes. *Frontiers in genetics,* 13**,** 873398-873398.

Krajewski, W. A., J. Li & Y. Dou (2018) Effects of histone H2B ubiquitylation on the nucleosome structure and dynamics. *Nucleic acids research,* 46**,** 7631-7642.

Kujirai, T., H. Ehara, Y. Fujino, M. Shirouzu, S.-i. Sekine & H. Kurumizaka (2018) Structural basis of the nucleosome transition during RNA polymerase II passage. *Science,* 362**,** 595-598.

Kulaeva, O. I., D. A. Gaykalova, N. A. Pestov, V. V. Golovastov, D. G. Vassylyev, I. Artsimovitch & V. M. Studitsky (2009) Mechanism of chromatin remodeling and recovery during passage of RNA polymerase II. *Nat Struct Mol Biol,* 16**,** 1272-8.

Kulaeva, O. I., F.-K. Hsieh, H.-W. Chang, D. S. Luse & V. M. Studitsky (2013) Mechanism of transcription through a nucleosome by RNA polymerase II. *Biochimica et biophysica acta,* 1829**,** 76-83.

Kulaeva, O. I., F.-K. Hsieh & V. M. Studitsky (2010) RNA polymerase complexes cooperate to relieve the nucleosomal barrier and evict histones. *Proceedings of the National Academy of Sciences,* 107**,** 11325-11330.

Kulaeva, O. I. & V. M. Studitsky (2010) Mechanism of histone survival during transcription by RNA polymerase II. *Transcription,* 1**,** 85-8.

Kulaeva, O. I., G. Zheng, Y. S. Polikanov, A. V. Colasanti, N. Clauvelin, S. Mukhopadhyay, A. M. Sengupta, V. M. Studitsky & W. K. Olson (2012) Internucleosomal interactions mediated by histone tails allow distant communication in chromatin. *The Journal of biological chemistry,* 287**,** 20248-20257.

Kuryan, B. G., J. Kim, N. N. H. Tran, S. R. Lombardo, S. Venkatesh, J. L. Workman & M. Carey (2012) Histone density is maintained during transcription mediated by the chromatin remodeler RSC and histone chaperone NAP1 in vitro. *Proceedings of the National Academy of Sciences,* 109**,** 1931-1936.

Kwak, H. & J. T. Lis (2013) Control of Transcriptional Elongation. *Annual Review of Genetics,* 47**,** 483-508.

Lai, W. K. M. & B. F. Pugh (2017) Understanding nucleosome dynamics and their links to gene expression and DNA replication. *Nat Rev Mol Cell Biol,* 18**,** 548-562.

Landré, V., B. Revi, M. G. Mir, C. Verma, T. R. Hupp, N. Gilbert & K. L. Ball (2017) Regulation of transcriptional activators by DNA-binding domain ubiquitination. *Cell Death Differ,* 24**,** 903-916.

Lee, C.-K., Y. Shibata, B. Rao, B. D. Strahl & J. D. Lieb (2004) Evidence for nucleosome depletion at active regulatory regions genome-wide. *Nature Genetics,* 36**,** 900-905.

Lee, J., J. B. Crickard, J. C. Reese & T.-H. Lee (2019a) Single-molecule FRET method to investigate the dynamics of transcription elongation through the nucleosome by RNA polymerase II. *Methods,* 159-160**,** 51-58.

Lee, J., J. B. Crickard, J. C. Reese & T. H. Lee (2019b) Single-molecule FRET method to investigate the dynamics of transcription elongation through the nucleosome by RNA polymerase II. *Methods,* 159-160**,** 51-58.

Lee, J. & T.-H. Lee (2019) How Protein Binding Sensitizes the Nucleosome to Histone H3K56 Acetylation. *ACS chemical biology,* 14**,** 506-515.

Lee, J. & T. H. Lee (2017) Single-Molecule Investigations on Histone H2A-H2B Dynamics in the Nucleosome. *Biochemistry,* 56**,** 977-985.

Lee, J. Y., J. Lee, H. Yue & T. H. Lee (2015) Dynamics of nucleosome assembly and effects of DNA methylation. *J Biol Chem,* 290**,** 4291-303.

Lee, J. Y., S. Wei & T.-H. Lee (2011) Effects of Histone Acetylation by Piccolo NuA4 on the Structure of a Nucleosome and the Interactions between Two Nucleosomes*. *Journal of Biological Chemistry,* 286**,** 11099-11109.

Lee, S., J. Lee & S. Hohng (2010) Single-molecule three-color FRET with both negligible spectral overlap and long observation time. *PLoS One,* 5**,** e12270.

Lee, T. H. (2019) Physical Chemistry of Epigenetics: Single-Molecule Investigations. *J Phys Chem B,* 123**,** 8351-8362.

Lerner, E., A. Barth, J. Hendrix, B. Ambrose, V. Birkedal, S. C. Blanchard, R. Börner, H. Sung Chung, T. Cordes, T. D. Craggs, A. A. Deniz, J. Diao, J. Fei, R. L. Gonzalez, I. V. Gopich, T. Ha, C. A. Hanke, G. Haran, N. S. Hatzakis, S. Hohng, S.-C. Hong, T. Hugel, A. Ingargiola, C. Joo, A. N. Kapanidis, H. D. Kim, T. Laurence, N. K. Lee, T.-H. Lee, E. A. Lemke, E. Margeat, J. Michaelis, X. Michalet, S. Myong, D. Nettels, T.-O. Peulen, E. Ploetz, Y. Razvag, N. C. Robb, B. Schuler, H. Soleimaninejad, C. Tang, R. Vafabakhsh, D. C. Lamb, C. A. Seidel & S. Weiss (2021) FRET-based dynamic structural biology: Challenges, perspectives and an appeal for open-science practices. *eLife,* 10**,** e60416.

Li, F., A. Allahverdi, R. Yang, G. B. Lua, X. Zhang, Y. Cao, N. Korolev, L. Nordenskiöld & C. F. Liu (2011) A direct method for site-specific protein acetylation. *Angew Chem Int Ed Engl,* 50**,** 9611-4.

Li, G., M. Levitus, C. Bustamante & J. Widom (2005) Rapid spontaneous accessibility of nucleosomal DNA. *Nat Struct Mol Biol,* 12**,** 46-53.

Li, J., Q. He, Y. Liu, S. Liu, S. Tang, C. Li, D. Sun, X. Li, M. Zhou, P. Zhu, G. Bi, Z. Zhou, J. S. Zheng & C. Tian (2017) Chemical Synthesis of K34-Ubiquitylated H2B for Nucleosome Reconstitution and Single-Particle Cryo-Electron Microscopy Structural Analysis. *Chembiochem,* 18**,** 176-180.

Li, W., P. Chen, J. Yu, L. Dong, D. Liang, J. Feng, J. Yan, P. Y. Wang, Q. Li, Z. Zhang, M. Li & G. Li (2016) FACT Remodels the Tetranucleosomal Unit of Chromatin Fibers for Gene Transcription. *Mol Cell,* 64**,** 120-133.

Lisica, A., C. Engel, M. Jahnel, É. Roldán, E. A. Galburt, P. Cramer & S. W. Grill (2016) Mechanisms of backtrack recovery by RNA polymerases I and II. *Proceedings of the National Academy of Sciences of the United States of America,* 113**,** 2946-2951.

Liu, Y., K. Zhou, N. Zhang, H. Wei, Y. Z. Tan, Z. Zhang, B. Carragher, C. S. Potter, S. D'Arcy & K. Luger (2020) FACT caught in the act of manipulating the nucleosome. *Nature,* 577**,** 426-431.

Ljungman, M., L. Parks, R. Hulbatte & K. Bedi (2019) The role of H3K79 methylation in transcription and the DNA damage response. *Mutat Res,* 780**,** 48-54.

Long, L., M. Furgason & T. Yao (2014a) Generation of nonhydrolyzable ubiquitin-histone mimics. *Methods (San Diego, Calif.),* 70**,** 134-138.

--- (2014b) Generation of nonhydrolyzable ubiquitin–histone mimics. *Methods,* 70**,** 134-138.

Lorch, Y., B. Maier-Davis & R. D. Kornberg (2006) Chromatin remodeling by nucleosome disassembly in vitro. *Proc Natl Acad Sci U S A,* 103**,** 3090-3.

Lowary, P. T. & J. Widom (1998) New DNA sequence rules for high affinity binding to histone octamer and sequence-directed nucleosome positioning11Edited by T. Richmond. *Journal of Molecular Biology,* 276**,** 19-42.

Lu, X., M. D. Simon, J. V. Chodaparambil, J. C. Hansen, K. M. Shokat & K. Luger (2008) The effect of H3K79 dimethylation and H4K20 trimethylation on nucleosome and chromatin structure. *Nat Struct Mol Biol,* 15**,** 1122-4.

Luger, K. (2003) Structure and dynamic behavior of nucleosomes. *Curr Opin Genet Dev,* 13**,** 127-35.

Luger, K., A. W. Mäder, R. K. Richmond, D. F. Sargent & T. J. Richmond (1997a) Crystal structure of the nucleosome core particle at 2.8 A resolution. *Nature,* 389**,** 251-60.

Luger, K., T. J. Rechsteiner, A. J. Flaus, M. M. Waye & T. J. Richmond (1997b) Characterization of nucleosome core particles containing histone proteins made in bacteria. *J Mol Biol,* 272**,** 301-11.

Luger, K., T. J. Rechsteiner & T. J. Richmond (1999a) Expression and purification of recombinant histones and nucleosome reconstitution. *Methods Mol Biol,* 119**,** 1-16.

--- (1999b) Preparation of nucleosome core particle from recombinant histones. *Methods Enzymol,* 304**,** 3-19.

Machida, S., S. Sekine, Y. Nishiyama, N. Horikoshi & H. Kurumizaka Structural and biochemical analyses of monoubiquitinated human histones H2B and H4. *Open Biology,* 6**,** 160090.

--- (2016) Structural and biochemical analyses of monoubiquitinated human histones H2B and H4. *Open Biol,* 6.

Mason, P. B. & K. Struhl (2003) The FACT complex travels with elongating RNA polymerase II and is important for the fidelity of transcriptional initiation in vivo. *Mol Cell Biol,* 23**,** 8323-33.

Mayanagi, K., K. Saikusa, N. Miyazaki, S. Akashi, K. Iwasaki, Y. Nishimura, K. Morikawa & Y. Tsunaka (2019) Structural visualization of key steps in nucleosome reorganization by human FACT. *Scientific reports,* 9**,** 10183-10183.

McBryant, S. J., Y. J. Park, S. M. Abernathy, P. J. Laybourn, J. K. Nyborg & K. Luger (2003) Preferential binding of the histone (H3-H4)2 tetramer by NAP1 is mediated by the amino-terminal histone tails. *J Biol Chem,* 278**,** 44574-83.

McQuibban, G. A., C. N. Commisso-Cappelli & P. N. Lewis (1998) Assembly, remodeling, and histone binding capabilities of yeast nucleosome assembly protein 1. *J Biol Chem,* 273**,** 6582-90.

Meng, H., K. Andresen & J. van Noort (2015) Quantitative analysis of single-molecule force spectroscopy on folded chromatin fibers. *Nucleic Acids Res,* 43**,** 3578-90.

Mersfelder, E. L. & M. R. Parthun (2006) The tale beyond the tail: histone core domain modifications and the regulation of chromatin structure. *Nucleic acids research,* 34**,** 2653-2662.

Mivelaz, M., A. M. Cao, S. Kubik, S. Zencir, R. Hovius, I. Boichenko, A. M. Stachowicz, C. F. Kurat, D. Shore & B. Fierz (2020) Chromatin Fiber Invasion and Nucleosome Displacement by the Rap1 Transcription Factor. *Mol Cell,* 77**,** 488-500.e9.

Morse, R. H. (1989) Nucleosomes inhibit both transcriptional initiation and elongation by RNA polymerase III in vitro. *The EMBO journal,* 8**,** 2343-2351.

Mosammaparast, N., C. S. Ewart & L. F. Pemberton (2002) A role for nucleosome assembly protein 1 in the nuclear transport of histones H2A and H2B. *EMBO J,* 21**,** 6527-38.

Murawska, M., T. Schauer, A. Matsuda, M. D. Wilson, T. Pysik, F. Wojcik, T. W. Muir, Y. Hiraoka, T. Straub & A. G. Ladurner (2020) The Chaperone FACT and Histone H2B Ubiquitination Maintain S. pombe Genome Architecture through Genic and Subtelomeric Functions. *Molecular Cell,* 77**,** 501-513.e7.

Neumann, H., S. M. Hancock, R. Buning, A. Routh, L. Chapman, J. Somers, T. Owen-Hughes, J. van Noort, D. Rhodes & J. W. Chin (2009a) A method for genetically installing site-specific acetylation in recombinant histones defines the effects of H3 K56 acetylation. *Mol Cell,* 36**,** 153-63.

--- (2009b) A Method for Genetically Installing Site-Specific Acetylation in Recombinant Histones Defines the Effects of H3 K56 Acetylation. *Molecular Cell,* 36**,** 153-163.

Ngo, T. T. & T. Ha (2015) Nucleosomes undergo slow spontaneous gaping. *Nucleic Acids Res,* 43**,** 3964-71.

Nguyen, A. T. & Y. Zhang (2011) The diverse functions of Dot1 and H3K79 methylation. *Genes Dev,* 25**,** 1345-58.

Nielsen, M., R. Ard, X. Leng, M. Ivanov, P. Kindgren, V. Pelechano & S. Marquardt (2019) Transcription-driven chromatin repression of Intragenic transcription start sites. *PLoS Genet,* 15**,** e1007969.

North, J. A., J. C. Shimko, S. Javaid, A. M. Mooney, M. A. Shoffner, S. D. Rose, R. Bundschuh, R. Fishel, J. J. Ottesen & M. G. Poirier (2012) Regulation of the nucleosome unwrapping rate controls DNA accessibility. *Nucleic Acids Research,* 40**,** 10215-10227.

Ozdemir, A., S. Spicuglia, E. Lasonder, M. Vermeulen, C. Campsteijn, H. G. Stunnenberg & C. Logie (2005) Characterization of lysine 56 of histone H3 as an acetylation site in Saccharomyces cerevisiae. *J Biol Chem,* 280**,** 25949-52.

Pagé, V., J. J. Chen, M. Durand-Dubief, D. Grabowski, E. Oya, M. Sansô, R. D. Martin, T. E. Hébert, R. P. Fisher, K. Ekwall & J. C. Tanny (2019) Histone H2B Ubiquitylation Regulates Histone Gene Expression by Suppressing Antisense Transcription in Fission Yeast. *Genetics,* 213**,** 161-172.

Park, Y. J., J. V. Chodaparambil, Y. Bao, S. J. McBryant & K. Luger (2005) Nucleosome assembly protein 1 exchanges histone H2A-H2B dimers and assists nucleosome sliding. *J Biol Chem,* 280**,** 1817-25.

Park, Y. J. & K. Luger (2006) Structure and function of nucleosome assembly proteins. *Biochem Cell Biol,* 84**,** 549-58.

--- (2008) Histone chaperones in nucleosome eviction and histone exchange. *Curr Opin Struct Biol,* 18**,** 282-9.

Qiu, Y., R. F. Levendosky, S. Chakravarthy, A. Patel, G. D. Bowman & S. Myong (2017) The Chd1 Chromatin Remodeler Shifts Nucleosomal DNA Bidirectionally as a Monomer. *Molecular Cell,* 68**,** 76-88.e6.

Ramachandran, S., K. Ahmad & S. Henikoff (2017) Transcription and Remodeling Produce Asymmetrically Unwrapped Nucleosomal Intermediates. *Mol Cell,* 68**,** 1038-1053.e4.

Rothbart, S. B. & B. D. Strahl (2014) Interpreting the language of histone and DNA modifications. *Biochimica et biophysica acta,* 1839**,** 627-643.

Sabantsev, A., R. F. Levendosky, X. Zhuang, G. D. Bowman & S. Deindl (2019) Direct observation of coordinated DNA movements on the nucleosome during chromatin remodelling. *Nat Commun,* 10**,** 1720.

Safaric, B., E. Chacin, M. J. Scherr, L. Rajappa, C. Gebhardt, C. F. Kurat, T. Cordes & K. E. Duderstadt (2022) The fork protection complex recruits FACT to reorganize nucleosomes during replication. *Nucleic Acids Res,* 50**,** 1317-1334.

Scheffer, M. P., M. Eltsov, J. Bednar & A. S. Frangakis (2012) Nucleosomes stacked with aligned dyad axes are found in native compact chromatin in vitro. *J Struct Biol,* 178**,** 207-14.

Schwabish, M. A. & K. Struhl (2004) Evidence for eviction and rapid deposition of histones upon transcriptional elongation by RNA polymerase II. *Mol Cell Biol,* 24**,** 10111-7.

Schübeler, D., D. M. MacAlpine, D. Scalzo, C. Wirbelauer, C. Kooperberg, F. van Leeuwen, D. E. Gottschling, L. P. O'Neill, B. M. Turner, J. Delrow, S. P. Bell & M. Groudine (2004) The histone modification pattern of active genes revealed through genome-wide chromatin analysis of a higher eukaryote. *Genes Dev,* 18**,** 1263-71.

Sengupta, B., M. Huynh, C. B. Smith, R. K. McGinty, W. Krajewski & T. H. Lee (2022) The Effects of Histone H2B Ubiquitylations on the Nucleosome Structure and Internucleosomal Interactions. *Biochemistry*.

Serra-Cardona, A. & Z. Zhang (2018) Replication-Coupled Nucleosome Assembly in the Passage of Epigenetic Information and Cell Identity. *Trends Biochem Sci,* 43**,** 136-148.

Shakya, A., C. Callister, A. Goren, N. Yosef, N. Garg, V. Khoddami, D. Nix, A. Regev & D. Tantin (2015) Pluripotency transcription factor Oct4 mediates stepwise nucleosome demethylation and depletion. *Mol Cell Biol,* 35**,** 1014-25.

Shoaib, M., Q. Chen, X. Shi, N. Nair, C. Prasanna, R. Yang, D. Walter, K. S. Frederiksen, H. Einarsson, J. P. Svensson, C. F. Liu, K. Ekwall, M. Lerdrup, L. Nordenskiöld & C. S. Sørensen (2021) Histone H4 lysine 20 mono-methylation directly facilitates chromatin openness and promotes transcription of housekeeping genes. *Nature communications,* 12**,** 4800-4800.

Simon, M., J. A. North, J. C. Shimko, R. A. Forties, M. B. Ferdinand, M. Manohar, M. Zhang, R. Fishel, J. J. Ottesen & M. G. Poirier (2011) Histone fold modifications control nucleosome unwrapping and disassembly. *Proc Natl Acad Sci U S A,* 108**,** 12711-6.

Simon, M. D., F. Chu, L. R. Racki, C. C. de la Cruz, A. L. Burlingame, B. Panning, G. J. Narlikar & K. M. Shokat (2007) The site-specific installation of methyl-lysine analogs into recombinant histones. *Cell,* 128**,** 1003-12.

Smith, E. & A. Shilatifard (2010) The chromatin signaling pathway: diverse mechanisms of recruitment of histone-modifying enzymes and varied biological outcomes. *Molecular cell,* 40**,** 689-701.

Spangler, C. J., S. P. Yadav, D. Li, C. N. Geil, C. B. Smith, G. G. Wang, T.-H. Lee & R. K. McGinty (2022) DOT1L activity in leukemia cells requires interaction with ubiquitylated H2B that promotes productive nucleosome binding. *Cell Reports,* 38**,** 110369.

Stehr, R., N. Kepper, K. Rippe & G. Wedemann (2008) The Effect of Internucleosomal Interaction on Folding of the Chromatin Fiber. *Biophysical Journal,* 95**,** 3677-3691.

Studitsky, V. M., E. V. Nizovtseva, A. K. Shaytan & D. S. Luse (2016) Nucleosomal Barrier to Transcription: Structural Determinants and Changes in Chromatin Structure. *Biochem Mol Biol J*, 2.

Swatek, K. N. & D. Komander (2016) Ubiquitin modifications. *Cell Research*, 26**,** 399-422.

Takahata, S., Y. Yu & D. J. Stillman (2009) FACT and Asf1 regulate nucleosome dynamics and coactivator binding at the HO promoter. *Mol Cell*, 34**,** 405-15.

Talbert, P. B. & S. Henikoff (2017) Histone variants on the move: substrates for chromatin dynamics. *Nat Rev Mol Cell Biol*, 18**,** 115-126.

Tanny, J. C., H. Erdjument-Bromage, P. Tempst & C. D. Allis (2007) Ubiquitylation of histone H2B controls RNA polymerase II transcription elongation independently of histone H3 methylation. *Genes Dev*, 21**,** 835-47.

Tomschik, M., K. van Holde & J. Zlatanova (2009) Nucleosome dynamics as studied by single-pair fluorescence resonance energy transfer: a reevaluation. *J Fluoresc*, 19**,** 53-62.

Tomschik, M., H. Zheng, K. van Holde, J. Zlatanova & S. H. Leuba (2005) Fast, long-range, reversible conformational fluctuations in nucleosomes revealed by single-pair fluorescence resonance energy transfer. *Proc Natl Acad Sci U S A*, 102**,** 3278-83.

Tsunaka, Y., Y. Fujiwara, T. Oyama, S. Hirose & K. Morikawa (2016) Integrated molecular mechanism directing nucleosome reorganization by human FACT. *Genes Dev*, 30**,** 673-86.

Tóth, K. F., J. Mazurkiewicz & K. Rippe (2005) Association states of nucleosome assembly protein 1 and its complexes with histones. *J Biol Chem*, 280**,** 15690-9.

Valencia-Sánchez, M. I., P. De Ioannes, M. Wang, N. Vasilyev, R. Chen, E. Nudler, J. P. Armache & K. J. Armache (2019) Structural Basis of Dot1L Stimulation by Histone H2B Lysine 120 Ubiquitination. *Mol Cell*, 74**,** 1010-1019.e6.

Valieva, M. E., G. A. Armeev, K. S. Kudryashova, N. S. Gerasimova, A. K. Shaytan, O. I. Kulaeva, L. L. McCullough, T. Formosa, P. G. Georgiev, M. P. Kirpichnikov, V. M. Studitsky & A. V. Feofanov (2016) Large-scale ATP-independent nucleosome unfolding by a histone chaperone. *Nat Struct Mol Biol*, 23**,** 1111-1116.

Valieva, M. E., N. S. Gerasimova, K. S. Kudryashova, A. L. Kozlova, M. P. Kirpichnikov, Q. Hu, M. V. Botuyan, G. Mer, A. V. Feofanov & V. M. Studitsky (2017) Stabilization of Nucleosomes by Histone Tails and by FACT Revealed by spFRET Microscopy. *Cancers (Basel)*, 9.

Vasudevan, D., E. Y. D. Chua & C. A. Davey (2010) Crystal structures of nucleosome core particles containing the '601' strong positioning sequence. *J Mol Biol*, 403**,** 1-10.

Vlijm, R., J. S. Smitshuijzen, A. Lusser & C. Dekker (2012) NAP1-assisted nucleosome assembly on DNA measured in real time by single-molecule magnetic tweezers. *PLoS One*, 7**,** e46306.

Wang, D., D. A. Bushnell, X. Huang, K. D. Westover, M. Levitt & R. D. Kornberg (2009) Structural basis of transcription: backtracked RNA polymerase II at 3.4 angstrom resolution. *Science (New York, N.Y.)*, 324**,** 1203-1206.

Wang, T., Y. Liu, G. Edwards, D. Krzizike, H. Scherman & K. Luger (2018) The histone chaperone FACT modulates nucleosome structure by tethering its components. *Life Sci Alliance*, 1**,** e201800107.

Wang, Z., C. Zang, J. A. Rosenfeld, D. E. Schones, A. Barski, S. Cuddapah, K. Cui, T. Y. Roh, W. Peng, M. Q. Zhang & K. Zhao (2008) Combinatorial patterns of histone acetylations and methylations in the human genome. *Nat Genet*, 40**,** 897-903.

Weake, V. M. & J. L. Workman (2008) Histone Ubiquitination: Triggering Gene Activity. *Molecular Cell*, 29**,** 653-663.

Wilkins, B. J., N. A. Rall, Y. Ostwal, T. Kruitwagen, K. Hiragami-Hamada, M. Winkler, Y. Barral, W. Fischle & H. Neumann (2014) A cascade of histone modifications induces chromatin condensation in mitosis. *Science,* 343**,** 77-80.

Winkler, D. D., U. M. Muthurajan, A. R. Hieb & K. Luger (2011) Histone chaperone FACT coordinates nucleosome interaction through multiple synergistic binding events. *J Biol Chem,* 286**,** 41883-41892.

Worden, E. J., N. A. Hoffmann, C. W. Hicks & C. Wolberger (2019) Mechanism of Cross-talk between H2B Ubiquitination and H3 Methylation by Dot1L. *Cell,* 176**,** 1490-1501.e12.

Worden, E. J. & C. Wolberger (2019) Activation and regulation of H2B-Ubiquitin-dependent histone methyltransferases. *Curr Opin Struct Biol,* 59**,** 98-106.

Wright, D. E. & C.-F. Kao (2015) (Ubi)quitin' the h2bit: recent insights into the roles of H2B ubiquitylation in DNA replication and transcription. *Epigenetics,* 10**,** 122-126.

Wu, L., L. Li, B. Zhou, Z. Qin & Y. Dou (2014) H2B ubiquitylation promotes RNA Pol II processivity via PAF1 and pTEFb. *Molecular cell,* 54**,** 920-931.

Xin, H., S. Takahata, M. Blanksma, L. McCullough, D. J. Stillman & T. Formosa (2009) yFACT induces global accessibility of nucleosomal DNA without H2A-H2B displacement. *Mol Cell,* 35**,** 365-76.

Xu, F., K. Zhang & M. Grunstein (2005) Acetylation in histone H3 globular domain regulates gene expression in yeast. *Cell,* 121**,** 375-85.

Yang, A., S. Ha, J. Ahn, R. Kim, S. Kim, Y. Lee, J. Kim, D. Söll, H. Y. Lee & H. S. Park (2016) A chemical biology route to site-specific authentic protein modifications. *Science,* 354**,** 623-626.

Yankulov, K. (2015) Book review: Epigenetics (second edition, eds. Allis, Caparros, Jenuwein, Reinberg). *Frontiers in Genetics,* 6**,** 315.

Yue, H., H. Fang, S. Wei, J. J. Hayes & T. H. Lee (2016) Single-Molecule Studies of the Linker Histone H1 Binding to DNA and the Nucleosome. *Biochemistry,* 55**,** 2069-77.

Zentner, G. E. & S. Henikoff (2013) Regulation of nucleosome dynamics by histone modifications. *Nat Struct Mol Biol,* 20**,** 259-66.

Zhang, L., L. Deng, F. Chen, Y. Yao, B. Wu, L. Wei, Q. Mo & Y. Song (2014) Inhibition of histone H3K79 methylation selectively inhibits proliferation, self-renewal and metastatic potential of breast cancer. *Oncotarget,* 5**,** 10665-77.

Zhang, Y. & T. G. Kutateladze (2019) Methylation of Histone H3K79 by Dot1L Requires Multiple Contacts with the Ubiquitinated Nucleosome. *Mol Cell,* 74**,** 862-863.

Zheng, C. & J. J. Hayes (2003) Intra- and inter-nucleosomal protein-DNA interactions of the core histone tail domains in a model system. *J Biol Chem,* 278**,** 24217-24.

Zhou, C. Y., S. L. Johnson, L. J. Lee, A. D. Longhurst, S. L. Beckwith, M. J. Johnson, A. J. Morrison & G. J. Narlikar (2018) The Yeast INO80 Complex Operates as a Tunable DNA Length-Sensitive Switch to Regulate Nucleosome Sliding. *Mol Cell,* 69**,** 677-688.e9.

Zhou, K., Y. Liu & K. Luger (2020) Histone chaperone FACT FAcilitates Chromatin Transcription: mechanistic and structural insights. *Curr Opin Struct Biol,* 65**,** 26-32.

Zorro Shahidian, L., M. Haas, S. Le Gras, S. Nitsch, A. Mourão, A. Geerlof, R. Margueron, J. Michaelis, S. Daujat & R. Schneider (2021) Succinylation of H3K122 destabilizes nucleosomes and enhances transcription. *EMBO Rep,* 22**,** e51009.

VITA

Mai Huynh

Education

2017 – Present	Ph.D. Candidate, Chemistry The Pennsylvania State University, PA
2013 – 2017	B.A., Biochemistry Mount Holyoke College, MA

Publications

Mai T. Huynh*, Bhaswati Sengupta*, Wladyslaw Krajewski and Tae-Hee Lee. The effects of histone H2B ubiquitylations and H3K79me$_3$ on transcription elongation. *ACS Chemical Biology* (2023) (* first co-authors)

Bhaswati Sengupta*, **Mai T.Huynh***, Charlotte Smith, Robert McGinty, Wladyslaw Krajewski, Tae-Hee Lee. The effects of histone H2B ubiquitylations on the nucleosome structure and internucleosomal interactions. *Biochemistry* (2022) 61(20): 2198-2205. (* first co-authors)

Mai T. Huynh, Satya Y. Prakash, Joseph C. Reese, and Tae-Hee Lee. Nucleosome dynamics during transcription elongation. *ACS Chemical Biology* (2020) 15: 3133–3142.

Subhra K. Das*, **Mai T. Huynh***, Jia Gao, Bhaswati Sengupta, Satya Yadav, and Tae-Hee Lee. Investigating nucleosome structure and dynamics with single-molecule FRET. Submitted to Methods. (* first co-authors)

Subhra K. Das, **Mai T. Huynh**, and Tae-Hee Lee. Spontaneous histone exchange between nucleosomes. Submitted to Biophysical Journal.

Conferences and Presentations

"The Effects of Histone H2B ubiquitylations and H3K79 trimethylation on Transcription Elongation", ASBMB Annual Meeting, 2023

"Nucleosome Dynamics during Transcription Elongation", ASBMB Annual Meeting, 2021

"Single-molecule Investigations of Nucleosome Dynamics during Transcription Elongation", ACS Macromolecular Chemistry: The Second Century, 2021

"How histone H3 K56 acetylation facilitates transcription through the nucleosome", ChemBio Student Seminar, University Park, PA (2020)